UNIVERSITAT DE BARCELONA

Esllavissaments submarins recents en el marge de l'Ebre i el canal d'Eivissa, Mediterrània occidental

Galderic Lastras Membrive

UNIVERSITAT DE BARCELONA
Departament d'Estratigrafia, Paleontologia i Geociències Marines

Esllavissaments submarins recents en el marge de l'Ebre i el canal d'Eivissa, Mediterrània occidental

Recent Submarine Landslides in the Ebro Margin and the Eivissa Channel, Western Mediterranean Sea

Realitzada per:

Galderic Lastras Membrive

sota la direcció del **Dr. Miquel Canals i Artigas**, al Departament d'Estratigrafia, Paleontologia i Geociències Marines de la Universitat de Barcelona dins del programa de doctorat en "Ciències de la Terra" de la Facultat de Geologia, bienni 1999-2000, per a optar al grau de Doctor en Geologia.

Barcelona, Abril de 2004

El Doctorand
Galderic Lastras

El Director de Tesi
Miquel Canals

CAPÍTOL 6

THE BIG'95 SLIDE: MODELING

Lastras, G., De Blasio, F.V., Canals, M., Elverhøi, A., 2004, Conceptual and numerical modeling of the BIG'95 debris flow, Western Mediterranean, Journal of Sedimentary Research (submitted).

Conceptual and numerical modeling of the BIG'95 debris flow, Western Mediterranean Sea[67]

G. Lastras
GRC Geociències Marines, Universitat de Barcelona, Spain

F.V. De Blasio
Department of Geology, University of Oslo, Norway

M. Canals[68]
GRC Geociències Marines, Universitat de Barcelona, Spain

A. Elverhøi
Department of Geology, University of Oslo, Norway

ABSTRACT

The BIG'95 debris flow affected 2,200 km^2 of the Ebro continental slope and rise in the Western Mediterranean Sea. The resulting deposit of sandy and silty mud has a volume of 26 km^3 and is up to 150 m thick. Dating yields a minimum failure age of ca. 11,500 cal yr BP. Swath bathymetry data, very-high resolution seismic reflection profiles, side-scan sonographs and sediment cores indicate that the debris flow consisted of two main components: relatively coarse, more mobile material, that was mostly remoulded during flow; and finer, more cohesive material, that moved as independent blocks and partially kept its internal coherence. These blocks, partially buoyant, were pushed and dragged up to 15 km by the mobile material. During transport the blocks broke into smaller fragments. The more mobile material kept on flowing, reaching almost 2,000 m water depth in the Valencia Channel after traveling ~110 km.

In this paper, a conceptual and numerical model of the BIG'95 debris flow is investigated. The more mobile component has been modeled as a Bingham fluid with assigned rheological properties. The more cohesive material has been idealized as consisting of rigid blocks. Without interaction with the mobile material, the blocks would stay at rest. As the mobile material comes into contact with the block, the latter is subjected to interaction forces: the impact force, static earth-pressure force, shear force and water drag, in addition to gravity and the Coulomb friction with the seafloor. Theoretical values for the internal friction angle of the block and the yield strength of the mobile material were adjusted to reproduce the observed run-outs of 15-20 km for the blocks and 70 km for the mobile material, a value which is less than observed to account for the topographical stretching of the Valencia Channel. The numerical results demonstrate that the proposed conceptual model is physically possible with input values of the order of 1° for the Coulomb frictional angle and 800 Pa for the yield strength. Such values, even if certainly low, are in line with recent estimates for other subaqueous debris flows, and might be explained by processes aiding mobilization such as hydroplaning, entrapment of more mobile material

[67] Manuscript submitted to Journal of Sedimentary Research.
Manuscript received July 21, 2003.
Revised manuscript received March 23, 2004.
[68] Corresponding author: miquel@natura.geo.ub.es

underneath the blocks. Alternatively, it might imply that the blocks were already in motion before the impact of the mobile material took place.

Keywords: Debris flow, conceptual modeling, numerical modeling, rheology, Western Mediterranean

6.1. INTRODUCTION

The BIG'95 debris flow affected 2,200 km^2 of the Valencia Trough in the southern Balearic Sea (Western Mediterranean Sea, Fig. 6.1), of which 2,000 km^2 are covered by the resulting deposit. The debrite has a total volume of 26 km^3 of remobilized sediment (Canals et al., 2000; Lastras et al., 2002), thus representing one of the largest mass-wasting events in the Mediterranean. It is located on the river-fed Ebro continental slope and rise at depths ranging from 200 m to almost 2,000 m water depth, roughly between 39°30'N and 40°10'N, and 0°50'E and 2°00'E (Fig. 6.2), offshore of the coastal city of Castelló and off the volcanic Columbretes Islets. AMS ^{14}C dating of a thin hemipelagic unit drapping the debris flow deposit yields a consistent minimum failure age of ca. 11,500 calendar years BP (Lastras et al., 2002).

Major advances have been made in recent years in our knowledge of the occurrence, extent, volume and dynamics of slope failures in both glacial (Evans et al., 1996; Boe et al., 2000; Laberg and Vorren, 2000; Canals et al., in press) and river-dominated (Rothwell et al., 1998; Droz et al., 2001; Canals et al., in press) European continental margins. Special efforts have been dedicated to the development of numerical models and simulations of debris flows (Mohrig et al., 1998; 1999; Imran et al., 2001; Marr et al., 2002). This paper presents a conceptual model of the BIG'95 debris flow, based on the available data, and its testing using numerical approaches with sensitivity tests, in order to achieve a better understanding of the physical processes that occurred during this particular event.

6.1.1. Geological Setting

The Valencia Trough extensional basin is bounded by the Balearic Promontory to the southeast, the Eivissa Channel to the south and the Ebro and Catalan continental margins to the northwest. To the northeast it opens to the Provençal Basin (Fig. 6.1). At present, the Valencia Trough is incised in its axis by the northeast trending

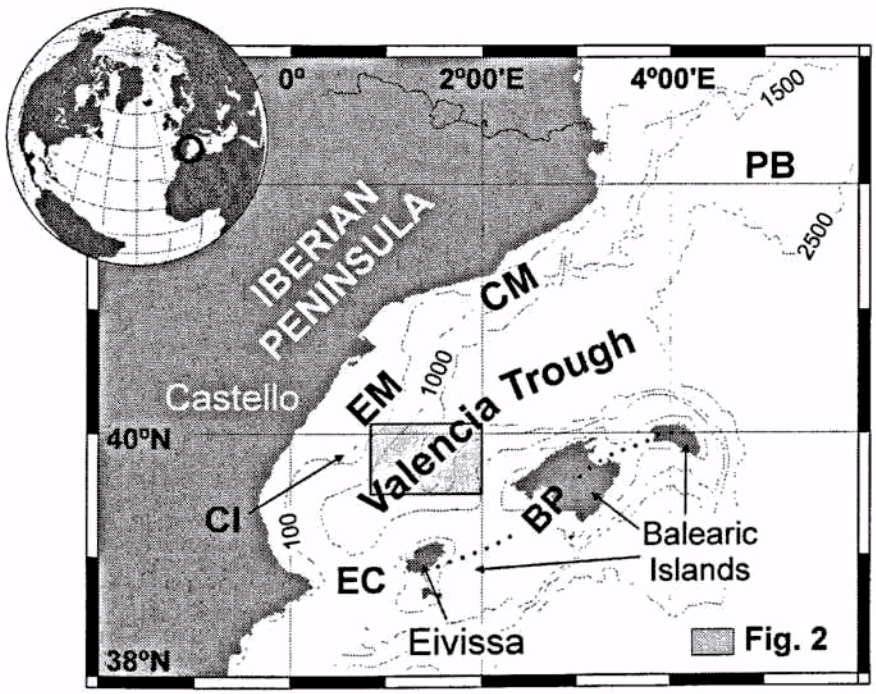

Figure 6.1. Regional map of the Valencia Trough and surroundings. Bathymetry extracted from Smith and Sandwell (1997) database. EM: Ebro margin, CM: Catalan margin, PB: Provençal Basin, CI: Columbretes Islets, EC: Eivissa Channel, BP: Balearic Promontory. Box shows location of the study area represented in Figure 6.2.

Valencia Channel (Canals et al., 2000). The passive Ebro continental margin, which is the source area of the BIG'95 debris flow material, is floored by siliciclastic sediment mainly fed by the 900 km long Ebro River. The shelf is amongst the widest in the Mediterranean Sea due to the sustained inputs from the Ebro. It reaches widths of 70 km and has a shelf break located at a mean depth of 130 m.

The narrow, 10 km wide Ebro slope is cut by a number of east—southeast trending submarine canyons often slightly incised into the shelf, and by several short, straight gullies (Fig. 6.2). The continental rise is occupied by meandering channel-levee complexes, smooth inter-channel areas, and debris flow and apron deposits, forming the Ebro Turbidite System (Nelson and Maldonado, 1988). None of the canyon—channel systems is connected with the Valencia Channel in the southern sector of the margin, south of 40°N (Fig. 6.2) (Canals et al., 2000). The growth patterns of the Ebro margin during the Quaternary were controlled by glacioeustatic sea-level oscillations, subsidence and changes in sediment supply (Farran and Maldonado, 1990). In contrast to the Ebro margin, the opposite Balearic margin is a starved margin fed by carbonate sediment and submarine valleys have not developed there (Fig. 6.2) (Canals et al., 1982).

There are several volcanic structures in the region, including the Columbretes Islets, a volcanic archipelago on the Ebro outer shelf (Aparicio et al., 1991) that is the topographic expression of a larger, mostly

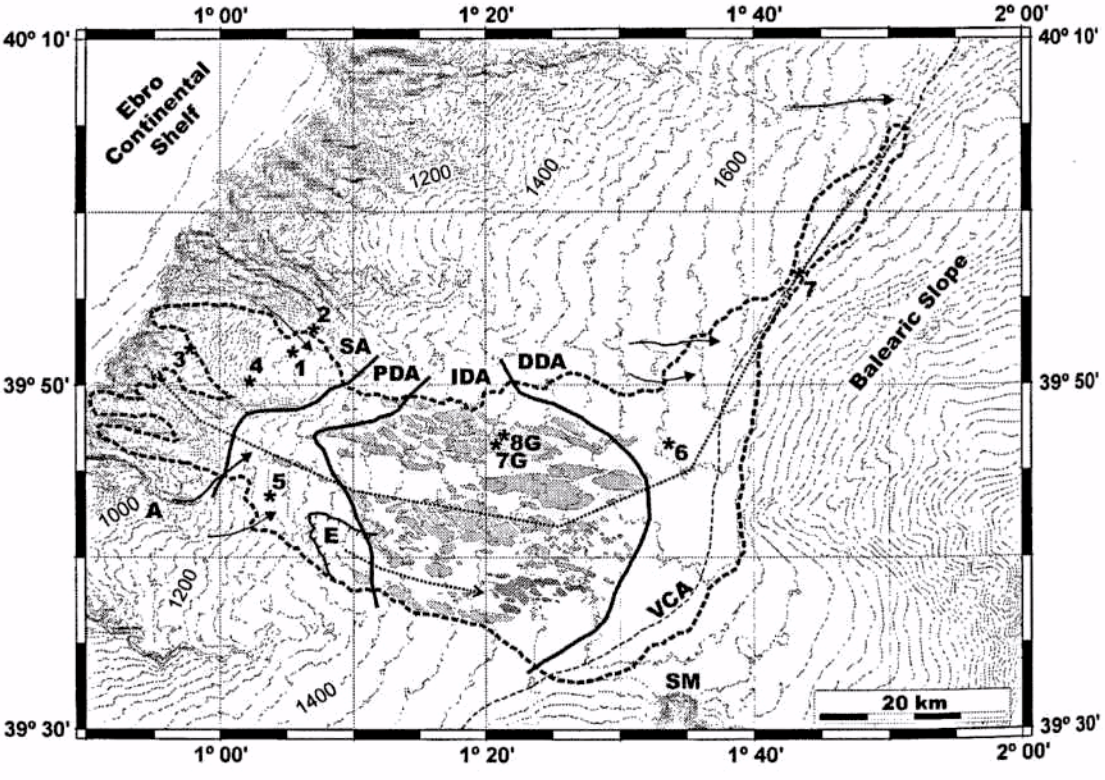

Figure 6.2. Swath bathymetry map of the BIG'95 debris flow area, bounded by the thick dashed line. Contour interval is 25 m. The source area (SA), proximal depositional area (PDA), intermediate depositional area (IDA) and distal depositional area (DDA) are separated by continuous lines. Grey patches in the IDA represent blocks as observed in swath bathymetry maps (see Fig. 1 in Lastras et al., 2002). The course of the Valencia Channel (VCA) is marked with a thin dashed line. The dotted line corresponds to the along-slide section in Figure 6.6. A: Canyon-channel system abruptly cut by the debris flow deposit. Other channels also cut are marked with thin arrows. E: Secondary scar downslope the main scar. SM: Seamount. Numbers 1 to 7 are core CLKS01 to CLKS07 locations, respectively (Fig. 6.3). 7G and 8G show core 277G and 278G locations.

buried volcanic field (Maillard and Mauffret, 1993). These volcanic structures likely played a significant role in the pre-conditioning of the BIG'95 debris flow (Lastras et al., 2002).

6.1.2. Data Set

Five surveys have been carried out to study the BIG'95 debris flow area: BIG-95 onboard R/V Hespérides in 1995, CALMAR onboard R/V L'Atalante in 1997, MATER-2 onboard R/V Hespérides in 1999, TTR-11 BIGIMAGE onboard R/V Professor Logachev in 2001 and GMO-2 onboard RV Le Suroit in 2002.

Swath bathymetry data (Fig. 6.2) and derivative products (Lastras et al., 2002) were obtained using EM-12S in 1995, EM12-Dual in 1997, EM-1002 in 1999, and EM-300 in 2002. Coupled towed deep-sea side-scan sonar and very high resolution seismic reflection data (Lastras et al., 2003) were obtained using Southampton Oceanography Centre's TOBI 30 kHz side-scan sonar and 7 kHz chirp sub-bottom profiler, and Professor Logachev's MAK-1M 30 kHz high-resolution side-scan sonar and 5 kHz chirp sub-bottom profiler, for a total coverage of 4000 km^2. Further high (HR) and very-high (VHR) resolution seismic reflection data (Lastras et al., in press) were obtained in 1995 and 1999 (3.5 kHz Simrad TOPAS PS 018 profiler), 1997 (3.5 kHz mud penetrator) and 1999 (0.1 kHz air-gun), totaling more than 5,000 km of profiles.

In addition, nine cores and seafloor videos and photos provide groundtruthing for geophysical data and geotechnical measurements to be used in numerical simulations.

6.2. BIG'95 DEBRIS FLOW: SETTING AND CONCEPTUAL MODEL

The complete data set available for the BIG'95 debris flow yields information on different aspects of the deposit. Geophysical and sedimentological characterization of the deposit provides clues to understand the triggering of the failure and the dynamics of the flowing sediment that are basic for the construction of a conceptual model for this particular mass-wasting event. In the following

sections we present a summary of the basic features of the BIG'95 debris flow that are necessary for the presentation of the conceptual model. Note that for further details on swath bathymetry data, HR and VHR seismic reflection data and side-scan sonar imagery have been published before (Lastras et al., 2002, in press, and 2003, respectively).

6.2.1. Geophysical Data

Merging of bathymetric, shaded relief and backscatter maps has proven to be particularly efficient in showing the seafloor features of the BIG'95 debrite. The deposit is displayed on VHR seismic reflection profiles as a huge, lens-shaped sediment body of mainly transparent but also chaotic to hyperbolic acoustic facies, with almost no internal reflectors, evidencing that it represents one single event (Fig. 3 in Lastras et al., 2002). It contrasts with the mainly stratified acoustic facies of the underlying Plio-Quaternary succession (Lastras et al., in press). An integrated study of the geophysical data allows the identification of the source area and the depositional areas within the affected region, the latter divided, in turn, into the proximal, the blocky intermediate and the distal depositional areas (Fig. 6.2).

The source area includes the main headwall, between 600 and 1,230 m of water depth, with a total length of ~20 km and a height up to 200 m. Several second-order scars, some of them of up to 100 m high, have also been identified. In this area, the debris flow deposit constitutes a thin, generally less than 18 m thick body of transparent seismic acoustic facies that turn into hyperbolic at the rim of the main headwall (Lastras et al., 2003). The proximal depositional area, located west of 1°15'E, is relatively flat and is the principal depocenter of the BIG'95 deposit, with sediment accumulations of up to 150 m

thick. Although this particular area represents only 15% of the total affected area, it contains more than 40% of the mobilized sediment. As a result of the BIG'95 event, pre-existing slope canyons and gullies were truncated, and ghosts of pre-landslide channels that were obliterated during the event are identified in the seafloor in this area. At its limit with the intermediate depositional area, there is another 40 m high secondary scar (scar E in Fig. 6.2). Seismic records show that other buried scars are located in this area (Lastras et al., 2002).

Material accumulated in the intermediate depositional area, mostly west of 1°30'E, has an average thickness of <15 m. This area is characterized by topographically elevated patches as large as 25 km^2 and up to 35 m high, surrounded and crossed by linear depressions (Lastras et al., in press). Both elements, the depressions and the elevated patches, display transparent acoustic facies with no internal reflectors (Lastras et al., 2002), demonstrating that they are part of the deposit and not remnants of the previous seafloor. The patches are interpreted as blocks or agglomerates of mobilized sediment and will be called blocks from here onwards for ease of reference.

Both the blocks and sediment in the depressions have their particular backscatter response, with the depressions displaying relatively higher backscattering (i.e. they are more reflective) than the blocks (Lastras et al., 2002). VHR seismic profiles do not show any reflectors at the contact between the two elements, which would indicate that they moved jointly during the same main event and probably interacted while moving. The edges of some blocks appear to fit together, as if they were the result of the fragmentation of larger remobilized blocks that broke to form clusters of smaller blocks. There is a particular block cluster ~20 km downslope from secondary scar E that looks as if it detached from that scar (Fig. 6.2; Lastras et al., 2002). Altogether the blocks represent a volume of ~5.5 km^3, while the total volume of the BIG'95 debris flow deposit is 26 km^3.

In VHR seismic reflection profiles the distal depositional area is shown as a homogeneous, thin, <10 m thick, layer of transparent acoustic facies with no internal structures (Lastras et al. in press). Its thickness increases where it partially buries the Valencia Channel after the flow turned north-eastwards due to the presence of the Balearic base-of-slope (Fig. 6.2). The seafloor reflector is of much higher amplitude in the distal depositional area than in the blocks of the intermediate depositional area.

6.2.2. Sedimentological Data

Different signatures for in situ, debris flow and post-debris flow deposits in piston cores (Fig. 6.3, location of cores in Fig. 6.2) were distinguished by direct observation and core logs obtained using a Geotek logging device onboard L'Atalante. A thin, 10 to 50 cm thick layer of post-landslide hemipelagic sediment tops the cores. Debris flow material underlies this layer in cores located in the deposit area (CLKS-01, CLKS-04, CLSK-05, CLKS-06 and CLKS-07), and consists of sandy and silty mud and sand debris that is unbedded or displays strongly contorted beds. The debrite contains clay chunks, mud chips, and other indicators of flow that are not present in cores outside the debris flow area (CLKS-02 and CLKS-03). Further analyses (Urgeles et al., 2003) yielded information on sedimentological, geotechnical and geochemical properties of the sediment. Values from some of the analyses are shown in Figure 6.3. Remoulded yield strength analyses show minimum values of 0,99 kPa in core CLKS-02. Palinological studies of some sections, as well as AMS ^{14}C dating, completed the study of the cores (Lastras et al., 2002).

Granulometry analyses showed high contents of silty sediment in cores located off the shelf break, and coarser sediment in the neighborhood of canyon-channel systems and channel-levee complexes. Cores obtained from the distal depositional area, which is dominated by high backscatter material similar to that present

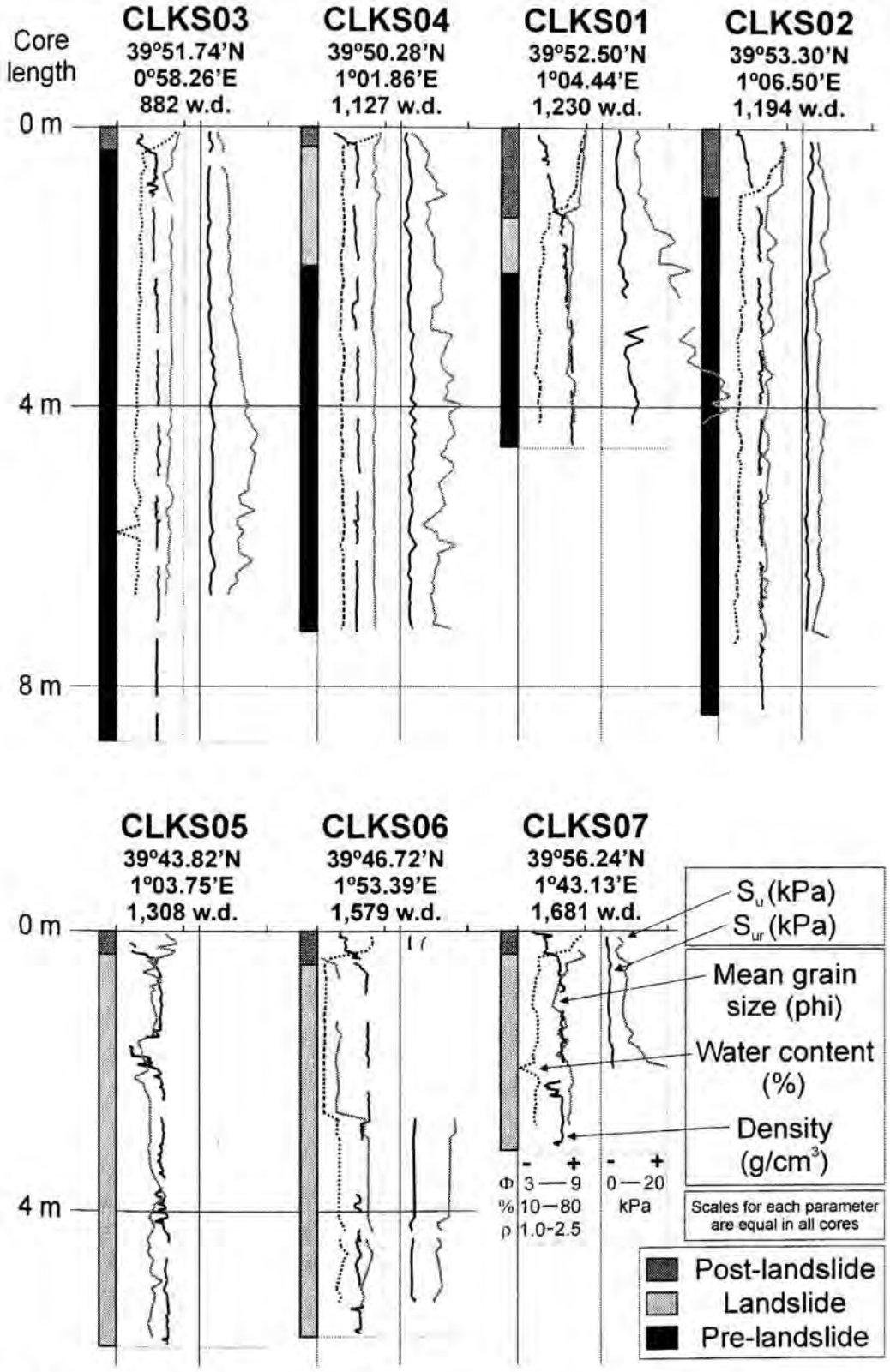

Figure 6.3. *Lithology, (left columns), mean grain size, water content and density (center columns), and intact (S_u) and remoulded (S_{ur}) yield strengths (right columns) logs for each core obtained in the BIG'95 debris flow area. Note scales, which are the same for all cores, below CLKS07 logs. Cores are sorted from left to right and top to bottom from source to distal depositional area. Location of cores (see also Fig. 6.2) and water depths in which they were obtained are shown. Cores 277G and 278G have not yet analyzed.*

in the depressions of the blocky intermediate area, as well as core CLKS-05 from the proximal area, display higher contents of coarser sediment compared to the debris flow sediment in the source area. Furthermore, core 277G, located in one of the intermediate area high backscatter depressions, is sandier at direct observation than core 278G recovered from one the blocks' top (location in Fig. 6.2). These grain size differences likely account for the variations in the backscatter response. The modern outer Ebro shelf and shelf edge are topped by sand dunes, possibly relict (GRC Geociències Marines, unpublished data). Although the debris flow upper scars did not reach the shelf break, the higher contents of sandy material observed in upper slope cores could have been deposited there either by shelf edge spillover or carried along gullies and canyons cut into the shelf edge that have been observed on swath bathymetry maps.

6.2.3. Conceptual Model

Based on the published data, we suggest that the debris flow deposit consists of two main sediment types. The first is a coarser, "loose fraction" that was presumably totally remoulded and liquefied during movement and is present in the proximal, the distal and the depressions in the intermediate depositional areas. The second sediment type is a finer, partially remoulded fraction, which probably maintained part of its initial cohesion during movement, forming the "blocky fraction" in the intermediate depositional area. We suggest that the loose fraction, which represents the greater part of the material involved, was released from the main headwall and secondary scars in the upper slope, where coarse material does exist, and also from the middle slope, in particular by the collapse of the channel-levee complex in the proximal depositional area named A in Figure 6.2. In turn, the blocky fraction was released from the base of the slope, at the limit between the proximal and the intermediate depositional areas, in particular from buried secondary scars similar to scar E. The presumed sequence of events following the triggering of the debris flow is described below (Fig. 6.4).

The formation of the main headwall was synchronous with or followed shortly after by the formation of secondary scars in the source area (Fig. 6.4A). As a result, large quantities of material were mobilized from water depths ranging from 200 to 1,250 m. A channel-levee complex was subsequently cut and collapsed adding more material to the mobile material (Fig. 6.4B). This fraction presumably accelerated downslope due to the slope gradient and became the loose material forming the bulk of the final deposit.

It is difficult to establish whether the blocks were already in motion when the loose material reached the intermediate depositional area, since release of blocks could have occurred either during initial destabilization or by the passage of the loose material (Fig. 6.4C). Blocks originated from water depths ranging from 1,250 to 1,400 m. Both the loose and the blocky fractions moved downslope, the first as a totally remoulded and likely liquefied mass of sediment that had gained speed after the noticeable distance already traveled. The mobile material traveled at higher speeds than the blocky fraction due to its distinct mechanical behavior and the difference in the slope gradient between their respective source areas. Both fractions presumably interacted while flowing. First, the loose material initiated or steered the mobilization of the blocks, which were partially buoyant in the loose material. And then later pushed, sheared and accelerated them. This flowing sediment probably caused fragmentation of blocks, flowed in-between them, and finally by-passed the blocky intermediate depositional area (Fig. 6.2). It is possible that blocks already surrounded by the mobile material trapped part of this fraction below them, thus decreasing the basal friction and easing movement.

As soon as the mobile material critically lost momentum while crossing the depositional area, transport energy became insufficient to continue carrying the blocks further downslope. Blocks were finally abandoned on the intermediate area. The mobile material kept on flowing, reached the distal area (Fig. 6.4D) and was forced to

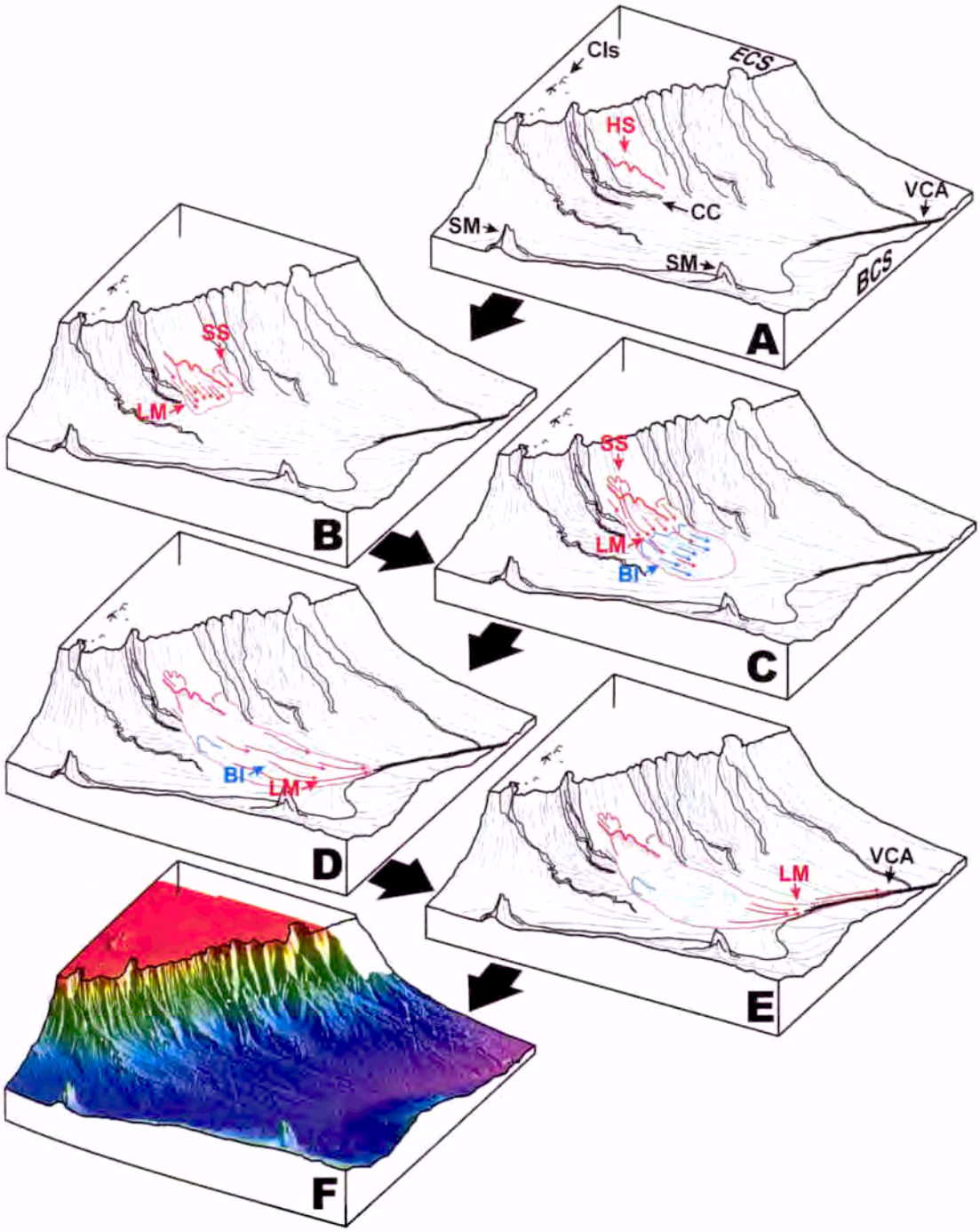

Figure 6.4. *Series of 3D block diagrams illustrating the presumed sequence of events on the Ebro margin after the triggering of the BIG'95 debris flow. ECS: Ebro continental shelf. BCS: Balearic continental slope. SM: Seamount. VCA: Valencia Channel. CC: Canyon-channel system. HS: Headwall scar. SS: Secondary scar. LM: Loose material. Bl: Blocks. After the triggering, loose material was released from the headwall scar (1) in the upper slope. The mobile material flowed downslope (2) while additional material released from secondary scars and from the collapse of a canyon-channel system added to the flow. The same triggering and/or the sudden overload of the lower slope produced by the flowing mobile material released large sediment blocks from the base-of-slope (3). These blocks traveled downslope being pushed and dragged by the mobile material, and finally stopped (4). The mobile material went on flowing downslope and turned northeast forced by the nearby presence of the Balearic base-of-slope (4) to finally bury the upper course of the Valencia Channel (5). Block number 6 shows the present configuration of this part of the Valencia Trough.*

turn northeastwards because of the presence of the Balearic slope. The mobile material finally stopped after filling most of the upper course of the Valencia Channel (Fig. 6.4E).

6.3. NUMERICAL MODELING

Several questions arise regarding the preceding possible scenario for the BIG'95 debris flow and its physical plausibility. Were the forces exerted by the mobile material on the blocks sufficiently great to mobilize the blocks in the depositional area? And conversely, if the conceptual model is correct, can we estimate, using a numerical approach, the properties of the materials based on the present geometrical features of the area together with estimates of the physical forces and energies at play? In order to understand in a more quantitative manner the flow and the mobilization of the blocks in the depositional area, a simplified model of the debris flow-block interaction has been constructed. Despite its practical importance in connection to industrial and geotechnical problems, the problem of the interaction forces between flowing mud and an obstacle is not fully understood. Even laboratory measurements of the force exerted by flowing mud on an obstacle are scarce (Coussot, 1997). In practical large-scale situations in which a gravity mass flow encounters a dam, a containing structure or other obstacles, empirical formulas have been devised (Takahashi, 1991).

The mobile material can be modeled as a Bingham fluid whose rheological properties are the viscosity μ and the yield strength τ_y. Other more sophisticated rheological models could be introduced, such as the bi-viscous model (Locat et al., 2004) or shear thinning or thickening (Imran et al., 2001). However, the uncertainties in the rheological behavior of soil in the BIG'95 event would not have justified the use of a more complex rheology. In a first model, which will be described in detail, these properties are considered time-independent. A second model for the mobile material is then introduced that accounts for remoulding, and in which the yield strength decreases as a function of the accumulated shear at the base of the debris flow. The blocks in the depositional area are assumed as perfectly rigid. As the interaction between different blocks probably did not play a major role in the dynamics, one single block is considered. The assumption that the behavior of the whole system (i.e. with all the blocks) can be inferred by studying just one single block is valid as long as the block width is much smaller than the distance between blocks. In fact, the mobilization of a large area formed by many blocks implies a re-arrangement of the velocity field of the loose material, which is not included in the present model.

6.3.1. 2D Conceptual Diagram

In the model, the block is a parallelepiped with the long axis oriented parallel to the flow (Fig. 6.5). The dimensions of the block are called L (the length), W (width) and H (height). These quantities do not change with time (a hypothetical height variation caused by sole erosion is not included in the model). The block interacts with the seafloor with a Coulomb frictional force specified by the apparent friction angle φ.

In order to run the two-dimensional numerical model, a cross-section along the seafloor area affected by the debris flow from the source to the distal area has been built (Fig. 6.6A). This cross-section shows the present seafloor topography obtained from swath bathymetry data (i.e., the shape of the top surface of the final deposit), and the basal profile of the final debris flow deposit, obtained by digitization of VHR seismic reflection profiles.

A tentative initial profile that represents the seafloor prior to the debris flow event has also been built (Fig. 6.6B). This profile represents the mobilized sediment distributed in two specific source areas, i.e. the mobile material and ideal block source areas. The first one has been defined by the location of the headwall scar and secondary scars in the source area for the shallower, upper source area; the second one by

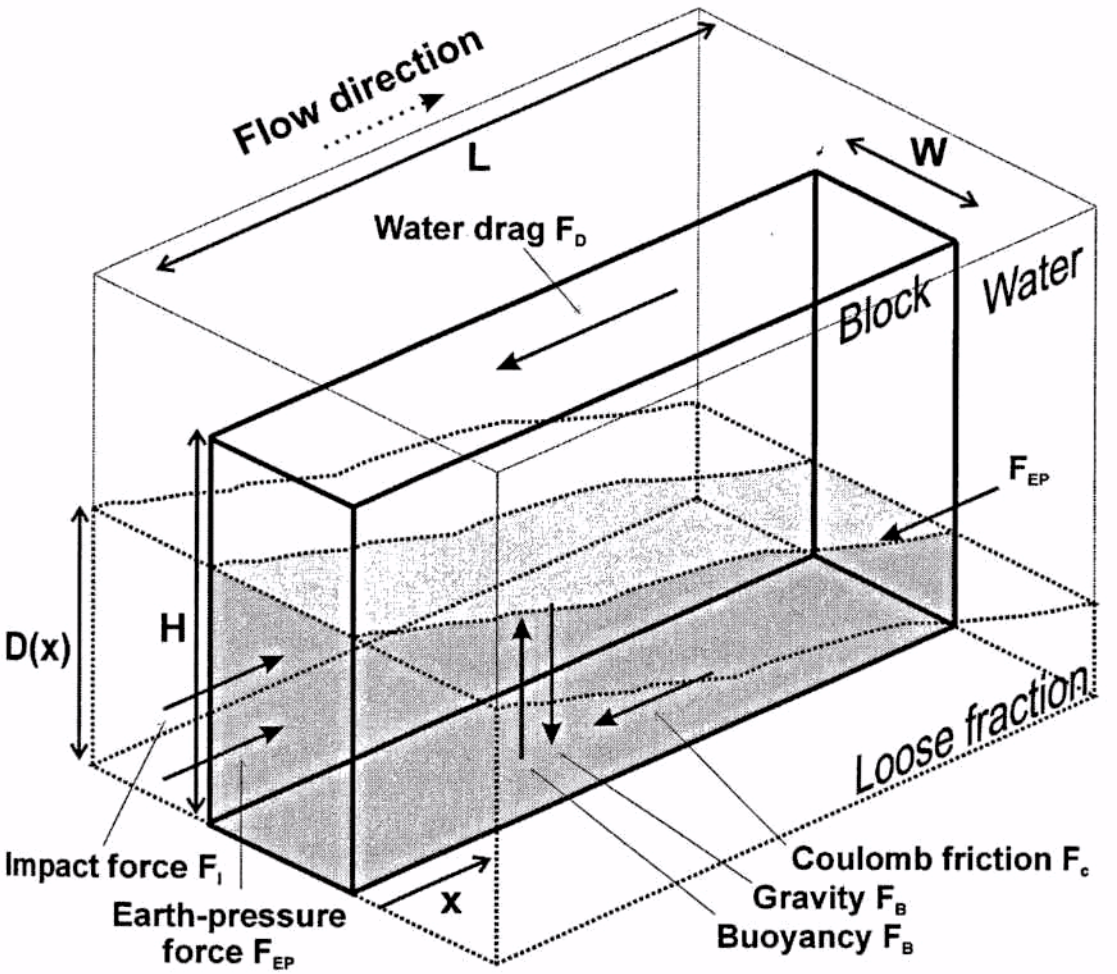

Figure 6.5. Representative sketch of the mobile material, a block and the forces acting upon it. Bold lines represent the edges of the block, dotted lines represent the loose material and thin lines represent water. Grey areas on the block surfaces are places of contact between the block and the mobile material.

locating the proximal and intermediate depositional areas limits and secondary scars in those areas, together with tentatively backstripping of blocks (Lastras et al., 2002). The idealized block is 5 km long, 2 km wide and 40 m high, roughly representing one of the largest blocks observed from swath bathymetry in the BIG'95 debris flow deposit.

The cross-section has been constructed taking into account that volume per unit width of the actual debris flow deposit and that resulting in the cross-section are coincident, as well as volumes per unit width of the real blocks in the debris flow deposit compared to the idealized block used in the runs.

6.3.2. Debris Flow-Block Interaction Model

For simplification, we assume that the blocks would stay at rest on the seafloor without the intervention of the loose fraction, although as explained in the conceptual model it is possible that the blocks were already in movement, released by the initial failure mechanism. As the mobile material comes into contact with the block (Figs. 6.4B and 6.4C), the latter is accelerated by several forces, as shown schematically in Figure 6.5. The motion of the block along the bedding parallel direction can be written equating the time derivative of the block velocity V parallel to the seabed (the acceleration) to the sum

of the forces acting on the block, and dividing by the mass of the block M

$$\frac{dV}{dt} = \frac{1}{M} \sum_{forces,i} F_i \qquad [1]$$

where the summation is extended to all the forces F_i acting on the block.

Since the mass is constant during the flow, we can simply write

$$\frac{dV}{dt} = \frac{1}{M}\left[F_B + F_C + F_I + F_{EP} + F_D + F_V + F_Y\right] = \qquad [2]$$
$$= a_B + a_C + a_I + a_{EP} + a_D + a_V + a_Y$$

where the terms on the right hand side represent the contribution to the acceleration of the block due to the different forces. These are, in order from left to right in equation (2): the bulk force (i.e., gravity) F_B, the Coulomb friction of the block with the seafloor F_C, the impact force exerted by the mobile material on the block front F_I, the static Earth-pressure force (originating from the differential height of the mobile material in contact with the block) F_{EP}, the drag shear stress of the sea water F_D, and finally the shear forces, which have a viscous the viscous and a yield component, F_V and F_Y respectively. In the following paragraphs, we expand the discussion on the different terms of the forces. Since the mass of the block remains constant, we refer indifferently to forces or accelerations.

Gravity and Coulomb frictional forces together give a total acceleration

$$a_B + a_C = g \sin\beta \left(1 - \frac{\tan\phi}{\tan\beta}\right)\left[\frac{\rho_B - \rho_W}{\rho_B} + \frac{\rho_W - \rho}{\rho_B}\frac{\bar{D}}{H}\right] \qquad [3]$$

where β is the slope angle, g is gravity acceleration, ρ_B and ρ_W are the block and water densities respectively, and $\bar{D}$ is the height of the mobile material in contact with the block averaged over the block length. The reduced density of the block is due to Archimedean buoyancy, partly from water and partly from the debris flow.

When some fluid material impacts against the front face of an obstacle, it exerts a force of the order $\sim\rho u^2 S$ where u is the impact velocity, ρ is the density of the impacting liquid and S is the front surface area of the obstacle. In the present case, we have to consider that the velocity of the mobile material is not uniform as it increases from zero at the bottom to a maximum value at the top. In addition, the block itself is in general moving with a finite velocity V. In order to calculate the relative velocity between the block and the mobile material we consider first the velocity profile of a Bingham fluid at equilibrium. In other words, we neglect the inertial terms in the Navier-Stokes equation. Calling the co-ordinate perpendicular to the seabed y, the velocity profile for $y<D_S$, where D_S is the thickness of the shear layer, is parabolic (Huang and Garcia, 1998; 1999):

$$u(y) = U_P\left[1 - \left(1 - \frac{y}{D_S}\right)^2\right] \qquad [4]$$

If $y>D_S$, the velocity is independent of y and equal to U_P, the velocity of the plug layer. Due to the fact that the block has in general a finite velocity V, the loose fraction layers below a certain height $\bar{y}$ from the seabed will not contribute to the impact, as their velocity is smaller than the velocity of the block itself. Accounting for this effect, one finds

$$a_I = c\frac{\rho}{\rho_B}\frac{\Omega}{LH} \qquad [5]$$

where c is a geometrical constant (we assume $c = 1/2$) and

$$\Omega = \int_{\bar{y}}^{D} \left(u(y) - V\right)^2 dy =$$
$$= U_P^2 D_S \left\{ \frac{8}{15} - \frac{4}{3}\frac{V}{U_P} + \left(\frac{V}{U_P}\right)^2 - \right.$$
$$\left. - \omega\left[\left(\frac{V}{U_P}\right)^2 - 2\omega\frac{V}{U_P} + \right.\right.$$
$$\left.\left. + \omega^2\left(\frac{4}{3} + \frac{2}{3}\frac{V}{U_P}\right) - \right.\right.$$
$$\left.\left. - \omega^3 + \frac{1}{5}\omega^4 \right]\right\} + \qquad [6]$$
$$+ \left[Min(D_{FRONT}, H) - D_{S,FRONT}\right]\left(U_P - V\right)^2$$

represents the integrated square of the velocity of the loose fraction impacting on the block front.

In equation (6), D_{FRONT} is the thickness of the mobile material at the block front and $D_{S,FRONT}$ is the thickness of the shear layer, while the function Min (a, b) returns the smaller of its arguments a and b. The parameter ω is

$$\omega = 1 - \sqrt{1 - \frac{V}{U_P}} \qquad [7]$$

while

$$\bar{y} = \omega D_s \qquad [8]$$

An additional contribution to the force, called the static Earth-pressure, is due to the weight of the material partially resting on the faces, front and rear sides, of the block. Such a force is identical to the force exerted on the faces of a bottle by a liquid in its interior. This force is independent of the velocity. The acceleration due to static Earth-pressure force is given by

$$a_{EP} = \frac{1}{2}\frac{\rho - \rho_W}{\rho_B} g \cos\beta \frac{D_{TAIL}^2 - D_{FRONT}^2}{LH} \qquad [9]$$

where D_{TAIL} is the depth of the mobile material at the tail of the block (Fig. 6.5).

For the lateral faces, it is the shear stress that enters into the calculations. As the shear stress for a Bingham fluid is the sum of a yield strength and a space derivative of the shear velocity, there are two terms contributing to the shear forces, the viscous and the yield components, which result in two contributions to the total acceleration of the block. This division is not physical but an artifact deriving from the assumption, implicit in the Bingham rheology, that there is no relative motion below the yield strength. Concerning the viscous part, it is necessary to integrate the shear stress from boundary layer theory both along the block and along the vertical direction. The equation for this acceleration takes the form

$$a_V = \frac{\rho}{\rho_B}\frac{f'(0)\nu^{1/2}}{HWL}\int_0^L \frac{dx}{\sqrt{x}}\int_{\bar{y}}^{D(x)} [u(y) - V]^{3/2}\, dy \qquad [10]$$

where x is the distance parallel to the bed, ν is the kinematic viscosity of the material, and $f'(0) \approx 0.3$ is the derivative of the Blasius function in drag theory (Batchelor, 1967; Guyon et al., 2001). The integral over the vertical co-ordinate can be handled to give the expression

$$a_V = \frac{3}{8}\pi\frac{\rho}{\rho_B}\frac{f'(0)\nu^{1/2}}{HWL}\int_0^L \frac{D_S(x)}{\sqrt{x}}\frac{[U_P - V]^2}{U_P^{1/2}(x)}\, dx \qquad [11]$$

and thus only the integration over x must be carried out numerically.

The shear stress due to the finite value of the yield strength is approximated as

$$a_Y = \frac{2\tau_y}{\rho_B WL}\int_0^L dx \frac{D(x) - \bar{y}}{H} \qquad [12]$$

Finally, the term representing the drag force exerted by water on the surface of the block volume not submerged into the mobile material must be accounted for. One can distinguish between a front drag due to water on the block face perpendicular to the velocity and the shear drag exerted on the lateral faces of the block parallel to the flow, of which only the upper face, due to its large area, contributes significantly. A direct calculation gives

$$a_D = \frac{1}{2}\frac{\rho}{\rho_B}\frac{V^2}{H}\left(c_1\frac{H - D_{right}}{L} + c_2\right) \qquad [13]$$

where c_1 and c_2 are coefficients representing the front and surface drag, respectively. The values of these numerical coefficients depend on the exact shape of the block and on the Reynolds number.

Water acceleration exerted by the block results in an increase of the effective mass of the block, or equivalently, a reduced acceleration for a given force. This effect is accounted for by multiplying the block mass with an added mass coefficient (see for example Newman, 1977 for a general discussion). In the present model, the acceleration is reduced by a factor

$$\gamma = 1 + \alpha\frac{\rho_W}{\rho}\frac{\sqrt{HW}}{L} \qquad [14]$$

where α is a constant of the order π. Evidently, the effect becomes important only for bodies whose section perpendicular to flow is large compared to their length along the flow, and is thus of minor importance for blunt block shapes such as the one considered here.

A typical model calculation starts with the block at rest. The motion of the mobile material is calculated using the two-dimensional, depth-integrated BING model

(Imran et al., 2001), which is a numerical code for non-Newtonian debris flows. When the mobile material reaches the block, its motion is calculated via direct numerical integration of the equations of motion with the acceleration given by equation (2). The block is assumed not to affect the velocity field of the mobile material.

The model is certainly simplified with respect to reality, particularly concerning the flow rheology, the geometrical shape of the block and consequently of the debris flow-block interface, and the dynamical forces acting upon it. Notwithstanding, all the significant components are accounted for by such a model, and the simplifications introduced in the dynamical equations are likely to be less relevant than the uncertainty in the rheological properties of the material, a situation which to some extent occurs in all the reported case studies on subaqueous mass gravity flows.

The model does not include processes related to the interaction between blocks and loose material, such as the breakage of the blocks, block erosion and incorporation of eroded sediment into the loose material, entrapment of loose material underneath the block, or rearrangement of the velocity field of the loose material due to the presence of the block. It does not also take into account the fact that blocks could be already moving when impact of the loose material occurred. Some of these processes and how they may have an influence on the results of the model runs are discussed later.

6.3.3. Mobile Material Run-Out

Field data suggest a value for the run-out of the mobile material on the order of 110 km or more, and a displacement of about 15-20 km for the blocks (Lastras et al., 2002). Such a run-out is remarkable, considering the relatively small volume of material. Undoubtedly, the long run-out was partly favored by the narrowing of the Valencia Channel along the basin axis and the nearby presence of the opposed Balearic base of slope. The width over which the BIG'95 debris flow event expanded is not constant from the headwall down to the distal part. In the source, proximal and intermediate depositional areas the width of the deposit is more or less constant and equal to nearly 20 km, and decreases to about 10-12 km in the distal area and less over the Valencia Channel upper course, which runs in S-SW to N-NE from about 60 to 120 km from the source area. One might assume that the channeling due to the presence of the Valencia Channel led to larger run-outs relative to the ideal case of unconfined flowing. Following the idealized model adopted here of a debris flow as a Bingham fluid, we remark that if inertial forces are neglected, a Bingham fluid comes to rest when the shear stress in all the fluid body is less than the yield strength of the fluid. This concept leads to the well-known relation between the thickness of the deposit, the slope angle and the yield strength of Johnson (1970):

$$D = \frac{\tau_y}{(\rho - \rho_w) g \sin\beta} \qquad [15]$$

If the debris flow has a total volume V_0, then the total run-out R can be calculated implicitly as

$$V_0 = \frac{\tau_y}{(\rho - \rho_w) g} \int_0^R W(x) \frac{dx}{\sin\beta} \qquad [16]$$

where $W(x)$ is the width of the basin as a function of the co-ordinate x.

A strong simplification is possible if one assumes a constant slope angle. Additionally, we introduce a simplified basin model whose width is equal to W_1 for the first Λ kilometers, and W_2 for distances larger than Λ. We define the effective run-out R' as the run-out that the debris flow would have with a constant width W_1 of the basin. The relation with the observed runout R is

$$R' = R + (R - \Lambda) \frac{W_2}{W_1} \qquad [17]$$

One can arrive to the same expression by equating the volume of the deposit in the two-widths and in the single-width basins (the same deposit thickness has to be assumed, which is consequence of the constant slope angle).

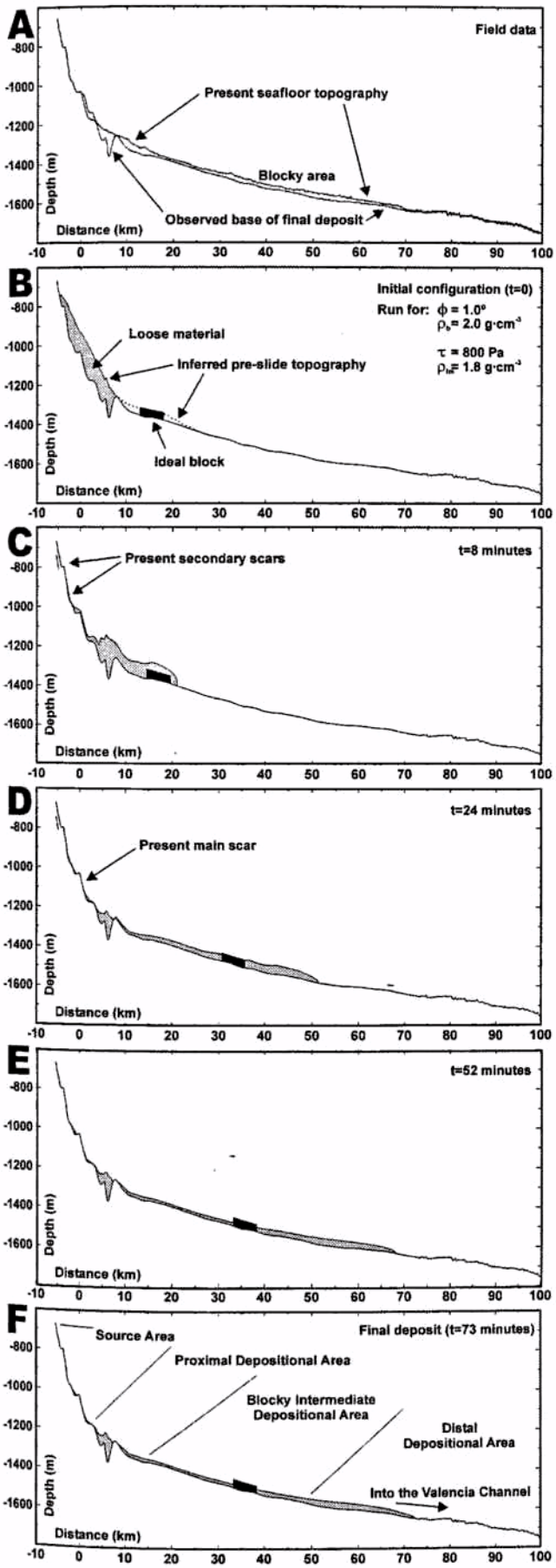

Figure 6.6. *Sequence of events from a calculation in which an internal friction angle of 1° for the block and a yield strength of 800 Pa for the mobile material have been applied. A: Bathymetric profile and base of the debris flow deposit as seen on swath bathymetry data and VHR seismic reflection profiles. B: Initial configuration for the run. C: Run after 8 minutes. D: Run after 24 minutes. E: Run after 52 minutes. F: Final deposit 73 minutes after the triggering of the debris flow.*

Adopting this simple view for the Valencia Trough, we estimate the following set of values: A=50 km, R=110 km, W_2=6 km, W_1=20 km, and R'=68 km. Therefore, due to the channeling effect in the distal area, the increase in the run-out of the debris flow can be estimated to be on the order 40 to 50 km. For this reason, our simulations should reproduce an effective run-out for the mobile material of the order of 60-70 km rather than the actual value of 110 km.

6.3.4. Numerical Results

Whereas the dimensions of the block have been deduced from swath bathymetry, the values of the physical constants (viscosity, yield strength and friction angle) are more uncertain. In the current case such constants were chosen so as to give results within the observational range both for the block and the mobile material, and will be discussed later. The sequence of configurations from a simulation is represented in Figure 6.6 for an internal friction angle (ϕ) of 1° for the block and a yield strength (τ_y) of 800 Pa for the mobile material, assuming densities of 1.8 and 2.0 g·cm^{-3} for the loose material and the block, respectively. Yield strength chosen is very close to the value of ~1 kPa, obtained from calculations based on field morphology (slope angle and thickness in the depositional zone), as proposed by Johnson (1984).

Figure 6.6B shows the configuration before failure. After 8 minutes (Fig. 6.6C) the loose material has already impacted and overtaken the block, displacing it for about 1 km. Configurations after 24 minutes (Fig. 6.6D), 52 minutes (Fig. 6.6E) and 73 minutes (the final one) (Fig. 6.6F) have also been plotted. The final run-out of the mobile material is about 62 km. The block has been moved forward by about 16 km. A comparison between the final deposit obtained from the simulation (Fig. 6.6F) and the real final deposit (Fig. 6.6F) shows the expected matches in the shape and thickness between both deposits for which the values above where chosen.

Figure 6.7 shows the various components of acceleration (or forces) of the block. The most important one in terms of maximum magnitude is found to be the impact force, even thought it is rather impulsive and decreases quickly with time as the front of the mobile material passes beyond the tail of the block. The other forces take over in conjunction with the rapid decrease of the impact force as the mobile material slows down. The static Earth-pressure force is found to be important, too, together with the gravity and the Coulomb friction. The remaining forces, water drag, viscous and yield, play a minor role and they have been multiplied by a factor 100 in order to illustrate their magnitude in Figure 6.7. Note that the block stops despite the fact that dynamical forces from the mobile material are still acting. At this point, forces are not large enough to move the block.

The velocities of the block and of the front of the mobile material, for an internal friction angle (ϕ) of 1° for the block and a yield strength (τ_y) of 800 Pa for the mobile material, are illustrated in Figure 5.8. Maximum velocities are much higher for the mobile material, yet the block reached a top velocity of about 20 m·s^{-1}.

6.3.5. Sensitivity Tests

In order to establish the critical parameters in the calculation, a sensitivity analysis was performed by running several simulations for a set of parameters. By direct sensitivity numerical tests we verified that viscosity plays a very minor role in the dynamics of the mobile material compared to the yield strength in the BIG'95 (Fig. 6.7), as previously found in other submarine debris flows (e.g., Elverhøi et al., 2002). The most important parameters in the sensitivity analysis are the internal friction angle (ϕ) of the block and the yield strength (τ_y) of the loose material. In principle, the run-out of the block will be sensitive to both parameters. However, given that our approach neglects any influence of the block on the mobile material, we imply that the run-out of the mobile material does not depend on the internal friction angle of the block.

Table 6.1 shows some results with different friction angles and yield strengths. As

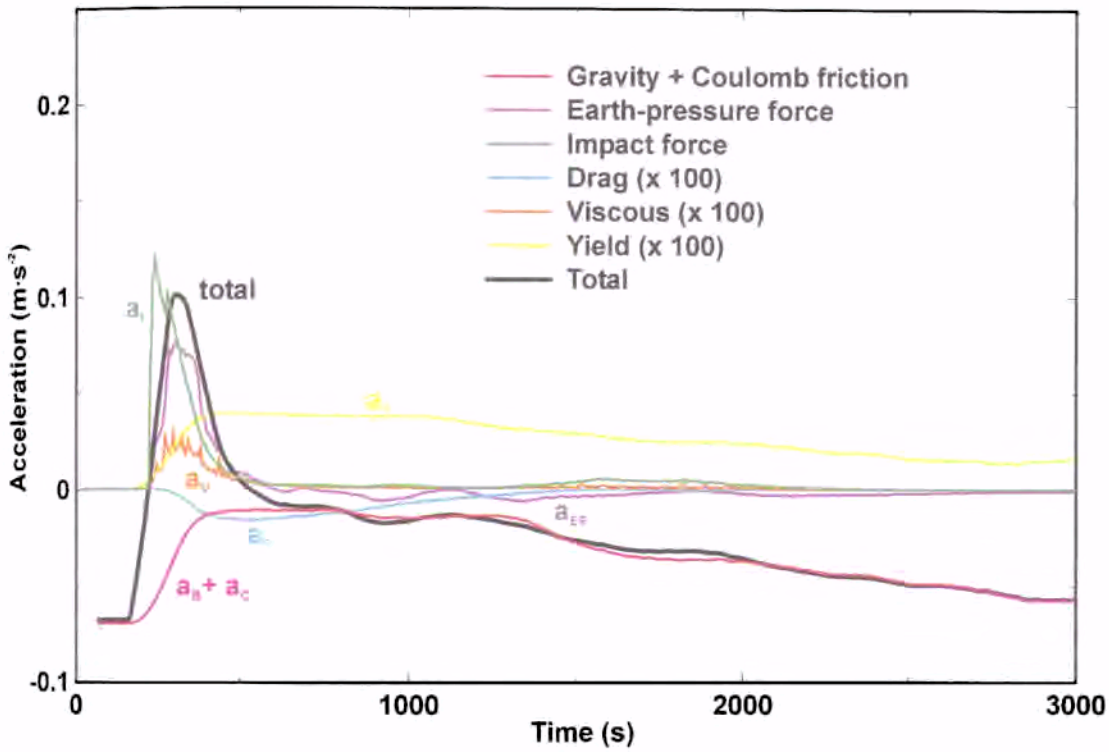

Figure 6.7. Contributions to the acceleration of the block by the different forces in equation (1) as a function of time after the triggering of the debris flow. The block is at rest until impacted by the mobile material. Note that the block stops moving after ~1,500 s (Fig. 6.6D). After this time, the plot shows the single forces divided by the mass, rather than the acceleration, since the latter is null.

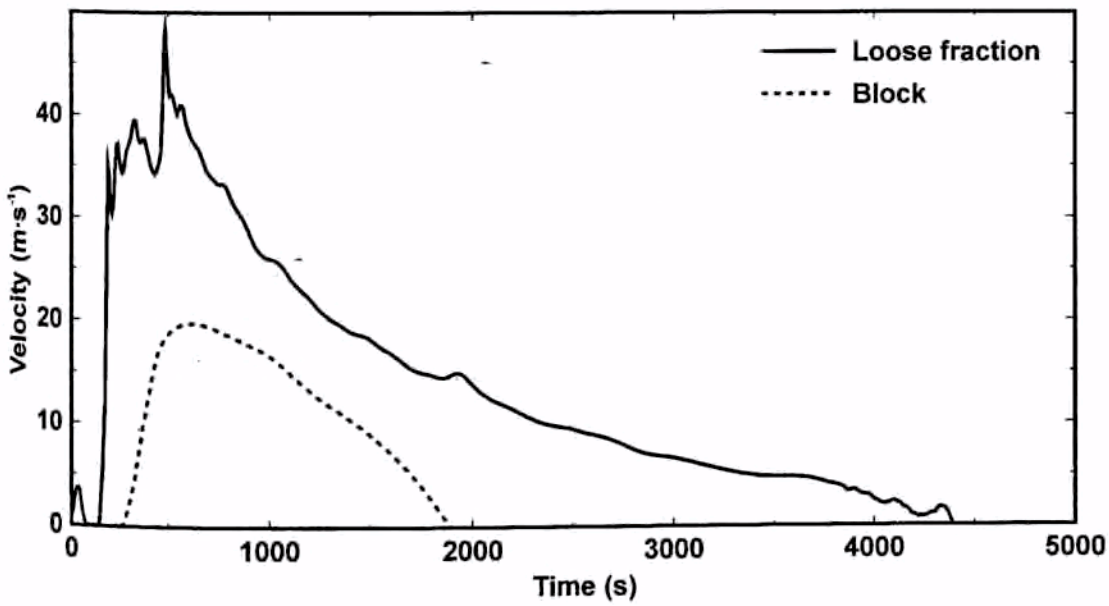

Figure 6.8. Velocities of the block and the front of the mobile material in seconds after the triggering of the debris flow.

τ_y (kPa)	ϕ (degrees)	Run-out Mobile material (km)	Block (km)
0.8	1	62.4	19.9
0.8	2	62.4	6.2
0.8	0.8	62.4	27.3
1	0.8	55.8	26.5
1	1	55.8	19.8
1	2	55.8	15.9
3	0.5	32.4	30.1
0.5	1	71.3	20.2
0.3	1	89.5	20.4

Table 6.1. *Results from some runs using different values of both the yield strength of the mobile material and the internal friction angle of the block.*

expected, the increase of the yield strength decreases the run-out of the mobile material. Concerning the block, the table shows that its run-out is very sensitive to the internal friction angle. A friction angle higher than 2° gives results incompatible with field data. The best correspondence with observations is obtained for an angle of about 1°. Note also that the run-out of the block depends little on the value of the yield strength. Only for much larger values of yield strength does the block run-out decrease. Considering the field data, we conclude that:

A. Values for the yield strength of the mobile material must have been between 500 and 800 Pa. If values were larger, the run-outs would have been too short; if smaller, very long run-outs would have resulted due to the Valencia Channel constriction.

B. Effective internal friction angles for the blocks must have been around 1°. For larger values the model block stands still or moves very little. Smaller values would be below the seabed inclination angle and this would result in perpetual block acceleration.

Evidently, the internal friction angle has a dramatic influence on the final result since even relatively small changes can produce great differences in model results. Unfortunately, the friction angle is basically unknown, being determined not only by the material properties, but also by the water pore pressure in the sediment.

6.4. DISCUSSION

To obtain simulation results that match the observational data (i.e., thickness distribution, mobile material run-out of 60-70 km and block run-out of 15-20 km), input values need to be ~1° for the internal friction angle and ~800 Pa for the yield strength. Remoulded yield strength data obtained from geotechnical analysis of the sediment cores (Fig. 6.3) differ from the yield strength used in simulation. These differences between measurements and models have also been encountered in other cases, like the Storegga debris flows off mid-Norway (De Blasio et al., 2003). Which parameters favoring movement have been left out of the model that, if added, would increase the minimum internal friction angle and yield strength needed to obtain run-outs matching the field data? Remarkably, parallel studies of submarine debris flows composed of fine material show a tendency to a very low shear strength (De Blasio et al., 2003) while other gravity mass flows composed by larger clasts seem to have higher shear strength (Locat et al., 2004).

Lower strength in the debris flow is attributed to wetting (i.e. dilution) of the clay material. As the debris flow moves, it incorporates sea water and thus reduces the strength of the material. Unfortunately, the quantitative knowledge of such effects is very poor. Measurements of wetted soils are performed by geotechnical standard techniques based on stirring and remolding of the material with a controlled fraction of

water introduced to gain the desired liquidity index. However, no data are available for the general case of an actual debris flow. In the following, a simple model (De Blasio et al., 2003) is introduced in which the yield strength is allowed to vary according to

$$\tau_y(t) = \tau_y(\infty) + \left[\tau_y(0) - \tau_y(\infty)\right] e^{-\Gamma\gamma(t)} \quad [18]$$

where

$$\gamma(t) = \int_0^t dt' \left(\frac{\partial U}{\partial u}\right)_{y=0} = 2\int_0^t dt' \frac{U_p}{D_s} \quad [19]$$

is the total accumulated shear at the base of the debris flow and Γ is a constant quantifying the wetting efficiency.

Table 6.2 contains some data from our simulations. In general, the findings are rather similar to the case with fixed yield strength, provided that the transformation from a strong to a weak soil proceeds relatively fast (i.e., Γ should be sufficiently large). Figure 6.9 shows the behavior of the yield strength, calculated for the front of the debris flow, as a function of the distance traveled by the debris flow itself. In our simulations, if a decrease in the yield strength occurs before the debris flow reaches the intermediate depositional area, the prediction of this modified model is very close to the basic model with constant yield strength equal to the lower limit $\tau_y(\infty)$. This would imply that the value of Γ must have been large enough for the mobile material to decrease down to values of about 500 to 800 Pa in the intermediate area. In fact, slope angles are so small in this area that a flow with higher yield strength would rapidly come to rest.

Another possibility for the long run-out of the mobile material is hydroplaning (Mohrig et al., 1998; Elverhøi et al., 2002), a process in which a thin water layer underneath the debris flow provides substantial lubrication and run-out enhancement. The computer program was implemented to evaluate hydroplaning according to the model described in De Blasio et al. (2004). In the model, for a yield strength of 3 kPa, run-out of the mobile material with hydroplaning increases to 47 km. On the other hand, the equations of hydroplaning flow are much more complex and calculations are affected by more uncertainties (De Blasio et al., 2004). The possibility of hydroplaning cannot be discarded solely on sedimentological grounds since according to laboratory measurements the clay content seems to be sufficiently high for hydroplaning to take place (Elverhøi et al., 2002). It is possible that both hydroplaning and wetting might have promoted the long run-out observed in BIG'95.

Other parameters left out of the model that may affect the final result are the entrapment of loose material underneath the blocks and the rearrangement of the velocity field of the mobile material due to the presence of the moving blocks. Once the loose material has bypassed the blocks, it could be incorporated at their bases, probably acting as a lubricant and reducing drastically the internal friction angle. Entrapment of water in the very first moments of block mobilization would also favor acceleration of the block.

$\tau_y(0)$ (kPa)	$\tau_y(\infty)$ (kPa)	Γ	Run-out	
			Mobile material (km)	Block (km)
3	0.8	0.00004	43.9	18.7
3	0.8	0.00001	34.5	15.5
3	0.5	0.00001	34.9	15.6
3	0.5	0.00008	67.9	19.4
2	0.5	0.00004	62.5	19.7
4	0.5	0.00008	65.0	19.0

Table 6.2. Data from simulations including a decrease of the yield strength as a function of the accumulated shear at the base of the debris flow. Other data as in the run in Figure 6.6.

Moreover, for simplicity it has been assumed that the blocks are at rest when impacted by the mobile material for simplification, although the actual moment of initial block mobilization remains unclear and could have coincided with the triggering of the debris flow. This would result in a larger distance traveled by the block for an assumed value of internal friction angle. The collective flow of several blocks and the breakage of large blocks into smaller ones (Lastras et al. 2002) could have resulted in an important rearrangement of the velocity field of the mobile material, which would have favored downslope flowing. Further modeling may be required to quantitatively assess the effects of block breakage and incorporation of the mobile material to the base of the blocks.

Finally, it has been assumed that the blocks are denser than the mobile material. If the opposite is true, blocks will float in the stream of the mobile material whenever the thickness of the latter is larger than $(\rho_B/\rho)\cdot H$. The friction with the sea bottom, which is the most important force opposing the motion, becomes overwhelmed by the static earth-pressure, gravity and impact forces, and the block would rapidly acquire a speed comparable to the one of the mobile material. Even neglecting gravity and static earth pressure, the acceleration of a rafted block subject to the continuous impact of the mobile material flowing at constant velocity U_0 is given by the differential equation

$$\frac{dV(t)}{dt} = \frac{\rho}{2L\rho_B}\left(V(t) - U_0\right)^2 \qquad [20]$$

where t is the time (t=0 corresponds to the instant of impact). The solution has the form

$$V(t) = \frac{\rho U_0^2}{2L\rho_B}\left[1 + \frac{\rho U_0 t}{2L\rho_B}\right]^{-1} t \qquad [21]$$

This equation shows that within a time of the order $\approx \frac{18L\rho_B}{\rho U_0}$ the block would be accelerated to 90 % of the velocity of the mobile material. With appropriate values for the parameters one finds a time length of some minutes, which is comparable to the time interval when the block is completely submerged by the debris flow.

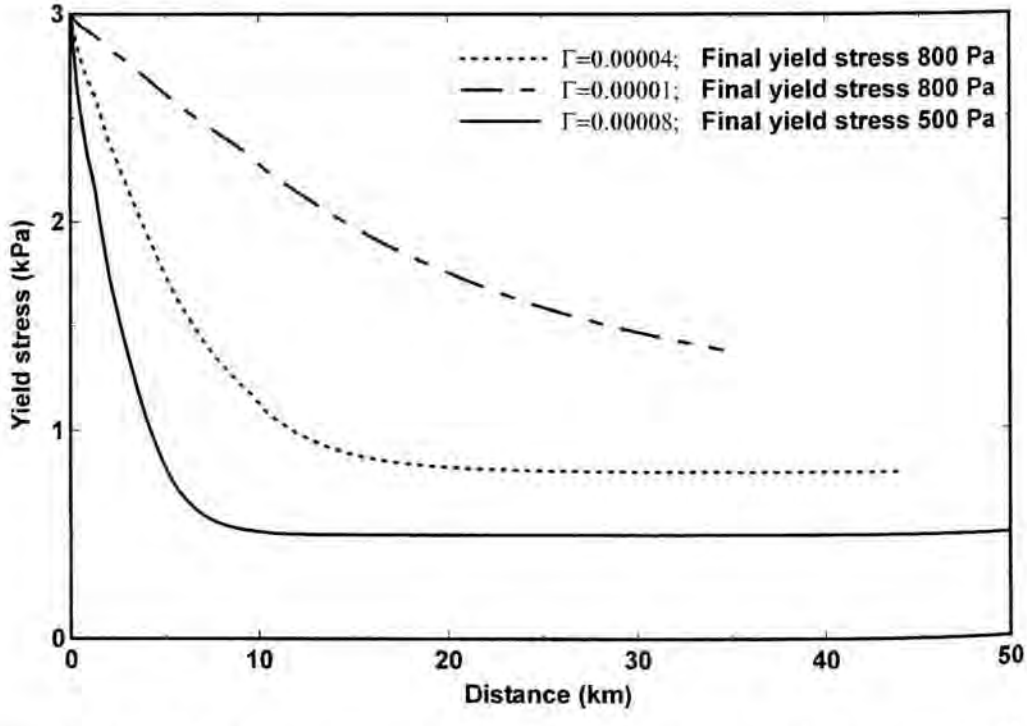

Figure 6.9. Strength loss due to wetting of the clay material as a function of the distance traveled by the debris flow for different Γ.

In conclusion, a light block detached from the bottom would be easily rafted by the dynamic forces. However, the condition that the mobile material is denser than the block probably never occurs in practice, mainly because the process of dilution of the debris flow in water causes a substantial decrease in density. These considerations, however, show that the results are very sensitive to the density difference between the blocks and the mobile material.

6.5. CONCLUSIONS

The dynamics of the BIG'95 debris flow event in the Ebro continental slope and base-of-slope has been modeled both conceptually and numerically. The conceptual model explains how a highly mobile sediment mass released from the middle slope flowed downslope pushing, shearing and accelerating slabs of cohesive sediment during more than 15 km, until the forces acting on them where not large enough and the blocks stopped. The mobile fraction went on flowing and stopped partly filling the upper course of the Valencia Channel, after ~110 km of run-out.

A numerical model incorporating the different forces acting on the blocks, including those exerted by the loose material, which in turn is modeled as a Bingham fluid with specific rheological properties, shows that the conceptual model proposed is physically plausible only if very low values of both the yield strength of the mobile material and the internal friction angle of an ideal block are used. Processes which have not been incorporated in the model but very likely to have occurred, such as the entrapment of mobile material underneath the block that would act as a lubricant to reduce the friction with the seafloor, as well as the fact that blocks could have been already at movement since the initial triggering, could at least partially account for such low values. Top velocities during mobilization are as high as 50 $m \cdot s^{-1}$ for the mobile material and 24 $m \cdot s^{-1}$ for the blocks. Sensitivity tests show that viscosity plays a very minor role compared to the yield strength in the dynamics of the mobile material.

Finally, even though the coupled conceptual and numerical modeling developed here was primarily aimed at the BIG'95 debris flow sedimentary dynamics, it could contribute to a better understanding of subaqueous mass gravity flows in general. Additionally, it may provide a relatively quick albeit simplified numerical framework in the analysis of the interaction forces between flowing material and an obstacle, a situation encountered in problems of debris flow mitigation.

6.6. APPENDIX

List of Symbols Used

H: block height
L: block length
W: block width
V: block velocity
ρ_B: block density
ρ_W: water density
ρ: density of the mobile material
β: slope angle
Φ: block friction angle with the sea bed
D: thickness of the mobile material
D_S: thickness of the shear layer in the mobile material
$\overline{D}$: average thickness of the mobile material on the lateral sides of the block.
U_P: plug velocity of the mobile material
g: gravity acceleration
D_{TAIL}: depth of the mobile material at the tail of the block
D_{FRONT}: depth of the mobile material at the front of the block
$D_{S,FRONT}$: thickness of the shear layer in the mobile material at the front of the block
ν: kinematic viscosity of the mobile material
τ_y: yield strength of the mobile material
x: co-ordinate parallel to the sea bed
y: co-ordinate perpendicular to the sea bed
$u(y)$: component x of the velocity of the mobile material as a function of the height y

6.7. ACKNOWLEDGEMENTS

This study was supported by the EC-VFP projects COSTA (Continental Slope Stability, EVK3-1999-00028) and EUROSTRATAFORM (European Margins

Strata Formation, EVK3-2002-00079), CYTMAR project GRANDES (MAR98-0347), a Generalitat de Catalunya Grups de Recerca Consolidats grant (2001 SGR-00076) and a Spanish Ministerio de Educación, Cultura y Deportes FPU fellowship to G. Lastras. The authors would like to thank everybody involved in the sedimentological and geotechnical study of the sediment cores, in the oceanographic surveys, and R. Urgeles for such interesting discussions on the conceptual model of the debris flow. H. Lee and J. Locat, associate editor P. Myrow and editor M. J. Kraus provided thoughtful and in-depth reviews that greatly improved this paper. The original version of the numerical code BING, which was modified in the present work, has been kindly provided by G. Parker. Support from the International Centre for Geohazards (ICG) in Oslo is gratefully acknowledged by F.V. De Blasio and A. Elverhøi. This is the ICG paper n. 30.

6.8. REFERENCES

Aparicio, A., Mitjavila, J.M., Araña, V., Villa, I.M., 1991, La edad del volcanismo de las islas Columbrete Grande y Alborán (Mediterráneo occidental): Boletín Geológico y Minero, v. 102-104, p. 565-570.

Batchelor, G. K., 1967, An Introduction to Fluid Dynamics: Cambridge University Press, Cambridge, UK, 615 p.

Boe, R., Hovland, M., Instanes, A., Rise, L., Vasshus, S., 2000, Submarine slide scars and mass movements in Karmsundet and Skudenesfjorden, southwestern Norway: morphology and evolution: Marine Geology, v. 167, p. 147-165.

Canals, M., Serra, J., Riba, O., 1982, Toponímia de la Mar Catalano-Balear, amb un glossari de termes genèrics. Bolletí d'Història Natural de les Balears, v. 26, p. 169-194.

Canals, M., Casamor, J.L., Urgeles, R., Lastras, G., Calafat, A.M., Masson, D., Berné, S., Alonso, B., De Batist, M., 2000, The Ebro continental margin, Western Mediterranean Sea: Interplay between canyon-channel systems and mass wasting processes; in Nelson, C.H., Weimer, P., eds., Deep-Water Reservoirs of the World: GCS SEPM Foundation 20th Annual Conference, Houston Texas (USA), p. 152-174 (CD Edition).

Canals, M., Lastras, G., Urgeles, R., Casamor, J.L., Mienert, J., Cattaneo, A., De Batist, M., Haflidason, H., Imbo, Y., Laberg, J.S., Locat, J., Long, D., Longva, O., Masson, D.G., Sultan, N., Trincardi, F., Bryn, P., in press, Slope failure dynamics and impacts from seafloor and shaloow sub-seafloor geophysical data: An overview: Marine Geology.

Coussot, P. C., 1997, Mudflow Rheology and Dynamics: IAHR-AIRH monographs, AA Balkema Publishers, Rotterdam, The Netherlands, 272 p.

De Blasio, F.V., Issler, D.D., Elverhøi, A., Harbitz, C.B., Ilstad, T., Bryn, P., Lien, R., Løvholt, F., 2003, Dynamics, velocity and run-out of the giant Storegga Slide; in Locat, J., Mienert, J., eds., Submarine Mass Movements and Their Consequences: Kluwer Academic Publishers, The Netherlands, p. 223-230.

De Blasio, F.V., Engvik, L., Harbitz, C.B., Elverhøi, A., 2004, Hydroplaning and submarine debris flows: Journal of Geophysical Research, v. 109, C01002, doi:10.1029/2002JC001714.

Droz, L., Kergoat, R., Cochonat, P., Berné, S., 2001, Recent sedimentary events in the western Gulf of Lions (western Mediterranean): Marine Geology, v. 176, p. 23-37.

Elverhøi, A., de Blasio, F.V., Butt, F.A., Issler, D.D., Harbitz, C.B., Engvik, L., Solheim, A., Marr, J., 2002, Submarine mass-wasting on glacially influenced continental slopes - processes and dynamics; in Dowdeswell, J.A., O'Cofaigh, C., eds., Glacier-influenced Sedimentation on High-latitude Continental Margins: Geological Society of London Special Publication, v. 203, p. 72-88.

Evans, D., King, E.L., Kenyon, N.H., Brett, C., Wallis, D., 1996, Evidence for long-term instability in the Storegga Slide region off western Norway: Marine Geology, v. 130, p. 281-292.

Farran, M., Maldonado, A., 1990, The Ebro continental shelf: Quaternary seismic stratigraphy and growth patterns; in Nelson, C.H., Maldonado, A., eds., The Ebro Continental Margin, Northwestern Mediterranean Sea: Marine Geology, v. 95, p. 289-312.

Guyon, E., Hulin J. P., Petit L., Mitescu C. D., 2001, Physical Hydrodynamics: Oxford University Press, USA, 528 p.

Huang, X., Garcia, M.H., 1998, A Herschel-Bulkley model for mud flow down a slope: Journal of Fluid Mechanics, v. 334, p. 305-333.

Huang, X., Garcia, M.H., 1999, Modeling of non-hydroplaning mud flows on continental slopes: Marine Geology, v. 154, p. 132-142.

Imran, J., Harff, P., Parker, G., 2001, A numerical model of submarine debris flow with graphical user interface: Computers and Geosciences, v. 27, p. 717-729.

Johnson, A.M., 1970, Physical Processes in Geology: Freeman, San Francisco, 577 p.

Johnson, A.M., 1984, Debris flows; in Brunsden, D., Prior, D.B., eds., Slope Instability, Wiley, p. 257-361.

Laberg, J.S., Vorren, T.O., 2000, The Trænadjupet Slide, offshore Norway – morphology, evacuation and triggering mechanisms: Marine Geology, v. 171, p. 95-114.

Lastras, G., Canals, M., Hughes Clarke, J.E., Moreno, A., De Batist, M., Masson, D.G., Cochonat, P., 2002, Seafloor imagery from the BIG'95 debris flow, western Mediterranean: Geology, v. 30, p. 871-874.

Lastras, G., Canals, M., Urgeles, R., 2003, Lessons from sea-floor and sub-seafloor imagery of the BIG'95 debris flow scar and deposit; in Locat, J., Mienert, J., eds., Submarine Mass Movements and Their Consequences: Kluwer Academic Publishers, The Netherlands, p. 425-431.

Lastras, G., Canals, M., Urgeles, R., De Batist, M., Calafat, A.M., Casamor, J.L., in press, Characterisation of a recent debris flow deposit after a variety of seismic reflection data, Ebro margin, Western Mediterranean: Marine Geology.

Locat, J., Lee, H. J., Locat, P., Imran, J., 2004, Numerical analysis of the mobility of the Palos Verdes debris avalanche, California, and its implication for the generation of tsunamis: Marine Geology, v. 203, p. 269-280.

Maillard, A., Mauffret, A., 1993, Structure et volcanisme de la fosse de Valence (Méditerranée nord-occidentale): Bulletin Société Geólogique France, v. 164, p. 365-383.

Marr, J.G., Elverhøi, A., Harbitz, C., Miran, J., Harff, P., 2002, Numerical simulation of mud-rich subaqueous debris flows on the glacially active margins of the Svalbard-Barents Sea: Marine Geology, v. 188, p. 351-364.

Mohrig, D., Whipple, K.X., Hondzo, N.H., Ellis, C., Parker, G., 1998, Hydroplaning of subaqueous debris flows: Geological Society of America Bulletin, v. 110, p. 387-394.

Mohrig, D., Elverhøi, A., Parker, G., 1999, Experiments on the relative mobility of muddy subaqueous and subaerial debris flows, and their capacity to remobilise antecedent deposits: Marine Geology, v. 154, p. 117-129.

Nelson, C.H., Maldonado, A., 1988, Factors controlling depositional patterns of Ebro Turbidite Systems, Mediterranean Sea: American Association of Petroleum Geologists Bulletin, v. 72, p. 698-716.

Newman, J.N., 1977, Marine Hydrodynamics: MIT press, Cambridge, Massachusetts, USA, 402 p.

Rothwell, R.G., Thomson, J., Kähler, G., 1998, Low sea-level emplacement of a very large Late Pleistocene "megaturbidite" in the Western Mediterranean: Nature, v. 392, p. 377-380.

Smith, W.H.F., Sandwell, D.T., 1997, Global seafloor topography from satellite altimetry and ship depth soundings: Science, v. 277, p. 1957-1962.

Takahashi, T., 1991, Debris Flows: AA Balkema Publishers, Rotterdam, The Netherlands, 165 p.

Urgeles, R., Lastras, G., Canals, M., Willmott, V., Moreno, A., Casas, D., Baraza, J., Berné, S., 2003, The BIG'95 debris flow in the NW Mediterranean Sea and adjacent unfailed sediments: geotechnical-sedimentological properties, and age dating; in Locat, J., Mienert, J., eds., Submarine Mass Movements and Their Consequences: Kluwer Academic Publishers, Dordrecht, The Netherlands, p. 479-487.

CAPÍTOL 7

SLIDES OF THE EIVISSA CHANNEL

Lastras, G., Canals, M., Urgeles, R., Hughes-Clarke, J.E., Acosta, J., 2004, Shallow slides and pockmark swarms in the Eivissa Channel, Western Mediterranean Sea, Sedimentology (accepted).

Shallow slides and pockmark swarms in the Eivissa Channel Western Mediterranean Sea[69]

G. Lastras, M. Canals[70], R. Urgeles
GRC Geociències Marines, Universitat de Barcelona, Spain

J.E. Hughes-Clarke
Ocean Mapping Group, University of New Brunswick, Canada

J. Acosta
Instituto Español de Oceanografía, Madrid, Spain

ABSTRACT

Four slides, the Ana, Joan, Nuna and Jersi slides, have been imaged on the seafloor along the Balearic margin of the Eivissa Channel, in the Western Mediterranean. They have areas of up to 16 km^2 and occur in water depths ranging between 600 and 900 m. Volumes range from 0.14 to 0.4 km^3. Their headwall scarps, internal architecture and associated deposits are characterised using a combination of swath bathymetry data and very-high resolution seismic reflection profiles. In general, they show horseshoe-shaped headwall scarps and distinct depositional lobes with positive relief. Internally, the slide bodies are mostly comprised of transparent seismic facies. Chaotic facies are observed at the toe of some of the slides, and blocks of coherent stratified facies embedded in the slide deposit have also been identified.

The reflection profiles demonstrate that the four slides share the same slip horizon that corresponds to a distinctive continuous, high amplitude reflector. Furthermore, the geometry of the headwall scars of the Nuna and Ana slides reveal evidence of pockmarks, and fluid escape features are also present further upslope. This indicates a possible link between fluid escape features and destabilisation of the upper sediment layers. In addition, these well-characterised slides demonstrate the pitfalls associated with calculating the volume of the slide masses using headwall scarp heights and the assumed pre-slide seafloor topography in the absence of seismic data. The internal structure also demonstrates that transport distances within the slides are generally low and poorly characterised by headwall scarp to slide toe lengths.

Keywords: Slides, pockmarks, swath bathymetry, Eivissa Channel, Western Mediterranean Sea.

Published in Sedimentology, in press.
ISSN: 0037-0746.
Manuscript received May 13, 2003.
Manuscript accepted August 28, 2003.
[70] Corresponding author: miquel@natura.geo.ub.es

7.1. INTRODUCTION

The advent of swath bathymetry techniques for seafloor mapping and their widespread application has given new insight into how the seafloor is shaped. However, seafloor features whose morphologic expression is close to the resolution limits of swath bathymetry and acoustic imaging techniques can be easily overlooked. Fine-scale swath mapping, even at great water depths, is becoming increasingly important for both academia and industry as illustrated by imaging of the giant Storegga Slide, offshore Norway. Recent work has used a high-resolution multibeam system mounted on an autonomous underwater vehicle to map the seabed above the Ormen Lange gas field area close to the Storegga Slide headwall scarp (Offshore Technology, 2003). The precision of the results strongly contrast with earlier mapping of the same area (Bugge, 1983). However, underwater vehicles are scarce and expensive, and beyond the scope of most swath mapping projects. In addition, they are slow, which means that a lot of time is required to map relatively large areas in the deep sea. Despite its limitations, fine-scale, beam-by-beam processing of swath bathymetry data from surface vessels offers results unachievable by conventional processing techniques. Another reasonably cheap alternative is to use surface picks from existing 3D high-resolution seismic reflection data (Bulat, 2003), or high-resolution 2D seismic data combined with swath bathymetry when these are available.

One of the areas in which swath bathymetry and high-resolution seismic data have demonstrated their potential during the last decade is the study of mass-wasting events in the deep-sea. Mass wasting represents a major geo-hazard both for offshore infrastructures (Campbell, 1999) and for nearby coastal areas (Synloakis et al., 1997). An extensive literature regarding submarine landslides on European and other margins is now available (see compilations in Mienert & Weaver, 2003; Locat & Mienert, 2003). A wide range of slide scars and deposits associated with gravitational mass movements have been identified in the western Mediterranean. These include small landslides on the flanks of some of the Balearic Islands (Acosta et al., 2002), the 2,000 km^2 BIG'95 debris flow on the Ebro slope and base-of-slope (Lastras et al., 2002), and the 60,000 km^2 Balearic Abyssal Plain megaturbidite described by Rothwell et al. (1998).

In this paper, the character of four small slides in the Eivissa Channel area, between the Iberian Peninsula and the Balearic Islands, is documented (Fig. 7.1; IEO-IHM, 1999; Acosta et al., 2001b). This study uses a combination of high resolution swath bathymetry and very-high resolution seismic data to investigate the geometry and internal structure of the slides, and to examine the relationship between sliding and gas escape features. The results also have implications for the characterisation of less well imaged submarine slides elsewhere.

7.2. DATA SET

The data presented in this paper were collected during two surveys onboard the *R/V Hespérides* in 1995 ('BIG'95' survey) and 2002 ('MARINADA' survey), when swath bathymetry data and very-high resolution (VHR) seismic reflection profiles were acquired simultaneously. The EM-12S swath bathymetry (13 kHz, 81 beams) data obtained in 1995, using Simrad's *Merlin/Mermaid* acquisition software, were processed using the *SwathEd* tools. The results from this processing guided the precise location of very-high resolution seismic reflection profiles collected during the 2002 cruise. A total of 2,287 km^2 of bathymetric data were obtained during the two surveys. The seismic reflection system employed was a hull-mounted Simrad topographic parametric source TOPAS PS 018 yielding a secondary frequency of 3.5 kHz, that allowed 642 km of good (1995) to high (Fig. 7.2b, 2002) quality profiling. Seismic facies have been described following a simplified Damuth (1980) classification. Positioning of the vessel was ensured by a GPS ASHTECH 3DF system.

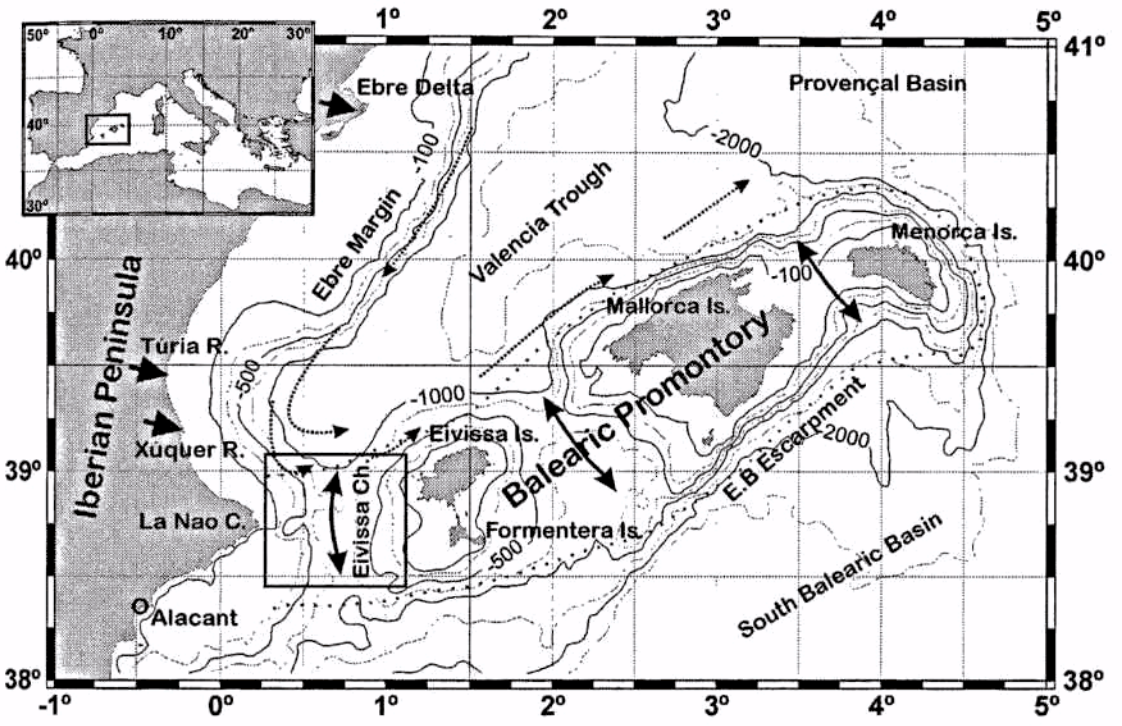

Figure 7.1. Bathymetric map of the Balearic Promontory and the surrounding area of the Western Mediterranean Sea. Bathymetry data extracted from the Smith & Sandwell (1997) database. Contours are at 100, 200, 500, 750, 1000, 1500, 2000 and 2500 m. Box shows location of the study area (Fig. 7.2). The bold arrows mark the areas where interchange of waters between the València Trough and the South Balearic Basin may occur. The dotted arrows show general direction of currents in the València Trough. The short arrows on the coast mark the location of discharge of the Ebre, Túria and Xúquer (Ebro, Turia and Júcar) rivers. Note that the Eivissa Channel is the deepest channel connecting the València Trough and the South Balearic Basin.

7.3. STRUCTURAL SETTING

The Eivissa Channel is situated between La Nao Cape north of the coastal city of Alacant (Alicante), on the Iberian Peninsula, to the west, and the islands of Eivissa (Ibiza) and Formentera, to the east (Fig. 7.1). It lies at the western end of the 348 km-long and 120 km-wide Balearic Promontory, which includes the Menorca, Mallorca and Eivissa structural blocks, the depressions between them, and the Eivissa Channel. The Promontory constitutes the northeastward prolongation of the external zone of the Betic Ranges from the Iberian Peninsula.

Westward migration of the Alboran microplate to the south along the Emile-Baudot (Fig. 7.1) and Mazarrón (southeast of the Iberian Peninsula) escarpments (Fontboté et al., 1990; Vegas, 1992; Sàbat et al., 1995; Acosta et al., 2001a) or subduction roll-back of the Alboran arc during the Tertiary (Gueguen et al., 1998), produced a clockwise rotation of the Mallorca and Eivissa blocks. The maximum height of the Balearic Promontory is ca. 3,000 m above the surrounding seafloor. Neogene volcanic centres are common both on the Balearic Promontory (Acosta et al., 2001a) and in nearby areas (e.g. Maillard & Mauffret, 1993).

7.4. PHYSIOGRAPHY

Three physiographic elements are distinguished in the Eivissa Channel: (1) the 100 to 130 m deep continental shelves off Alacant and SW Eivissa – Formentera, (2) the continental slopes down to 800 m deep, and (3) a generally smooth median depression that only locally exceeds 900 m water depth. Overall, the saddle morphology of the north-south trending

Eivissa Channel is slightly asymmetric, with the Iberian Margin to the west steeper than the Balearic Margin to the east (Fig. 7.2).

The smoothness of the median depression is interrupted by a prominent ca. 200 m high east-west trending seamount (Fig. 7.2), here named the "Xàbia Seamount" after a nearby coastal town. According to Palomo et al. (1976), this seamount consists of a tilted horst of Cainozoic and possibly older strata. However, unpublished magnetic data suggest a volcanic origin. This latter interpretation is consistent with the presence of other volcanic seamounts in the area around the Eivissa Channel (Maillard & Mauffret, 1993).

The Xàbia Seamount divides the deep Eivissa Channel into two sectors, the southern sector double the area of the northern one. The northern Eivissa Channel opens to the north to the València Trough, while the southern sector is connected to the South Balearic Basin across the tectonic escarpments bounding the Balearic Promontory to the south. The maximum water depths in the Eivissa Channel reach 826 m and 925 m in the northern and southern sectors respectively, the latter in an elongated east-west oriented depression at the foot of the Xàbia Seamount (Fig. 7.2).

7.5. SEDIMENTATION AND CIRCULATION

Most of the sediment reaching the Eivissa Channel is thought to come from the Iberian Peninsula. Since the regional circulation along the Iberian Margin north of the Eivissa Channel is oriented southward, the channel should receive an influx of fines from rivers to the north such as the Ebre, Túria and Xúquer (Ebro, Turia and Júcar). The Ebre is the largest river in the Mediterranean watershed of the Iberian Peninsula, and the Túria and Xúquer are also amongst the most important rivers in terms of water and sediment discharge to the València Trough, especially during the intense flood events typical of the Mediterranean climate (Barriendos-Vallvé & Martín-Vide, 1998). Small mountain rivers whose mouths are located closer to the Eivissa Channel such as the Serpis and Gorgos can also occasionally carry large amounts of sediment during flood events. Despite the likely riverine influence on the Iberian Margin of the Eivissa Channel, patches of benthic carbonate-dominated sedimentation exist on the Balearic continental shelf west of the channel axis according to studies in nearby areas by Canals & Ballesteros (1996) and Cebrián et al. (2000).

Since rainfall is low and the terrain is karstic, no permanent rivers exist on the Balearic Islands. This favours very transparent, oligotrophic waters where sunlight can penetrate to greater depths thus enhancing the development of carbonate-producing benthic communities on the continental shelf (Canals & Ballesteros, 1996).

The two sectors in the deep median depression of the Eivissa Channel display contrasting seafloor textures, as seen on swath bathymetry imagery (Fig. 7.2a), but both sectors are dominated by stratified seismic facies. A rough northern sector, with the seafloor often disrupted by fluid escape features that give it an orange peel texture (Acosta et al., 2001b), contrasts markedly with the essentially smooth-bottomed southern sector. The latter possibly behaves as a sediment trap limited by the Iberian and Eivissa slopes to west and east, and the Xàbia Seamount to the north. Its subdued connection with the South Balearic Basin and the dominant current regime (see below) would favour effective sediment trapping in the southern sector.

The Eivissa Channel plays a major role in the exchange of water masses between the South Balearic Basin and the València Trough (Fig. 7.1). Surface waters with Atlantic influence enter the València Trough through the Eivissa Channel. Northward-directed bottom current velocities range from 23 cm/s during fall and winter to less than 5 cm/s during spring and summer (López-Jurado & Díaz del Río, 1994). When the flow of water from the

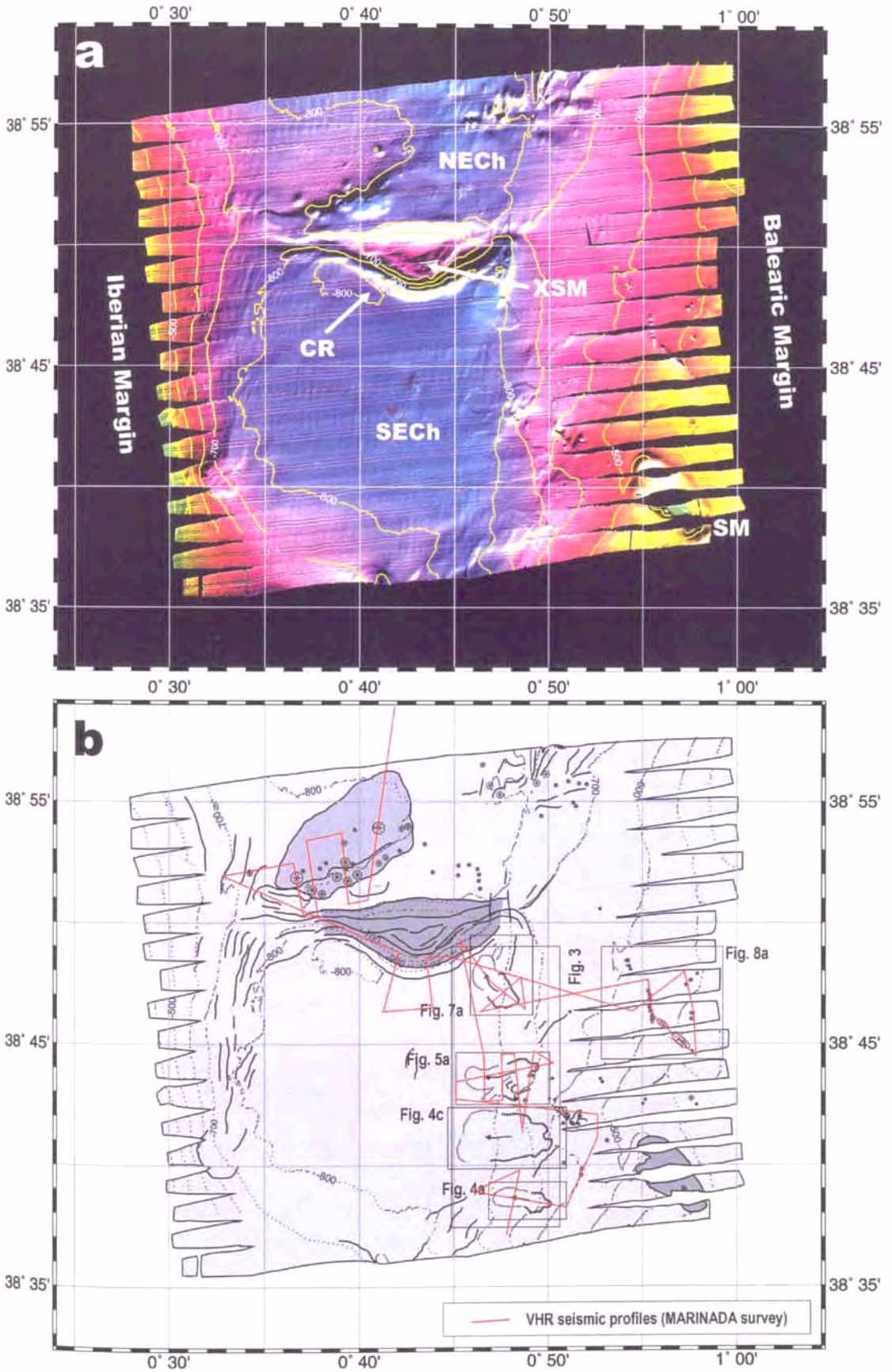
a
0° 30'
0° 40'
0° 50'
1° 00'
38° 55'
38° 45'
38° 35'
NECh
SECh
XSM
CR
SM
Iberian Margin
Balearic Margin
b
Fig. 3
Fig. 8a
Fig. 7a
Fig. 5a
Fig. 4c
Fig. 4a
VHR seismic profiles (MARINADA survey)

Figure 7.2. *(previous page) a: Shaded relief image and swath bathymetry map of the Eivissa Channel, illuminated from the north. Contours are every 100 m. The east-west trending Xàbia Seamount (XSM) forms the boundary between the northern (NECh) and southern (SECh) Eivissa Channel. Another seamount is also labelled (SM), as well as the contouritic ridge (CR) south of the Xàbia Seamount. b: Interpretation of the swath bathymetry map of Fig. 7.2a. Dark grey areas represent seamounts while the light grey area corresponds to the pockmark field in the northern Eivissa Channel. Contours every 100 m. Encircled stars show the location of the larger pockmarks. Bold lines represent morphologic alignments such as sediment drifts. Boxes show the location of Figs. 7.3, 7.4a, 7.4c, 7.5a, 7.7a and 7.8a.*

south weakens, deep waters originating in the Ligurian Sea and the Gulf of Lions exit the València Trough through the Eivissa Channel. The interaction between near-bottom currents and the seafloor topography associated with the Eivissa Channel have important implications for the sediment dynamics in the area.

The east-west oriented depression at the foot of the Xàbia Seamount and the associated parallel sedimentary ridge bounding the depression to the south resemble typical contouritic ridges and associated base-of-slope depressions (Fig. 7.2; Canals, 1985; Stow et al., 1998; Faugères et al., 1999). The Xàbia Seamount is an obstacle that opposes the northward-moving bottom current. Flow lines concentrate, as the bottom current strengthens around the seamount and scours the base of the slope. The eroded material accumulates to the south forming a linked contouritic ridge. No depression or contouritic ridge are observed on the northern side of the Xàbia Seamount, thus demonstrating that the prevailing long-term direction of near-bottom currents is to the north.

7.6. MASS WASTING

After refined processing, the swath bathymetry data obtained in 1995 identified four headwall scars and associated slide deposits roughly aligned along the 0°48'E meridian on the Balearic Margin flanking the southern sector of the Eivissa Channel. These occur in water depths ranging between 600 and 900 m (Figs. 7.2 and 7.3). The slides, named from south to north, the Ana, Joan, Nuna, and Jersi slides, were revisited in 2002 in order to obtain VHR parametric seismic reflection profiles to image their geometry and internal structure in detail. The area of individual slides varies from 6 to 16 km^2.

7.6.1. Ana slide

The Ana slide (Fig. 7.4a and b) is located between 38°38'N and 38°39'N and between 0°47'E and 0°50'E, at water depths ranging

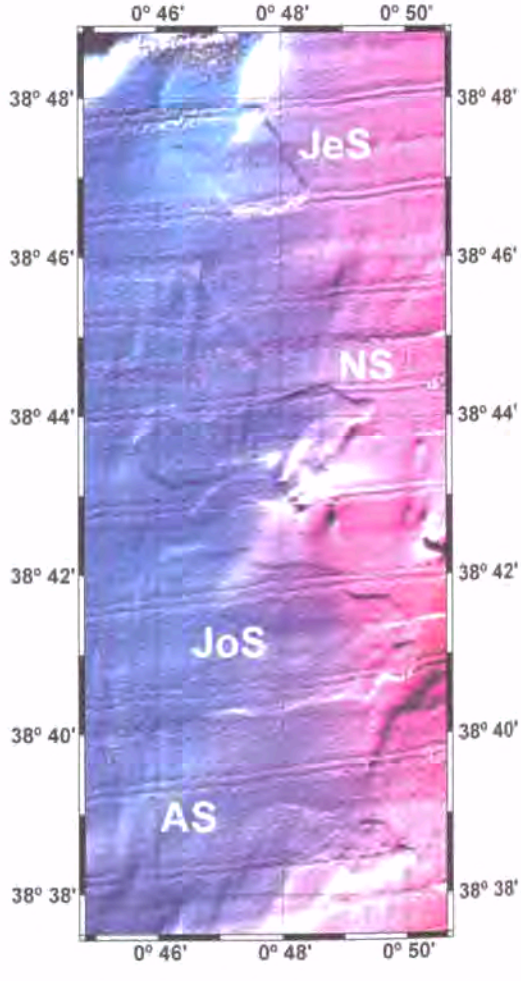

Figure 7.3. *Shaded relief image of the Eivissa Channel slides, illuminated from the north. From south to north, the slides have been named for the Ana slide (AS), Joan slide (JoS), Nuna slide (NS) and Jersi slide (JeS).*

from 635 m at the rim of the headwall scarp to 815 m at its toe, with an average slope angle of 1.6°. The headwall scar extends from 635 m to 740 m water depth, has a horseshoe shape and is up to 30 m high. The slide has a total length of 4.9 km and a mean width of 1.3 km. It has affected an area of 6 km^2 (Fig. 7.4a).

Seismic reflection profiles along the length of the Ana slide (Fig. 7.4b) show three seismic facies that succeed one another downslope. At shallower water depths, the slide deposit consists of transparent seismic facies. Slightly rotated, glide blocks with stratified seismic facies can be observed in the central part of the slide. The deposit facies become chaotic at the slide toe, as if in this lower reach there was a lesser degree of sediment disruption compared to the upper part of the slide. Material did not significantly outflow over the slide toe.

The slide deposit has a mean thickness of 23 m (assuming a velocity of 1,500 $m \cdot s^{-1}$ for the sediment) and a maximum of 44 m, which is greater than the headwall scarp height. The disturbed sediment thickens downslope towards the distal part of the deposit. Such thickening contrasts with the minimal bathymetric expression of the edge of the depositional lobe in terms of height difference. These observations suggest that modest material transfer is accompanied by the downslope propagation of deformation front that extensively remoulds the slope sediment without necessarily translating it very far downslope. Most of the sediment in the central and lower slide deposit remains *in situ* or is only slightly displaced, but it is highly disrupted. Thus, the total length of the slide does not correspond to the run-out of sediment. Overall, the total volume of sediment affected is ca. 0.14 km^3.

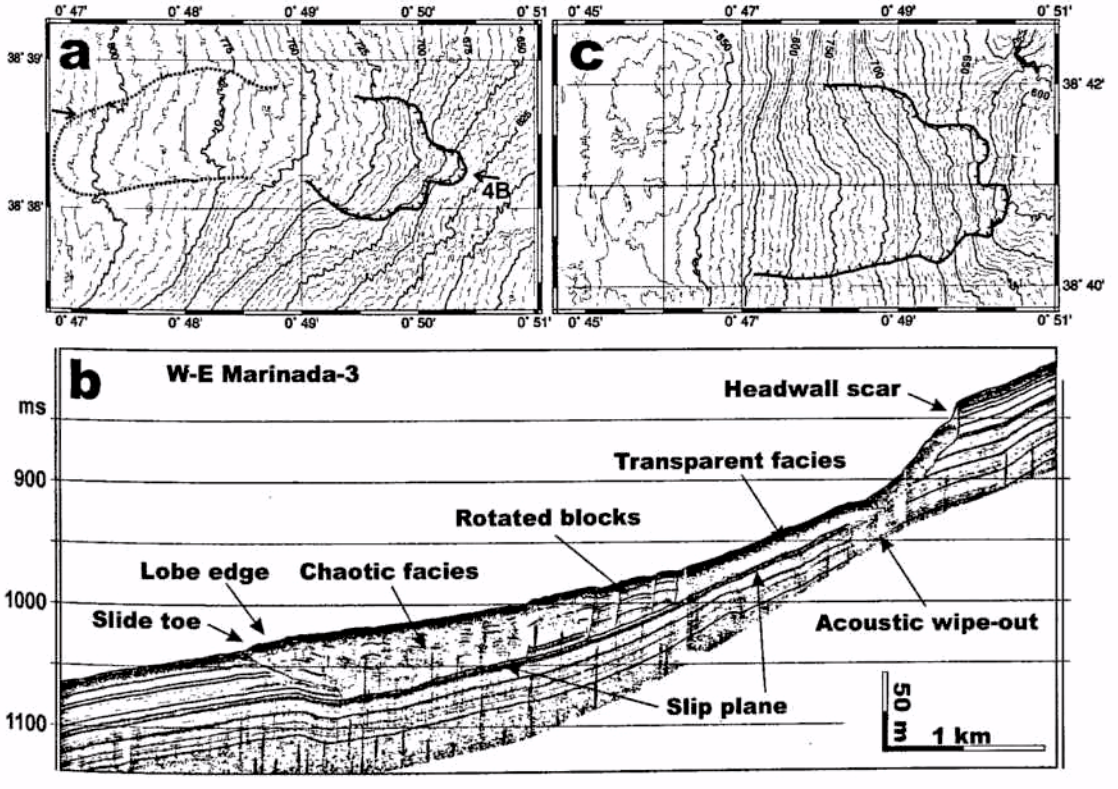

Figure 7.4. a: Swath bathymetry map of the Ana slide. Contours every 5 m. The dotted line outlines the limit of the depositional lobe and the bold line is the trace of the headwall scarp. Arrows show the location of the profile in Fig. 7.4b. b: Interpreted very high resolution reflection seismic profile along the Ana slide. Main features within the profile are indicated. See text for explanation. c: Swath bathymetry map of the Joan slide. Contours every 5 m. The bold line is the headwall scarp. See text for explanation.

The slip plane for the Ana slide exploits a characteristic high amplitude reflector within the seismically well-stratified slope deposits outside the slide. At a short distance from the slide headwall there is an acoustic wipe-out masking the stratified facies beneath the slide (Fig. 7.4b). In plan view, this part of the headwall is complicated by a semi-circular embayment (Fig. 7.4a). Acoustic wipe-out zones can be indicative of the presence of gas in the sediment (O'Leary & Laine, 1996), and the headwall embayment could mark the location of a former large pockmark (cf. fluid escape features; e.g. Hovland & Judd, 1988; Acosta et al., 2001b).

7.6.2. Joan slide

The Joan slide (Fig. 7.4c) is located approximately between 38°40'N and 38°42'N and between 0°45'E and 0°50'E. It is the largest slide in the region, disturbing 16 km^2 of the Eivissa Channel seafloor. The slide occurs between 600 and ca. 870 m water depth and the average slope angle is 2.5°. It has a horseshoe-shaped headwall scarp, which is up to 20 m high, and extends from a water depth of 600 to 820 m on the basis of multibeam bathymetric mapping (Fig. 7.4c). The outer limit of the depositional lobe resulting from the Joan slide is poorly defined on swath bathymetry because of its low relief. Since no seismic reflection profiles were acquired across the deposit, the thickness has to be inferred from those obtained from the other three slides in the Eivissa Channel (cf. discussion). The total volume is thus estimated at about 0.4 km^3 based on an estimated thickness of 25 m.

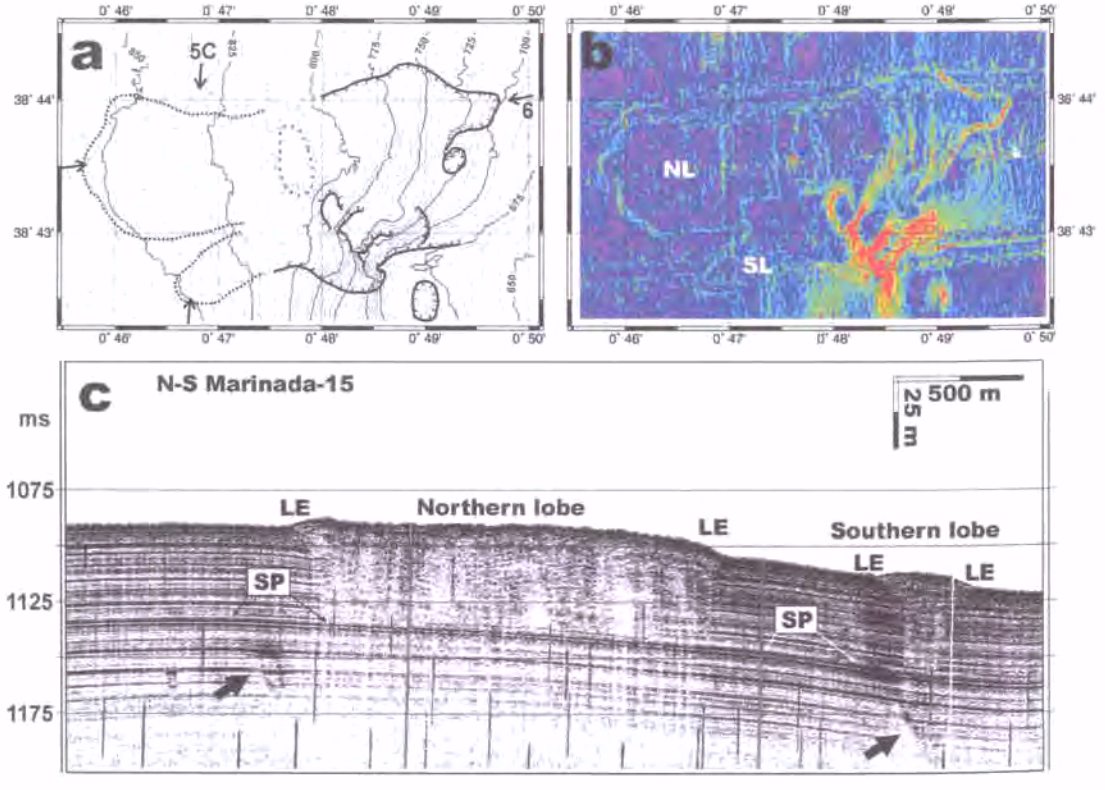

Figure 7.5. *a: Swath bathymetry map of the Nuna slide. Contours every 5 m. The dotted line follows the limit of the depositional lobe and the bold line tracks the headwall scarp. The oval of spaced dots marks a depression within the slide deposit. Arrows show the location of profiles in Figs. 7.5c and 7.6. b: Slope gradient map of the Nuna slide. Red, yellow, green and light blue represent high gradients whereas dark blue and purple represent low gradients. The northern (NL) and southern (SL) lobes are clearly identifiable. See text for explanation. c: Seismic reflection profile across the toe of the Nuna slide, showing the internal structure and sub-surface expression of the two lobes identified, their edges (LE), and the slip plane (SP) of the slide. Black arrows point to "bright spots" indicative of the presence of gas in the sediment.*

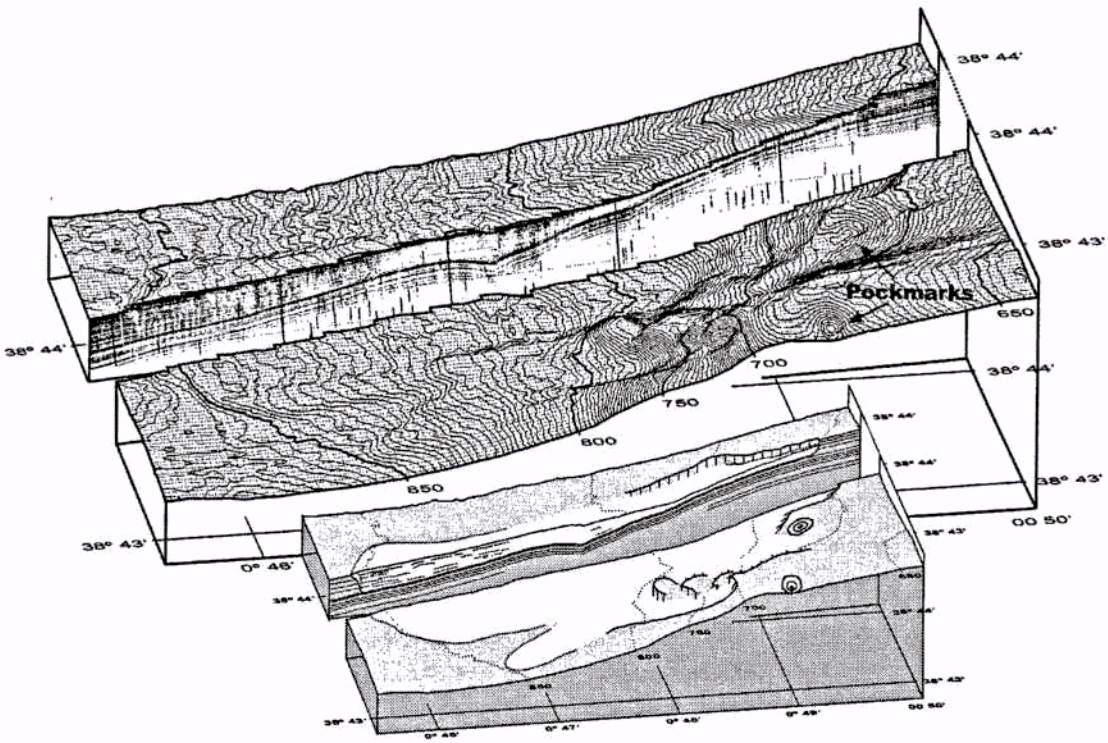

Figure 7.6. *Bathymetric 3D block model of the Nuna slide area, split along the seismic reflection profile located in Fig. 7.5a and its interpretation below. Note the different seismic facies within the deposit, as explained in the text, and the presence of two pockmarks close to the headwall scar area.*

7.6.3. Nuna slide

The Nuna slide complex (Figs. 7.5 and 7.6) results from two events forming two separate headwalls and lobes to the north and south that are identified on the swath bathymetry imagery and derivative slope maps (Figs. 7.5a and b), and on VHR seismic reflection profiles (Fig. 7.5c). The slide complex is located between 38°42'30"N and 38°44'N, and between 0°46'E and 0°50'E in an area with an average slope angle of 3°. Including the depositional lobes, it affects 10.3 km^2 of the seafloor at water depths from 675 to 860 m. The headwall scarp has an irregular morphology and ranges from 20 m high for the northern slide to more than 50 m high for the southern slide, where steps up to 30 m high occur (Figs. 7.5a and 7.6) due to the presence of shallow acoustic basement seen on seismic reflection profiles (Fig. 7.2b). Swath bathymetry reveals the presence of two pockmarks up to 15 m deep in the headwall scar area. The ca. 400 m in diameter, <10 m deep pockmark to the north is almost connected to the northern scar upper rim (Figs. 7.5a and 7.6).

Seismic reflection profiles across (Fig. 7.5c) and along (Fig. 7.6) the Nuna slide complex show the deposit to be mainly made up of transparent seismic facies, but it is also chaotic and discontinuously stratified at its distal most part. It lies on top of the continuously stratified facies that forms the stable Plio-Quaternary sequence. As already seen on the Ana slide, short distance transport was sufficient to obliterate the internal stratification of the slide mass. Both lobes are characterised by areas of positive and rougher relief with respect to the surrounding undisturbed seafloor (Fig. 7.5c). The mean thickness of the deposit is ca. 30 m, rising to a maximum of 50 m locally. The total volume of disturbed sediment is about 0.31 km^3. A small, <5 m deep, north-south oriented, oval-shaped depression observed on top of the deposit at ca. 810 m water depth results from the accommodation of the deposit to the topography of the

underlying slip plane reflector (Figs. 7.5a and 7.6). This slip plane reflector displays very high amplitude and continuity, and can be identified at the base of both lobes of the Nuna Slide complex. Reflector enhancements or "bright spots" (black arrows in Fig. 7.5c), which could relate to the presence of free gas in the sediment, are occasionally observed.

7.6.4. Jersi slide

The Jersi slide (Fig. 7.7) is located between 38°46'30"N and 38°48'30"N, and between 0°46'E and 0°48'30"E, in an area with an average slope angle of 1.9°. The Jersi slide has a 15 m high headwall scarp and affects 7.9 km^2 of the seafloor in the northeastern corner of the southern sector of the Eivissa Channel, close to the Xàbia Seamount. Due to the local topographic influences, the sediment moved northwestwards and not westwards as in the rest of the slides in the area (Fig. 7.7a).

Seismic reflection profiles along the Jersi slide (Fig. 7.7b) show that the deposit is characterized by transparent seismic facies. Chaotic seismic facies such as those observed at the toes of the Ana and Nuna slide deposits are not present in this case. Instead, small patches of broken stratified facies can be identified in the upper part of the slide below the headwall step suggesting that sediment was only slightly disturbed here. The slide deposit overlies the stable stratified Plio-Quaternary sequence of the Eivissa Channel and, as in the other slides, it represents the last sedimentary event in the area. It has a mean thickness of 25 m, giving a total volume of 0.19 km^3. Seismic reflection profiles also show that the height of the headwall scarp is not representative of the final thickness of the deposit, since disturbed sediment was not totally evacuated from the headwall scar area. Once again, a prominent high-amplitude reflector forms the slip plane of this slide for which a tentative reconstruction of the seafloor profile prior to the slide has been made (Fig. 7.7b).

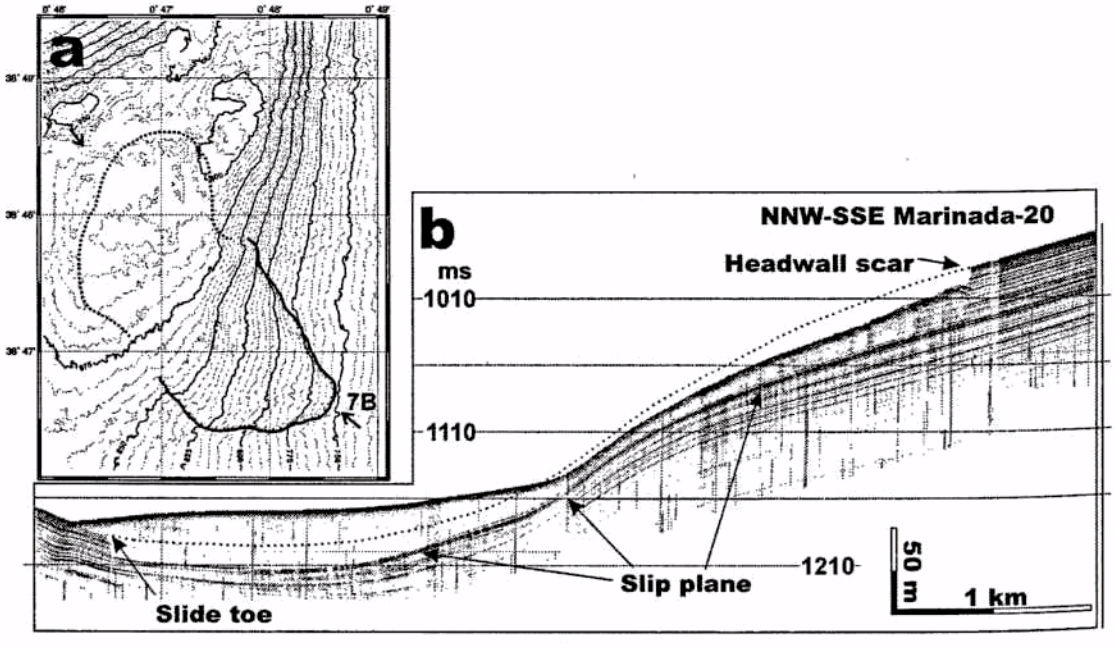

Figure 7.7. *a: Swath bathymetry map of the Jersi slide. Contours every 5 m. The dotted line marks the limit of the depositional lobe and the bold line is the headwall scarp. Arrows show the location of the profile in Fig. 7.7b. b: Seismic reflection profile along the Jersi slide. Main features within the profile are indicated. The dotted line illustrates a tentative reconstruction of the seafloor profile previous to the slide. See text for explanation.*

7.7. FLUID ESCAPE FEATURES

Fluid escape features have been described in the Balearic Promontory by Acosta et al. (2001b), both in the Eivissa Channel and in the Mallorca Channel between the islands of Eivissa and Mallorca. These authors relate those features, mostly pockmark fields, to the occurrence of 30 Ma – Recent submarine volcanism as well as to local sagging caused by recent faulting forcing the expulsion of hydrothermal gas and water. They identified the pockmark field north of Xàbia Seamount, in the northern Eivissa Channel region (Fig. 7.2), but finer processing of the swath bathymetry data in this study has allowed the identification of additional pockmark fields and isolated pockmarks in the Balearic Margin south of the Xàbia Seamount (Figs. 7.2b and 7.8).

In the pockmark field in the northern Eivissa Channel, two families of pockmarks have been identified. The first consists of a group of about ten large pockmarks up to 500 m in diameter and up to 50 m in depth. The second is made of more than fifty small pockmarks with a mean diameter of 10 m and less than 5 m in depth. Seismic reflection profiles across this pockmark field show that the larger pockmarks are rooted in deep strata beyond the penetration of the seismic system used, while the smaller pockmarks are rooted in a seismic reflector located ca. 70 m below the seafloor. Pockmark distribution north of the Xàbia Seamount does not show any clear spatial pattern.

By contrast, pockmarks in the southern Eivissa Channel are often aligned (Fig. 7.8a). These are rather similar in size, ~100 m in diameter and ~15 m in depth, occur at water depths of ca. 500 m, and are also rooted deeper than the penetration range of the seismic acquisition system (Fig. 7.8b). The few isolated pockmarks in the southern Eivissa Channel occur at greater water depths and have different sizes. Two of these pockmarks are situated in the vicinity of the headwall scar of the Nuna slide, while a third seems to be related to the headwall scar of the Ana slide. This suggests that fluid escape processes in the upper Plio-Quaternary sedimentary sequence of the Eivissa Channel are closely linked to the observed landslides.

Pockmarks in the Eivissa Channel are either currently active or have been active in recent times. This view is supported by the lack of buried pockmarks in the seismic reflection profiles and by the fact that all of them disturb not only the uppermost sediment layers but also the seafloor. What appears to be active gas venting plumes

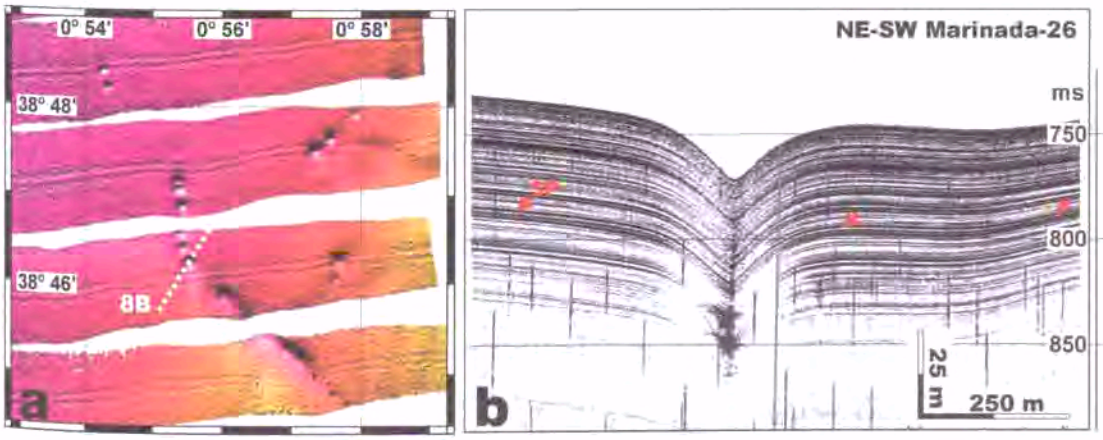

Figure 7.8. a: Shaded relief image of part of the southern Eivissa Channel showing aligned pockmarks, illuminated from the north. The dotted line shows the location of the profile in Fig. 7.8b. b: Seismic reflection profile crossing a large pockmark in the southern Eivissa Channel. Note that the pockmark is rooted below the penetration range of the VHR seismic acquisition system. Red arrows point to the slip plane (SP) of the slides in the Eivissa Channel.

have been observed north of the study area by means of a single beam, high-frequency Simrad EA500 echo-sounder during a cruise in summer 2002 on board the Spanish research vessel *Hespérides*. The relation of pockmarks and gas hydrates is discarded since the oceanographic setting of this part of the Mediterranean does not allow the presence of gas hydrates (Klauda & Sandler, 2003). Origin of the fluids has not been studied. These are presumably thermogenic and related with the numerous volcanic structures observed in the Balearic Promontory and its surroundings (e.g. Acosta et al., 2002), although a biogenic contribution can not be discarded.

7.8. DISCUSSION

Shallow gravity failure of sediment packages may be more likely at certain stratigraphic levels where interstratified layers with contrasting mechanical properties occur. These levels, often identified as weak layers, are strata having sedimentological and geotechnical properties that make them prone to act as slip planes for overlying sediment (e.g. Lykousis et al., 2002). In the case of the four slides studied here, the slip plane can be identified wherever seismic reflection profiles are available, i.e. the Ana, Nuna and Jersi slides. Correlation of seismic reflectors between the various slides reveals that the slip planes for these three slides correspond to the same seismic reflector. A correlation panel of seismic units and reflectors beneath the three slides is plotted in Fig. 7.9, illustrating how the SP reflector acted as a slip plane in all three cases. This reflector is easily identifiable on most of the seismic profiles (Fig. 7.2b) and must represent a mechanically weak layer over large areas of the Eivissa Channel.

Such a weakness could be enhanced because of the escape of fluids from the sediment, as indicated by the observation of numerous pockmarks and other fluid-related features such as "bright spots" seen on the seismic reflection profiles. Pockmarks are frequently observed in regions where mass wasting processes have occurred (e.g., Piper et al., 1999; Hovland et al., 2002). As the pockmarks in the southern Eivissa Channel are rooted below the penetration range of the seismic reflection profiles (~100 m), the source of the fluids is from below the SP reflector, which in the area of aligned pockmarks is ca. 30 m below the seafloor (Fig. 7.8).

The role of pockmarks in triggering the slides may be dual. On the one hand escaping fluids forming the pockmarks may have been injected into SP reflector, thus increasing the pore pressure; on the other hand pockmarks represent a bedding discontinuity presumably reducing the shear resistance along the potential failure plane. These effects would further promote destabilisation when combined with maximum slope angles. Indication of this relation is that the Ana, Joan and Nuna slides display curved embayments in the uppermost parts of their headwall scars (Figs. 7.4a, 7.4c, 7.5a and 7.5b). These embayments open downslope towards depositional areas. Normally, such geometries may be taken as an indication of retrogressive failure and secondary sliding and degradation of the headwall (Lastras et al., 2003). However, in this case they could correspond to the remnants of pockmarks that led to the collapse of the upper sediment layers located immediately downslope. Furthermore, the size of the observed uppermost headwall embayments is similar to the size of uncollapsed pockmarks seen in the study area, often at short distance from embayed headwalls (e.g. Nuna slide, Figs. 7.5a and 7.6). In addition, acoustic wipe-out zones that appear below the embayment further support the interpretation of an origin related to fluid escape (e.g. Ana slide, Fig. 7.4b).

The fact that all the slides in the Eivissa Channel occupy the same stratigraphic position and share the same slip horizon could indicate that they occurred simultaneously following a common triggering mechanism. Significant seismic events have occurred in historic times in nearby areas, e.g. a shock with a local magnitude of 4.8 occurred in Mula, Murcia, in 1999 (URSPA, 2003), and seismogenic faults exist both onshore and offshore

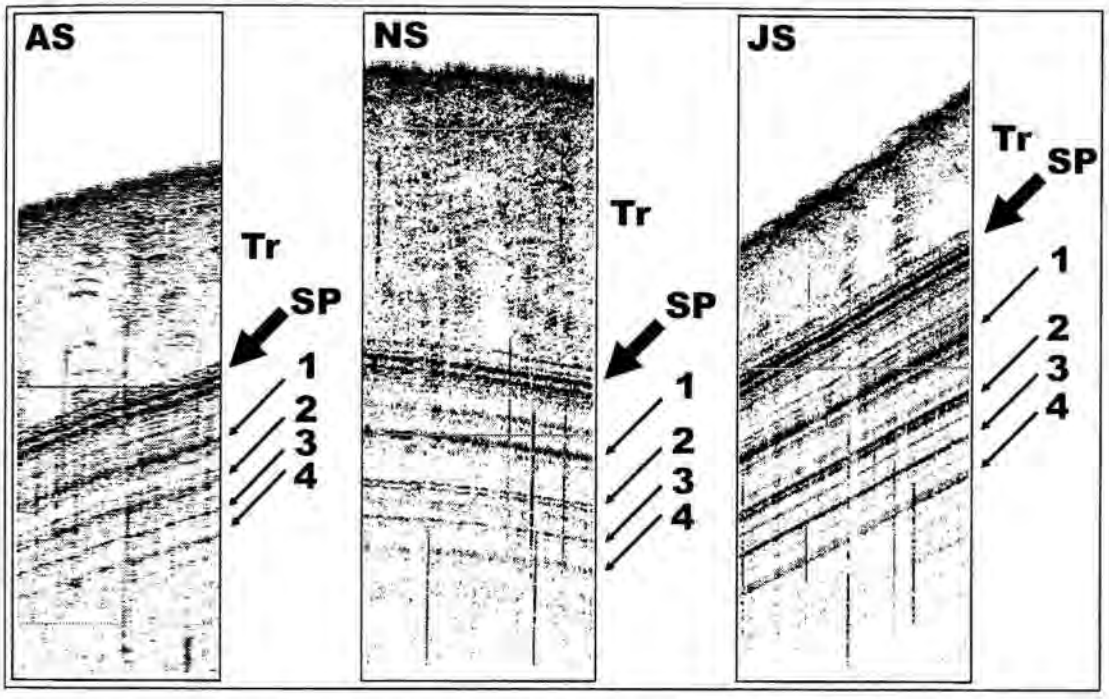

Figure 7.9. Correlation of seismic reflectors underlying the Ana (AS), Nuna (NS) and Jersi (JS) slides. Large arrows (SP) under transparent units (Tr) point to common slip plane horizon. Correlated reflectors 1 to 4 are also labelled for ease of comparison.

capable of generating earthquakes that could induce the failure of sediment piles overlying a weak layer.

An additional lesson arising from the study of the slides in the southern Eivissa Channel relates to the methodology employed to calculate the volume of submarine slide and debris flow deposits using the height of the headwall scarp to infer the thickness and, when combined with areal extent, the volume of the final deposit. Such a calculation is normally done in cases when no seismic profiles are available or when they do not penetrate to the base of the disturbed sediment (e.g. McAdoo et al., 2000). This method appears to be inapplicable for the Eivissa Channel slides since the thickness of the deposit is often greater than the height of the headwall scarp (Fig. 7.7b). Furthermore, the seafloor expression of slide depositional lobes can be subtle when compared to their sub-surface expression (Figs. 7.4b and 7.5c). This implies that the volumes of sediment released from slide scars and transported downslope can be relatively small compared to the volume of mostly *in situ* sediment disturbed by the passage of materials moving downslope. The sharp lateral change in seismic facies, from chaotic to stratified, below the edge of the depositional lobe of the Nuna slide is a good example of this (Fig. 7.5c).

Lastly, run-out distance is used as one of the key inputs for slide and debris flow modelling. Usually the total length from the headwall scarp to the slide toe is taken as a measure of run-out due to the difficulty of calculating the displacement of the failed sediment mass centre (e.g. McAdoo et al., 2000). The internal character of the Eivissa Channel slides indicates that the headwall-to-toe distance (ca. 5 km) greatly overestimates the actual transport distance of the remobilised slope sediments caught up in the slides.

The Eivissa Channel slides have yet to be cored. However, the seismic reflection data indicate that the features must be young, as the high resolution seismic profiling precludes draping of the features by more than 10 cm of sediment. A coring programme is now needed to date the slide

events more precisely, and to recover samples of the mechanically weak SP layer on which the sliding occurred.

7.9. CONCLUSIONS

Four small slides have been imaged in the southern Eivissa Channel in the Western Mediterranean, at water depths ranging from 600 to 900 m, as a result of a fine-scale processing of swath bathymetry data and subsequent acquisition of strategically located very high resolution seismic reflection profiles. Individual slides are no larger than 16 km^2 in area and 0.4 km^3 in volume. Their small size allows them to be studied in great detail using seismic reflection profiling, which provides information on the sedimentary architecture of the resulting deposits. A common slip plane for the four slides has been identified and characterised as a layer that extends at least along the whole slope west of Eivissa Island. The presence of fluid escape structures and other features suggesting the occurrence of gas in the sediment combined with the existence of a mechanically weak layer is thought to be the main factor controlling instability in the area. The slides possibly occurred simultaneously, and may have been triggered by a seismic event of a magnitude larger than the usual magnitude of 3 to 4 events in the Eivissa Channel.

In addition, these slides provide a salutary lesson for the study of submarine landslides in absence of seismic data. Thus using the height of headwall scars to infer the thickness of the deposits, and the total length to infer the actual run-out of a remobilised sediment mass may not be appropriate.

7.10. ACKNOWLEDGEMENTS

This study was supported by the V Framework Program Projects COSTA (EVK3-1999-00028) and EUROSTRATAFORM (EVK3-2002-00079), and Research Training Network EURODOM (HPRN-CT-2002-00212 from the Human Potential Programme) from the European Community; Projects SPACOMA (01-LEC-EMA14F) and WEST-MED (01-LEC-EMA22F) of EUROCORES Program about EUROMARGINS of the European Science Foundation; CYTMAR Project GRANDES (MAR98-0347), a Generalitat de Catalunya Grups de Recerca Consolidats grant (2001 SGR-00076), a Spanish "Ministerio de Educación, Cultura y Deportes" FPU fellowship (Lastras), and a Spanish "Ministerio de Ciencia y Tecnología" "Ramón y Cajal" fellowship (Urgeles). The authors would also like to thank the scientific parties and *R/V Hespérides* crews who helped to obtain the best data possible during the BIG'95 and MARINADA cruises. The manuscript greatly benefited from thorough comments by reviewers Martin Hovland and Peter Croker, and the editor, Peter Haughton.

7.11. REFERENCES

Acosta, J., Muñoz, A., Herranz, P., Palomo, C., Ballesteros, M., Vaquero, M., Uchupi, E., 2001a, Geodynamics of the Emile Baudot Escarpment and the Balearic Promontory, western Mediterranean: Marine and Petroleum Geology, v. 18, p. 349-369.

Acosta, J., Muñoz, A., Herranz, P., Palomo, C., Ballesteros, M., Vaquero, M., Uchupi, E., 2001b, Pockmarks in the Ibiza Channel and western end of the Balearic Promontory (western Mediterranean) revealed by multibeam mapping: Geo-Marine Letters, v. 21, p. 123-130.

Acosta, J., Canals, M., López-Martínez, J., Muñoz, A., Herranz, P., Urgeles, R., Palomo, C., Casamor, J.L., 2002, The Balearic Promontory geomorphology (western Mediterranean): morphostructure and active processes: Geomorphology, v. 49, p. 177-204.

Barriendos-Vallve, M., Martín-Vide, J., 1998, Secular climatic oscillations as indicated by catastrophic floods in the Spanish Mediterranean coastal area (14th – 19th centuries): Climatic Change, v. 38, p. 473-491.

Bugge, T., 1983, Submarine slides on the Norwegian continental margin, with special emphasis on the Storegga area: Continental Shelf Institute Publications, v. 110, 152 p.

Bulat, J., 2003, Imaging the Afen slide from commercial 3D seismic – methodology and

comparisons with high-resolution data; in Locat, J., Mienert, J., eds., Submarine Mass Movements and Their Consequences: Kluwer Academic Publishers, The Netherlands, p. 205-213.

Campbell, K.J., 1999, Deepwater geohazards: How significant are they?: The Leading Edge, v. 18, p. 514-519.

Canals, M., 1985, Estructura sedimentaria y evolución morfológica del talud y el glacis continentales del Golfo de León: Fenómenos de desestabilización de la cobertura plio-cuaternaria [Ph.D. Thesis]: Universitat de Barcelona, Spain, 618 p.

Canals, M., Ballesteros, E., 1996, Production of carbonate particles by phytobenthic communities on the Mallorca-Menorca Shelf, Northwestern Mediterranean Sea: Deep-Sea Research, v. 44, p. 611-629.

Cebrián, E., Ballesteros, E., Canals, M., 2000, Shallow rocky bottom benthic assemblages as calcium carbonate producers in the Alboran Sea (southwestern Mediterranean): Oceanologica Acta, v. 23, p. 311-322.

Damuth, J.E., 1980, Use of high-frequency (3.5–12 kHz) echograms in the study of near-bottom sedimentation processes in the deep-sea: A review: Marine Geology, v. 38, p. 51-75.

Faugères, J.C., Stow, D.A.V., Imbert, P., Viana, A., 1999, Seismic features diagnostic for contouritic drifts: Marine Geology, v. 162, p. 1-38.

Fontboté, J.M., Guimerà, J., Roca, E., Sàbat, F., Santanach, P., Fernández-Ortigosa, F., 1990, The Cenozoic geodynamic evolution of the Valencia Trough (western Mediterranean): Revista de la Sociedad Geológica de España, v. 3, p. 249-259.

Gueguen, E., Doglioni, C., Fernández, M., 1998, On the post 25-Ma geodynamic evolution of the Western Mediterranean. Tectonophysics, v. 298, p. 259-269.

Hovland, M., Judd, A.G., 1988, Seabed pockmarks and seepages. Impact on Geology, Biology and the Marine Environment: Ed. Graham and Trotman, London (UK), 293 pp.

Hovland, M., Gardner, J.V., Judd, A.G., 2002, The significance of pockmarks to understanding fluid flow processes and geohazards: Geofluids, v. 2, p. 127-136.

IEO-IHM, 1999, Zona Económica Exclusiva, Hoja M-13. Mapa Batimétrico: Ed. Ministerio Agricultura, Pesca y Alimentación: Instituto Español de Oceanografía, Departamento de Geología y Geofísica Marina, Madrid, Spain.

Klauda, J.B., Sandler, S.I., 2003, Predictions of gas hydrate phase equilibria and amounts in natural sediment porous media. Marine and Petroleum Geology, (in press).

Lastras, G., Canals, M., Hughes-Clarke, J.E., Moreno, A., De Batist, M., Masson, D.G., Cochonat, P., 2002, Seafloor imagery from the BIG'95 debris flow, western Mediterranean: Geology, v. 30, p. 871-874.

Lastras, G., Canals, M., Urgeles, R., 2003, Lessons from sea-floor and subsea-floor imagery of the BIG'95 debris flow scar and deposit; in Locat, J., Mienert, J., eds., Submarine Mass Movements and Their Consequences: Kluwer Academic Publishers, The Netherlands, p. 425-431.

Locat, J., Mienert, J., (eds.), 2003, Submarine Mass Movements and Their Consequences: Kluwer Academic Publishers, Dordrecht. Holland, 552 p.

López-Jurado, J.L., Díaz del Río, G., 1994, Dinámica asociada a las masas de agua en el Canal de Ibiza en noviembre de 1990 y marzo de 1991: Boletín del Instituto Español de Oceanografía, v. 10, p. 3-22.

Lykousis, V., Roussakis, G., Alexandri, M., Pavlakis, P., Papoulia, P., 2002, Sliding and regional slope stability in active margins: North Aegean Trough (Mediterranean): Marine Geology, v. 186, p. 281-298.

Maillard, A., Mauffret, A., 1993, Structure et volcanisme de la Fosse de Valence (Méditerranée nord-occidentale): Bulletin Societe Géologique France, v. 164, p. 365-383.

McAdoo B.G., Pratson, L.F., Orange D.L., 2000, Submarine landslide geomorphology, US continental slope: Marine Geology, v. 169, p. 103-136..

Mienert J., Weaver, P.P.E., (eds.), 2003, European Margins Sediment Dynamics: Side-Scan Sonar and Seismic Images: Springer-Verlag Publishers, Heidelberg, Germany, 310 pp.

Offshore Technology, 2003, Offshore Technology – gas field project – Ormen Lange – North Sea, Northern Norway: [WWW document], URL: http://www.offshore-technology.com/projects/ormen/

O'Leary, D.W., Laine, E., 1996, Proposed criteria for recognizing intrastratal deformation features in marine high resolution seismic reflection profiles: Geo-Marine Letters, v. 16, p. 305-312.

Palomo, C., Acosta, J., de Andrés, J., Herranz, P., Rey, J., Sanz, J.L., 1976, Perfiles geofísicos entre la península y las Islas Baleares: 2ª Asamblea Nacional de Geodesia y Geofísica, Comunicaciones, v. 3, p. 1615-1627.

Piper, D.J.W., Cochonat, P., Morrison, M.L., 1999, The sequence of events around the epicentre of the 1929 Grand Banks earthquake: initiation of debris flow and turbidity current inferred from sidescan sonar: Sedimentology, v. 46, p. 79-97.

Rothwell, R.G., Thomson, J., Kähler, G., 1998, Low sea-level emplacement of a very large late Pleistocene "megaturbidite" in the western Mediterranean Sea: Nature, v. 392, p. 377-380.

Sàbat, F., Roca, E., Muñoz, J.A., Vergés, J., Santanach, P., Sans, M., Masana, E., Estévez, A., Santisteban, C., 1995, Role of extension and compression in the evolution of the eastern margin of Iberia: the ESCI-Valencia Trough seismic profile: Revista de la Sociedad Geológica de España, v. 8, p. 431-448.

Smith, W.H.F., Sandwell, D.T., 1997, Global seafloor topography from satellite altimetry and ship depth soundings: Science, v. 277, p. 1957-1962.

Stow, D.A.V., Faugères, J.C., Viana, A., Gonthier, E., 1998, Fossil contourites: a critical review: Sedimentary Geology, v. 115, p. 3-31.

Synloakis, C.E., Liu, P., Carrier, G., Yeh, H., 1997, Tsunamigenic sea-floor deformation: Science, v. 278, p. 598-600.

URSPA (Unidad de Registro Sísmico de la Provincia de Alicante), 2003, Unidad de Registro Sismológico: [WWW document], URL: http://www.ua.es/ursua/ [March 27th, 2003].

Vegas, R., 1992, The Valencia Trough and the origin of the western Mediterranean basins: Tectonophysics, v. 203, p. 249-261.

CAPÍTOL 8

INTEGRACIÓ DELS RESULTATS

En aquest capítol s'ofereix una visió integrada dels resultats descrits en els articles i capítols de llibre precedents sobre els esllavissaments BIG'95 i del canal d'Eivissa. S'hi han inclòs també algunes dades i resultats no publicats, referits sobretot als testimonis de sediment.

8.1. BIG'95: morfologia del dipòsit

L'àrea afectada pel *debris flow* BIG'95 és de ~2.200 km^2, i el dipòsit resultant cobreix ~2.000 km^2 del talús i el glacis continentals de l'Ebre (Fig. 4.2) **amb 26 km^3 de sediment remobilitzat**. Aquest és, doncs, l'esllavissament recent del marge de l'Ebre més gran identificat fins ara i, juntament amb els esllavissaments del golf de Lleó (Droz, 1983; Méar, 1984; Canals, 1985; Gaullier et al., 1998; Berné et al., 1999; Droz et al., 2001) i la megaturbidita de la plana abissal de Balears (Rothwell et al., 1998; 2000), un dels moviments de massa més extensos i amb més volum de sediment involucrat de la Mediterrània occidental. **El recorregut** descrit pel sediment esllavissat no va ésser lineal, sinó que primer **va seguir una direcció WNW-ESE** a favor del màxim pendent del talús de l'Ebre, i **després girà cap al NE** obligat per la topografia del talús oposat de les Balears, canalitzant-se finalment dins el canal de València (Fig. 4.3). Hom pot considerar que **en els darrers 40 km del seu recorregut**, l'esllavissament BIG'95 **va ser un flux topogràficament confinat**, fet que tingué importants implicacions en la dinàmica del moviment.

Per a la caracterització de la superfície de l'esllavissament, hom ha emprat diferents combinacions de mapes de batimetria de multifeix i d'intensitat de retrodifusió (Figs. 1.18, 2.1 i 8.1). A grans trets, hom ha diferenciat **dues grans àrees** dins la regió afectada per l'esllavissament: **l'àrea font**[71] i **l'àrea deposicional**[72]. **A la primera**, des de la qual va evacuar-se pràcticament tot el sediment mobilitzat, quedant només en alguns indrets un dipòsit de gruix inferior a 10 m, **s'hi situen la cicatriu principal i** gairebé totes **les cicatrius secundàries. La segona àrea ha estat dividida en** tres sub-àrees, **l'àrea deposicional proximal**[73], **l'àrea deposicional intermèdia**[74] **i l'àrea deposicional distal**[75], a partir de criteris morfològics i llur resposta acústica. **L'àrea deposicional proximal presenta un relleu** relativament **suau i regular, i una retrodifusió intermèdia. L'àrea deposicional intermèdia mostra un relleu molt irregular, amb** nombrosos **monticles** de fins a 35 m d'alçada **separats per depressions** allargassades, **i una retrodifusió molt variable i lligada als elements morfològics**, amb intensitats molt altes a les depressions i relativament baixes als monticles. **L'àrea deposicional**

[71] *source area*
[72] *depositional area*
[73] *proximal depositional area*
[74] *intermediate depositional area*
[75] *distal depositional area*

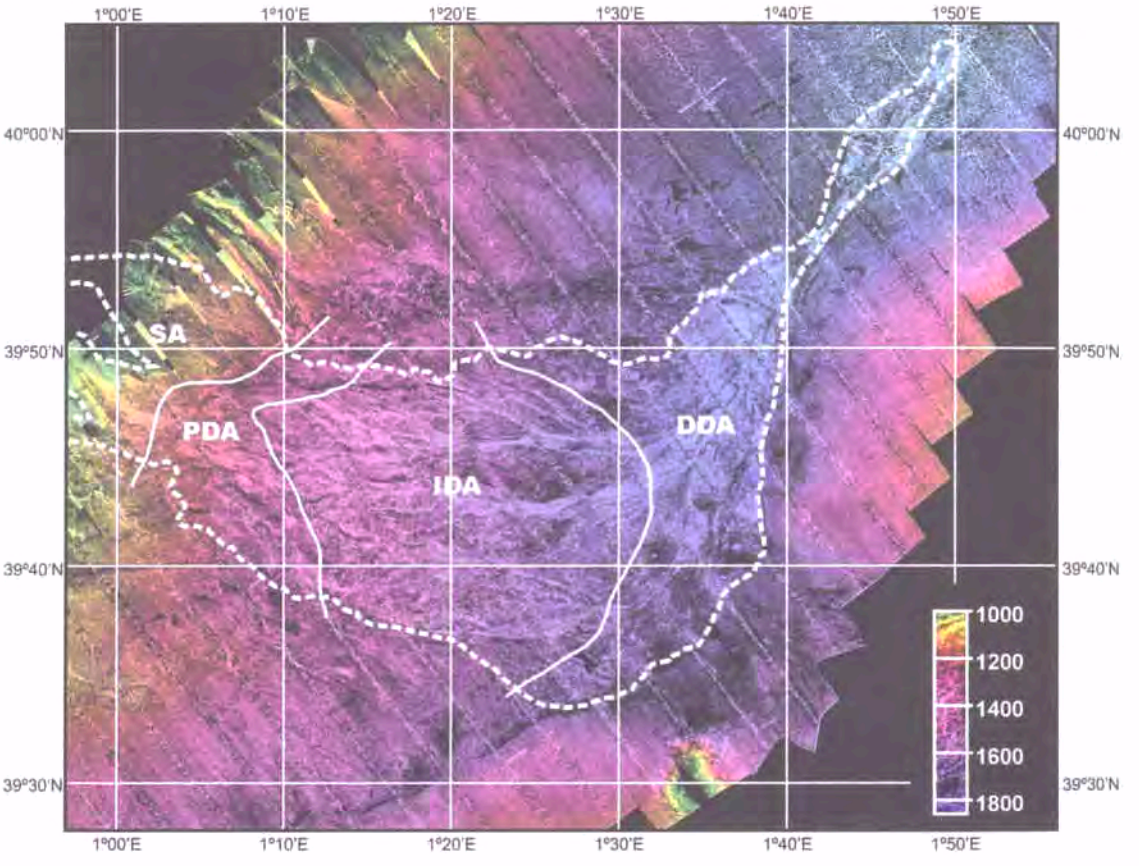

Figura 8.1. *Combinació de batimetria de multifeix (color) i d'intensitat de retrodifusió (tons clars, retrodifusió alta; tons foscos, retrodifusió baixa). Juntament amb altres productes de l'ecosonda de multifeix (Fig. 2.1), ha estat la base per a la distinció de les quatre àrees diferenciades a la regió afectada pel BIG'95: SA (àrea font), PDA (àrea deposicional proximal), IDA (àrea deposicional intermèdia), DDA (àrea deposicional distal). L'escala de profunditats està en metres.*

distal torna a presentar un relleu suau, però la retrodifusió és relativament alta. En el conjunt de l'esllavissament, la intensitat de retrodifusió té una distribució en forma de cua de cavall (Fig. 8.1).

El principal tret morfològic de l'àrea font (Fig. 4.4) és **una gran cicatriu de capçalera** en forma de ferradura oberta cap al SE. **Té una longitud de 20 km, fins a 200 m d'alçada, i un pendent mitjà de 17°**. Les dades d'ecosonda de multifeix i de sonars d'escombrada lateral il·lustren perfectament la seva geometria i morfologia (Figs. 1.23, 3.2, 3.3, i 4.5). Hom pot diferenciar-hi tres seccions. A la part més oriental, la cicatriu està formada per una sèrie d'entre sis i deu esglaons de fins a 10 m d'alçada, a la part central forma un pendent regular, i a la part occidental el salt topogràfic es resol mitjançant dos o tres esglaons de fins a 50 m d'alçada. La morfologia esglaonada de la part oriental de la cicatriu principal del *debris flow* BIG'95 és molt semblant a l'observada en sonografies de TOBI en alguns segments de la cicatriu principal de l'esllavissament gegant de Storegga, al marge noruec (Fig. 8.2; Canals et al., 2004). Hom ha

pogut apreciar, a més, que la cicatriu principal de l'esllavissament BIG'95 mostra certa degradació per petits esllavissaments posteriors (Fig. 8.2).

A banda de la cicatriu principal, a l'àrea font de l'esllavissament BIG'95 **s'han identificat tres cicatrius secundàries** de certa importància (Taula 4.2), totes talús amunt de la cicatriu

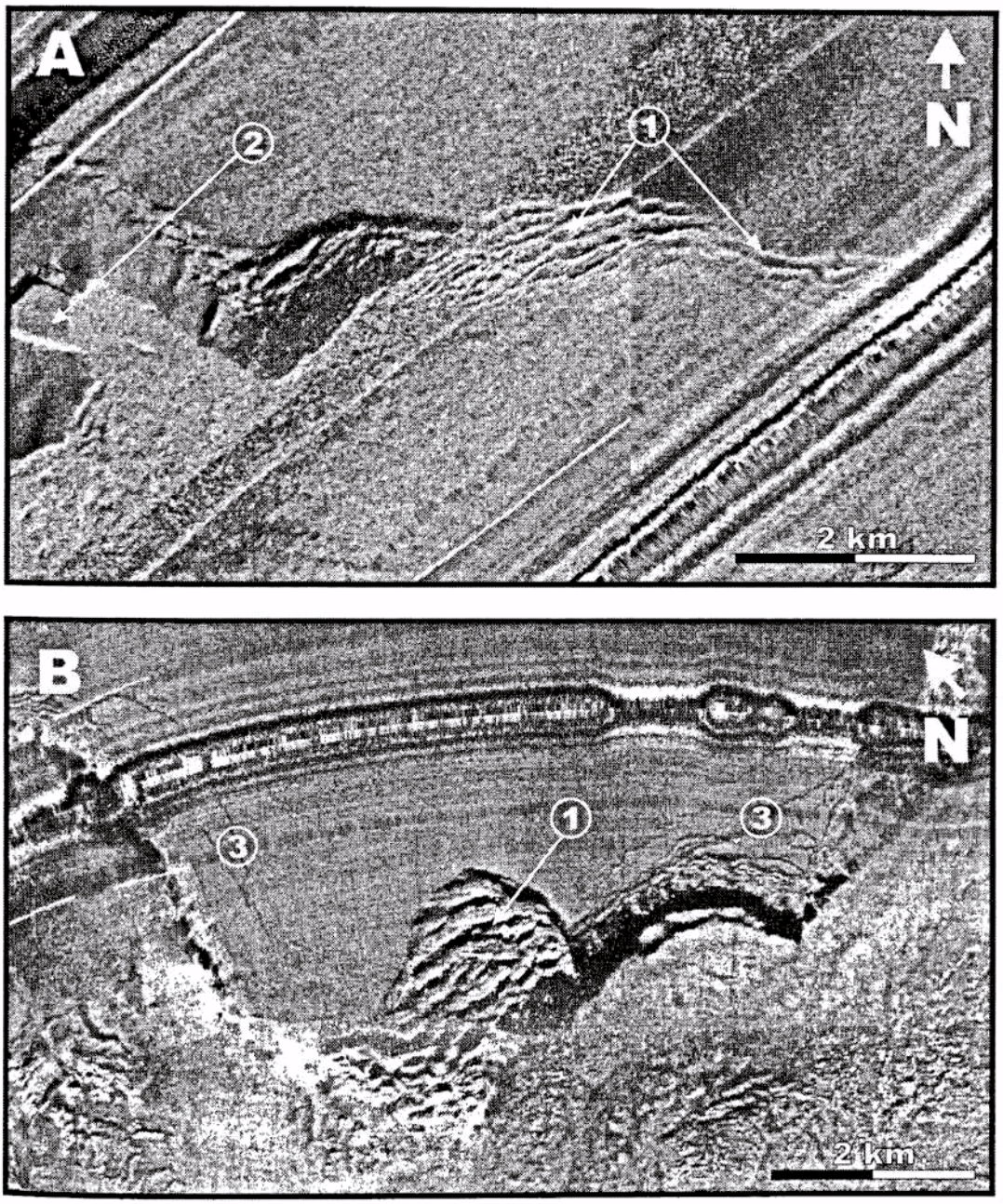

Figura 8.2. Comparació de la cicatriu principal de l'esllavissament BIG'95 (A) amb un petit segment de la cicatriu de l'esllavissament d'Storegga, la qual té més de 500 km de longitud total (B). (1) Morfologia esglaonada, (2) esllavissament posterior que degrada la cicatriu inicial, i (3) cicatrius o fractures de corona. Les dues imatges foren obtingudes amb el sonar d'escombrada lateral immergit en profunditat TOBI (cf. Aptat. 1.3.5). Modificada de Canals et al. (2004).

principal (Figs. 4.4 i 4.7). **Hom ha identificat una quarta cicatriu secundària a l'àrea deposicional proximal** (Fig. 4.3). Les dimensions d'aquestes cicatrius són de fins a 100 m d'alçada, 15 km de longitud i pendents de fins a 11° (Taula 4.2). Llurs geometries són força variables. Els materials alliberats des d'aquestes cicatrius s'incorporaren a la massa esllavissada seguint trajectòries diverses (Fig. 4.4). Hom ha observat cicatrius secundàries en molts esllavissaments: les observades a l'esllavissament GEBRA, a la península Antàrtica, es troben en unes posicions relatives similars a les del BIG'95 (Fig. 8.3; Canals et al., 2004).

L'esllavissament BIG'95 va truncar (Figs. 2.2 i 4.4) diferents **sistemes de canyó-canal i de canal-levée**, en especial a l'àrea font, **mentre que va fossilitzar-ne d'altres** (Figs. 4.13 i 4.15), sobretot **a l'àrea deposicional proximal**. L'ablació gairebé total del curs baix del sistema de canyó-canal de la Figura 8.4, a més d'il·lustrar la capacitat destructiva dels esllavissaments submarins i llur repercussió en la dinàmica sedimentària dels marges continentals, tingué probablement una importància cabdal en la **incorporació de sediment de mida més grollera a la massa esllavissada**.

L'àrea deposicional proximal constitueix el principal depocentre de l'esllavissament, amb acumulacions sedimentàries de fins a 135 m de potència. És una àrea relativament plana, amb pendents de menys d'1°, i de relleu molt suau, amb l'excepció de la part més meridional, on hi ha una de les cicatrius secundàries, de fins a 40 m d'alçada.

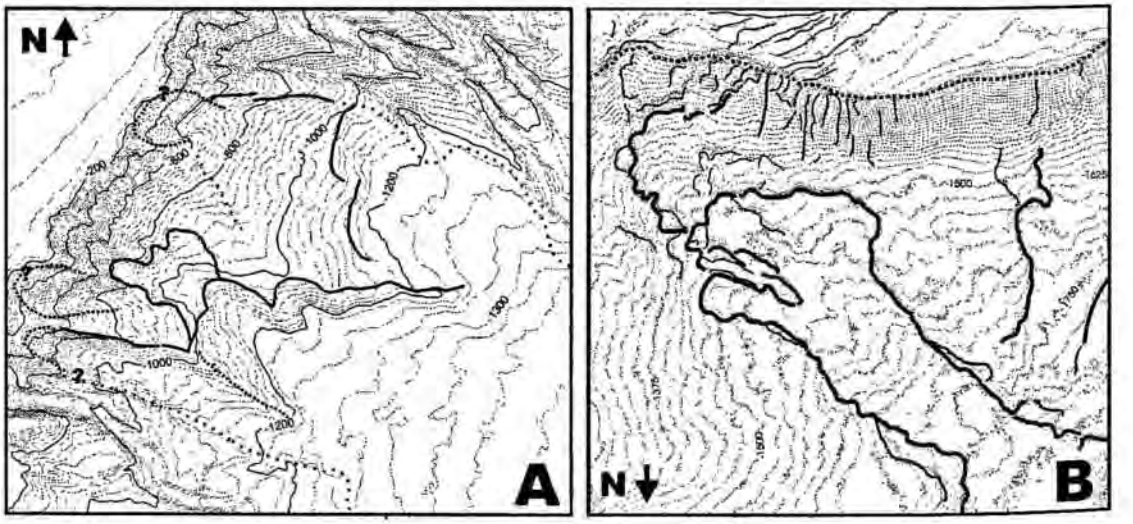

Figura 8.3. *Comparació entre les àrees font dels esllavissaments BIG'95 (A) i GEBRA (B), el segon situat a la península Antàrtica. Tant l'un com l'altre presenten cicatrius secundàries (línies gruixudes, sense tenir en compte la cicatriu principal), talús amunt de la cicatriu principal, gairebé a tocar de la vora de la plataforma continental. Modificada de Canals et al. (2004).*

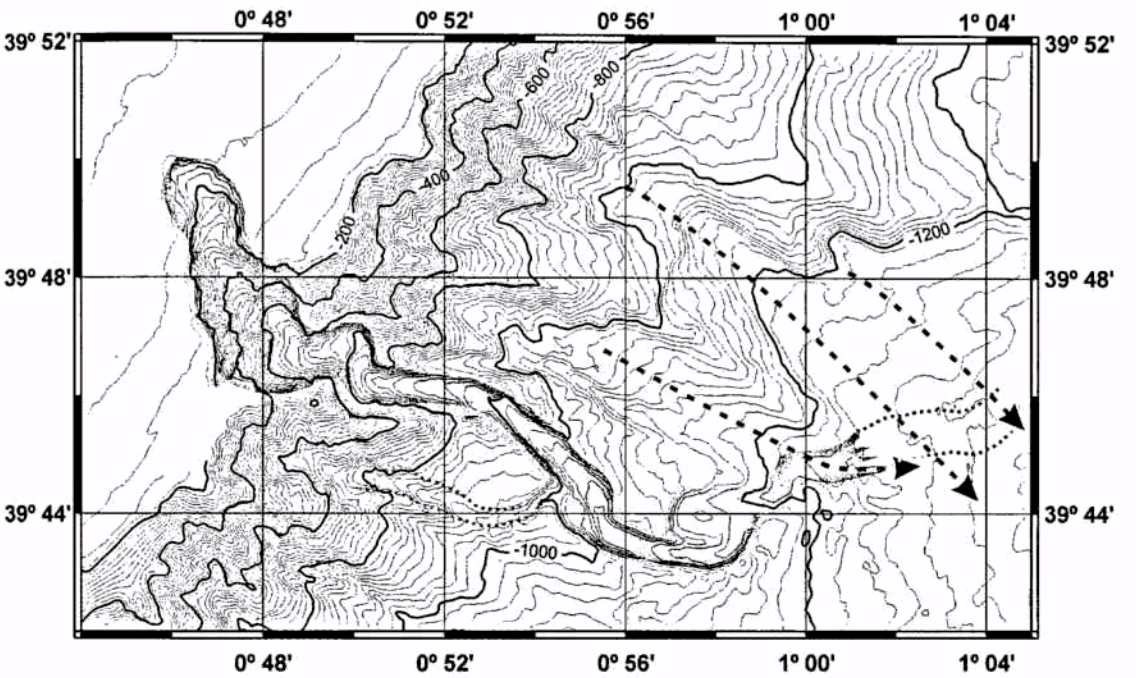

Figura 8.4. Mapa batimètric del talús de l'Ebre al límit meridional de l'esllavissament BIG'95, mostrant l'ablació gairebé total del curs baix d'un sistema de canyó-canal. La destrucció d'aquest sistema comportà la incorporació de sediment més groller a la massa esllavissada. En gris, curs actual del sistema de canyó-canal. Les fletxes en línia discontínua mostren la trajectòria de la massa esllavissada. Isòbates cada 20 m.

L'àrea deposicional intermèdia és la més complexa. **Presenta una sèrie de monticles de sediment de fins a 25 km^2 d'extensió i 35 m d'alçada, de relleu irregular, baixa intensitat de retrodifusió i fàcies sísmica transparent, separats per depressions més o menys lineals, de fons pla i alta intensitat de retrodifusió.** Tant l'ecosonda de multifeix (Figs. 2.1 i 8.1) com el sonar MAK-1M (Fig. 3.5) s'han demostrat molt útils per a estudiar aquesta àrea, encara que amb resolucions molt diferents (Fig. 8.5). Tot i que podria semblar que **els monticles** fossin petits turons testimoni, als perfils de sísmica de molt alta resolució tant de TOPAS (Fig. 2.3) com de 5 kHz (Fig. 8.6) aquests **presenten fàcies sísmica transparent**, posant de manifest el trencament de l'estratificació interna i, per tant, **indicant que el sediment que els conforma també es veié involucrat a l'esllavissament**. De fet, en alguns perfils sísmics s'ha observat el reflector basal de l'esllavissament tant sota les depressions com sota els monticles (Fig. 8.6).

L'àrea deposicional distal es caracteritza per una topografia molt més suau que l'àrea precedent i, en general, **mostra una resposta a la insonificació** molt **similar a** la del material que omple **les depressions** de l'àrea deposicional intermèdia. En els darrers 40 km del seu recorregut, la massa esllavissada es desplaçà confinada dins el canal de València.

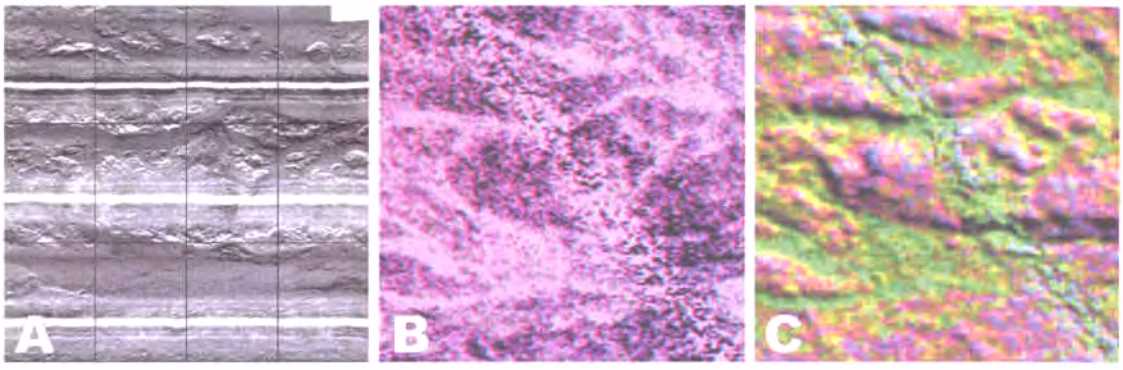

Figura 8.5. *Imatges de sonar d'escombrada lateral MAK-1M (A) i d'ecosonda de multifeix (B, combinació similar a la Fig. 8.1; C, combinació similar a la Fig. 2.1) d'una part de l'àrea deposicional intermèdia entre 39°45' i 39°48'N i entre 1°18' i 1°22'E, mostrant la complexa topografia d'aquesta àrea i les diferències entre els resultats segons el mètode emprat.*

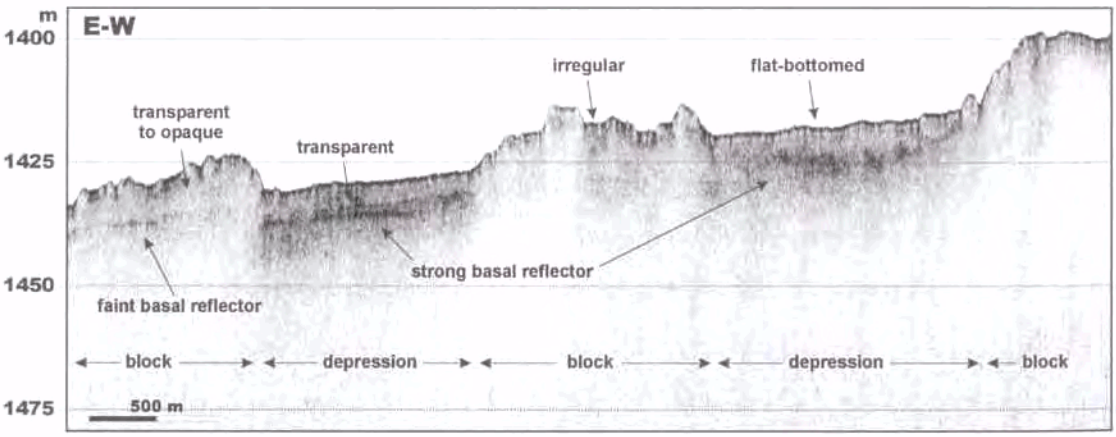

Figura 8.6. *Perfil de sísmica de reflexió de molt alta resolució de 5 kHz pres durant l'adquisició de dades amb el sonar d'escombrada lateral MAK-1M a l'àrea deposicional intermèdia, mostrant la distribució del dipòsit esllavissat, amb fàcies sísmica transparent, en monticles i depressions. Observi's la presència de reflector basal tant sota les depressions, que tenen un fons pla i regular, com, tot i que més difuminat, sota els monticles amb relleu apreciablement irregular.*

8.2. BIG'95: testimonis de sediment

Hom obtingué un total de nou testimonis de sediment de l'esllavissament BIG'95 i rodalies (Fig. 4.3), dos a l'àrea font (Fig. 8.7), un a l'àrea deposicional proximal (Fig. 8.8), dos a la intermèdia (Fig. 8.9), dos a la distal i dos més fora de l'esllavissament (Taula 4.1). **En tots els testimonis hom pogué identificar el sediment de pre-, sin- i post-esllavissament** (cf. Capítol 5 i Fig. 6.3) mitjançant l'observació directa i les dades obtingudes amb el *core logger* (per exemple, la densitat del sediment, il·lustrada a la Fig. 8.10). **El sediment de post-esllavissament està representat per** una capa de 20 a 120 cm de gruix de **sediment hemipelàgic** fangós i oxidat, i és present en tots els testimonis (Figs. 8.7, 8.8, 8.9 i 8.10).

Aquesta capa està **en contacte directe amb el sediment esllavissat** en els testimonis situats dins l'àrea deposicional (per exemple, Figs. 8.7 i 8.10). El sediment esllavissat és **constituït per fang llimós i arenós i sorres, amb laminació** trencada, plegada i **convoluta** o, simplement, sense laminació, i amb **còdols tous** (vegi's, per exemple, el sostre de la tercera secció a la Fig. 8.7, o l'interval de 25 a 80 cm de la segona secció a la Fig. 8.8). Les característiques del sediment de pre-esllavissament poden observar-se a partir dels 55 cm de la tercera secció a la Figura 8.7.

Les anàlisis granulomètriques (Fig. 6.3) indiquen un **alt contingut de material groller als testimonis CLKS-05** (àrea deposicional proximal), **CLKS-06** i **CLKS-07** (àrea deposicional distal), i **CLKS-02** (fora de l'esllavissament, al flanc d'un sistema de canyó-canal). Els dos testimonis de gravetat de l'àrea deposicional intermèdia no han estat analitzats, però llurs descripcions visuals indiquen sediments més grollers al testimoni **278G**, situat en una de les depressions, que al testimoni 277G, situat en un monticle.

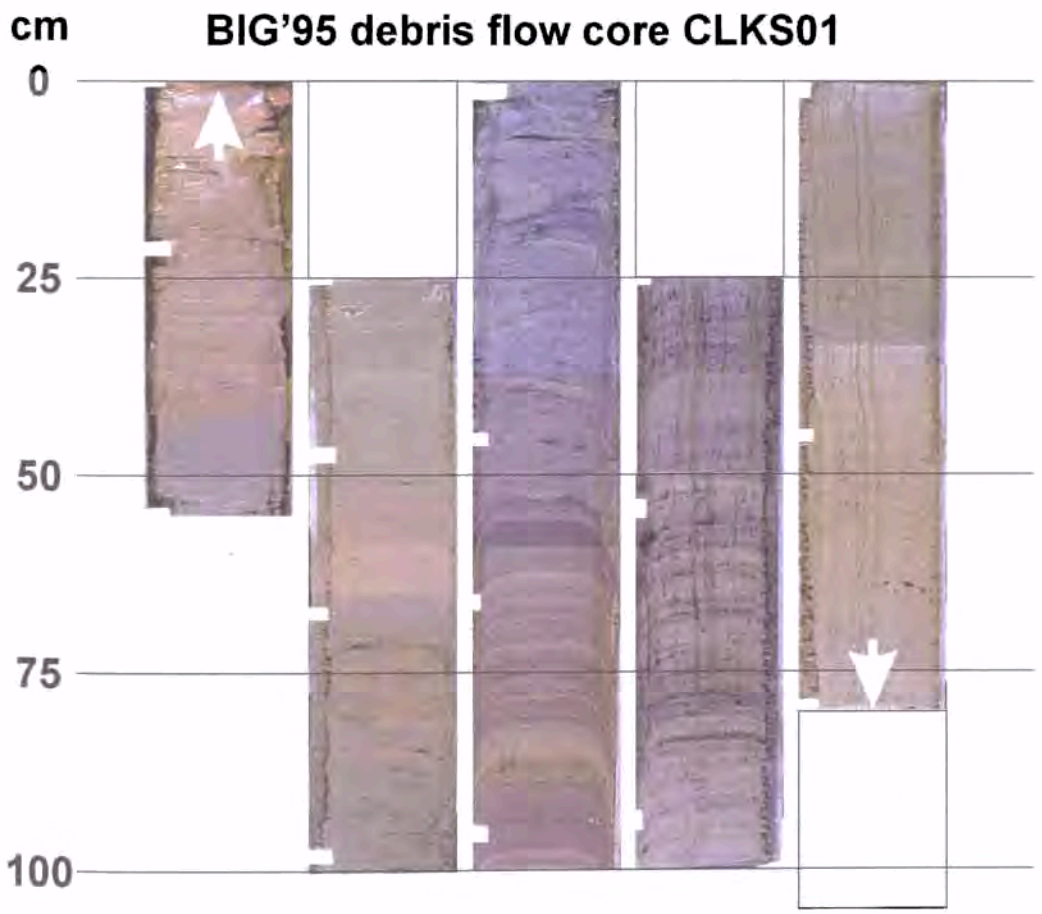

Figura 8.7. *Fotografia en fals color del testimoni de pistó CLKS-01. Observi's la capa hemipelàgica de post-esllavissament entre els 0 cm de la primera secció i els ~70 cm de la segona, i la debrita fins els 55 cm de la tercera secció. Els rectangles blancs representen seccions tallades per a fer assaigs edomètrics. Interpretació i anàlisis a la Fig. 8.10.*

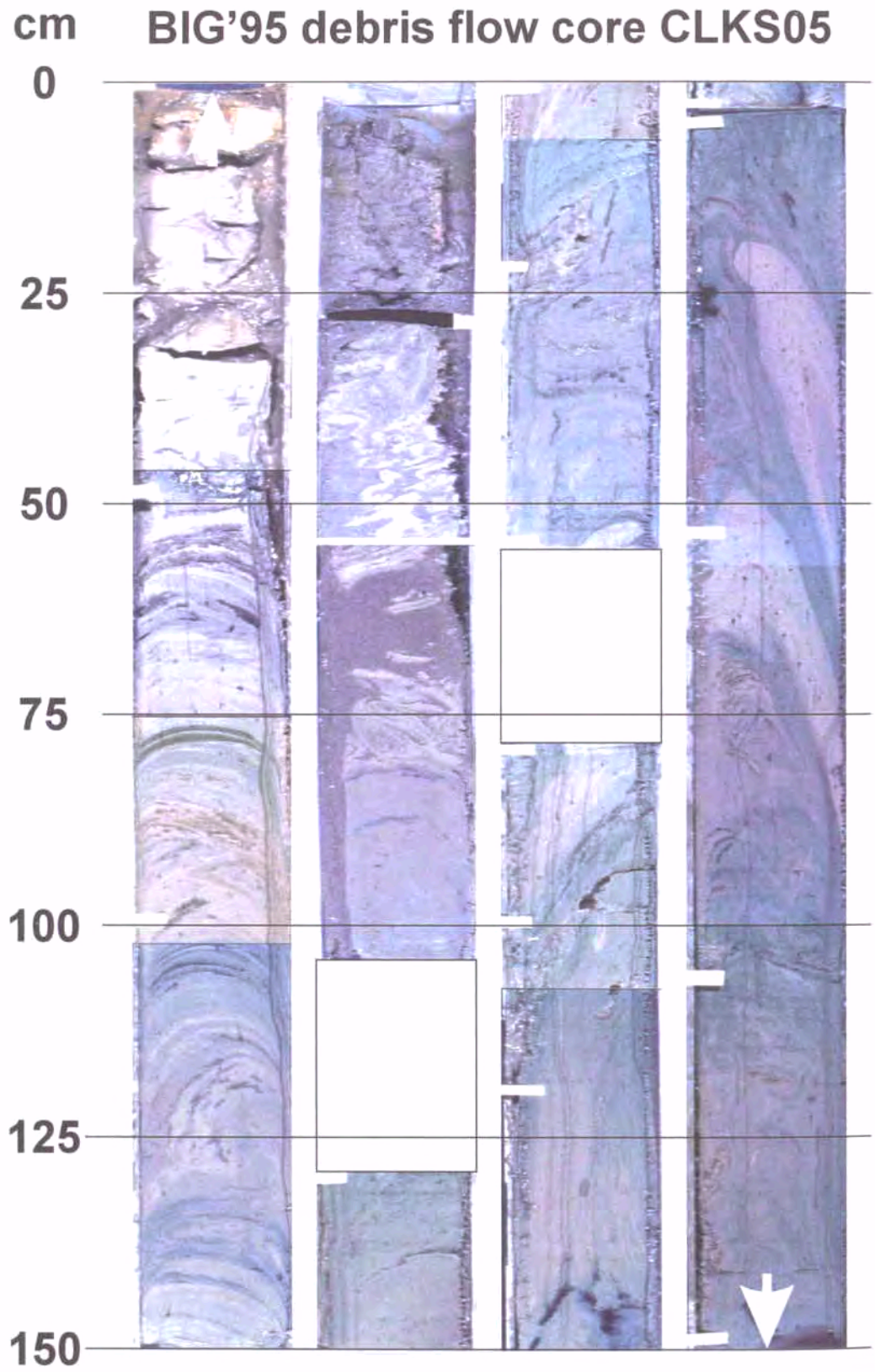

Figura 8.8. *Fotografia en fals color del testimoni de pistó CLKS-05. Observi's la capa hemipelàgica de post-esllavissament entre els 0 i els 35 cm de la primera secció, i la debrita que ocupa la resta del testimoni, amb còdols d'argila en una matriu sorrenca (secció 2, 50 cm), i laminació convoluta (secció 1, 120 cm, o tota la secció 4). Els rectangles blancs representen seccions tallades per a fer assaigs edomètrics.*

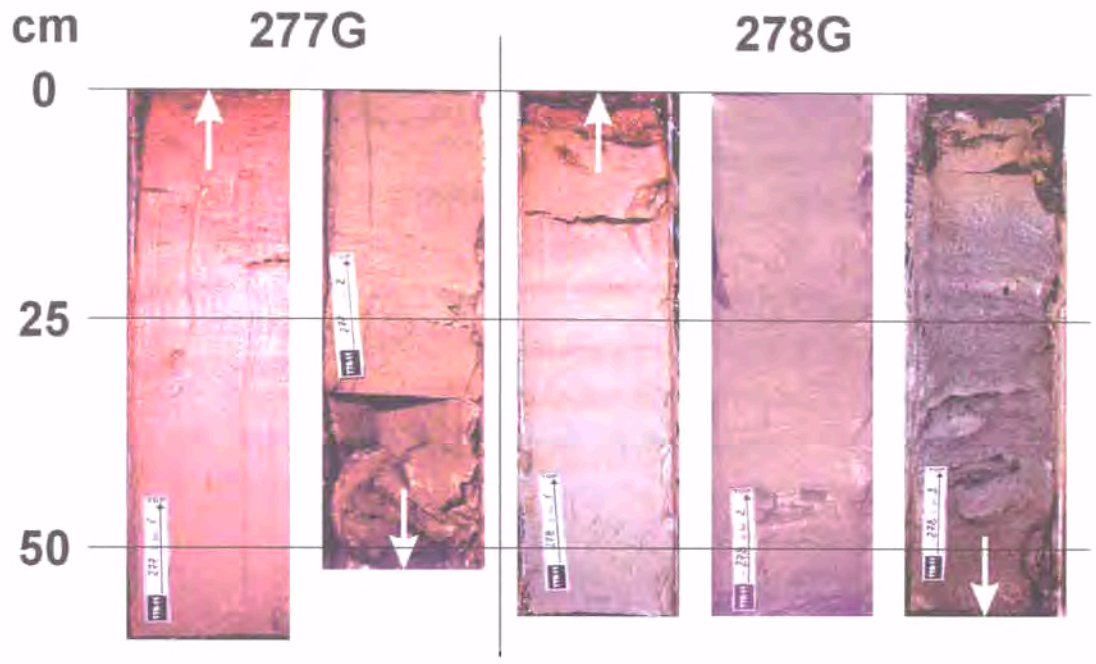

Figura 8.9. *Fotografia en falsos color dels testimonis de gravetat 277G (les dues seccions de l'esquerra) i 278G (les tres seccions de la dreta). El 277G va ésser obtingut en un monticle i el 278G en una depressió de l'àrea deposicional intermèdia. A grans trets, el segon sembla contenir sediment més sorrenc que el primer.*

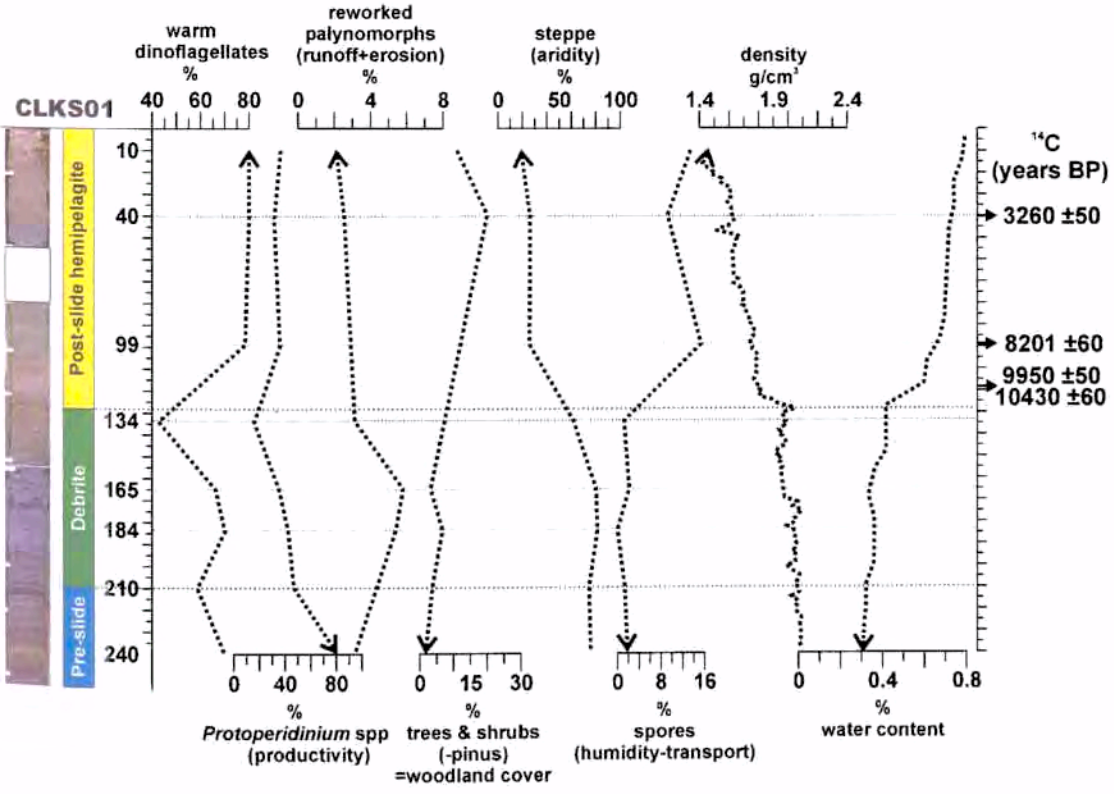

Figura 8.10. *Interpretació del testimoni de pistó CLKS-01 (Fig. 8.7), resultats dels comptatges de dinoflagel·lats i pol·len, de les mesures de densitat i contingut d' aigua en el sediment, i datacions per ^{14}C AMS.*

Per a realitzar les anàlisis de ^{14}C AMS hom decidí mostrejar el sediment hemipelàgic de post-esllavissament, en especial la seva base, molt a prop del contacte amb la unitat esllavissada, cosa que havia de permetre obtenir una data mínima per a l'esllavissament. Els resultats obtinguts (Taula 4.4, Fig. 8.10) daten l'esllavissament entre 10.490 i 10.190 anys de ^{14}C BP o, el que és el mateix, entre **11.647 i 11.129 anys de calendari AP**.

Les mostres de la unitat esllavissada tenen menys quantitat d'espècimens de dinoflagel·lats d'ambients càlids, menys espores i més espècimens esteparis que les mostres de la unitat hemipelàgica (Fig. 8.10). Això indicaria que **el sediment remobilitzat es dipositá en un ambient més fred, àrid i sec que l'actual**. Aquestes dades s'adiuen amb els resultats de la datació per ^{14}C de l'esllavissament, molt a prop del final de l'Últim Màxim Glacial.

8.3. BIG'95: modelització

El model conceptual de la dinàmica de l'esllavissament BIG'95 s'elaborà a partir de la morfologia del dipòsit esllavissat, la intensitat de retrodifusió, les estructures observades i l'anàlisi dels testimonis de sediment. Segons aquest model, **a les depressions i als monticles hi hauria materials d'origen diferent**. **Les depressions** estarien ocupades **per material relativament més groller**, més ric en sorra, **provinent de la cicatriu principal i de les secundàries situades talús amunt, i de l'ablació del sistema de canyó-canal** (Fig. 8.4) que era alimentat amb material sorrenc provinent de la plataforma continental (Fig. 1.5). **Els monticles estarien formats per material més fi i compacte, alliberat en** el límit entre **l'àrea deposicional proximal** i l'àrea deposicional intermèdia; per exemple, de la cicatriu secundària "E" de la Fig. 4.3, i de cicatrius en una posició similar recobertes pel dipòsit de l'esllavissament). **Durant el moviment**, aquests materials, constituïts en blocs de sediment, **haurien mantingut parcialment la seva cohesió interna** de manera suficient per a mantenir-se prou compactes i formar els monticles actuals, tot i que insuficientment per a mostrar estratificació als perfils sísmics. En canvi, **el material més groller** de les depressions **hauria estat completament remotllat** i podria haver incorporat força aigua durant el moviment, cosa que hauria afavorit l'acceleració del mateix. **Aquest material hauria empès i accelerat els blocs de sediment**, facilitant alhora el seu trencament. Donat que **l'energia involucrada** anà disminuint per la suavització del pendent i per la fricció interna, arribà un moment en què **deixà de ser suficient per a mantenir els blocs en moviment**. Aquests quedaren aleshores "congelats" **a l'àrea deposicional intermèdia**. En canvi, **el material solt més groller continuà el seu moviment fins a l'àrea deposicional distal**. A l'etapa final, el moviment es veié possiblement **reforçat per la canalització del flux** dins el canal de València.

Hom ha pogut demostrar que aquest model conceptual, basat en la interpretació dels fets observats, és físicament possible. Així, s'ha dut a terme una simulació numèrica amb el programari *BING* modificat per tal d'incloure la presència de blocs. Les limitacions de la simulació numèrica han fet, però, que s'hagin hagut de prendre valors de resistència a la cisalla del material groller per sota dels mesurats en els testimonis de sediment. Aquests podrien ésser justificats per la incorporació d'aigua[76] al sediment durant l'esllavissada. Tampoc es va tenir en compte a la simulació el possible atrapament de material groller sota els blocs en moviment ni l'hidroplanament basal de la massa esllavissada.

8.4. BIG'95: mecanismes de dispar

La interpretació de les dades obtingudes **ha proposat els següents mecanismes de dispar** per a l'esllavissament BIG'95: (1) un **comportament mecànic diferencial** entre les roques que formen el dom volcànic observat sota l'esllavissament (Fig. 4.10) i el recobriment sedimentari Plio-Quaternari, **resolt mitjançant la formació** i la propagació **d'una falla normal** que travessa tota la columna sedimentària fins al fons marí; (2) la sobrecàrrega i la sobreinclinació del talús superior degut a una **sedimentació molt ràpida** possiblement lligada amb nivells del mar baixos i amb antigues goles de l'Ebre (Farran i Maldonado, 1990; Fig. 5.6); (3) **l'escapament de fluids del sediment associat al canvi en la temperatura de l'aigua** propera al fons marí ocorregut durant la transició glacial-Holocè, tot i que no s'han observats indicis evidents d'estructures d'escapament de fluids a l'àrea del BIG'95; (4) **la sismicitat** que afecta secularment al marge oriental de la península Ibèrica, tot i ésser de tipus passiu, amb esdeveniments sísmics prou importants per a donar llocs a acceleracions que provoquin la liqüefacció del sediment.

No hi ha forma de demostrar quin fou el factor de dispar definitiu de l'esllavissament BIG'95, però **tot apunta a una combinació dels quatre citats**. Els dos primers representen factors d'inestabilitat persistents i inherents del marge de l'Ebre. Fan minvar la resistència a la cisalla del sediment. Els altres dos són factors d'inestabilitat puntuals que podrien haver provocat l'esfondrament d'un marge propens a desestabilitzar-se. La presència d'altres masses esllavissades intercalades dins la seqüència sedimentària (Fig. 4.11) demostra la inestabilitat recurrent del marge de l'Ebre, on sembla probable que alguns esdeveniments responguin a dispars sísmics mentre que altres ho facin a canvis ambientals d'abast global.

[76] *wetting*

8.5. Esllavissaments del canal d'Eivissa

Hom ha identificat quatre esllavissaments al marge balear del sector meridional del **canal d'Eivissa, tots ells a profunditats d'entre 600 i 900 m, amb àrees afectades per sota dels 16 km^3 i volums inferiors a 0.4 km^3** (Fig. 7.3). En general, llurs cicatrius de capçalera tenen forma de ferradura i els seus respectius lòbuls deposicionals mostren relleu positiu respecte la resta del canal d'Eivissa. Els dipòsits d'esllavissament estan constituïts per fàcies sísmica transparent, localment caòtica a la part més distal dels lòbuls, tot i que hom ha pogut observar blocs amb fàcies sísmica estratificada dins els mateixos dipòsits esllavissats.

Els quatre esllavissaments estudiats **comparteixen el mateix pla de lliscament**: un reflector continu de gran amplitud que pot identificar-se a tot el marge balear del canal d'Eivissa (Fig. 7.9). **La presència de gran quantitat d'estructures relacionades amb l'escapament de fluids suggereix certa existència de fluids en el sediment**, la qual cosa, sumada a l'ocurrència d'un nivell feble[77], o nivell predisposat a la inestabilitat, afegeix elements de judici a l'hora d'apuntar quin és el mecanisme de dispar capaç de produir quatre esllavissaments, presumiblement simultanis, a la mateixa àrea.

8.6. Comparació amb altres esllavissaments arreu del món

L'esllavissament BIG'95 és un dels més extensos i voluminosos de la Mediterrània occidental (Taula 8.1), només comparable als observats al golf de Lleó, alguns dels quals superen els 100 km^3 de volum (Droz et al., 2001), i a la megaturbidita de la plana abissal de Balears, d'uns 500 km^3 de volum (Rothwell et al., 2000). És, en canvi, molt modest si el comparem amb els observats al marge de Noruega: l'esllavissament de Storegga gairebé afecta una àrea dos ordres de magnitud superior (Taula 8.1). Canals et al. (2004) presenta l'estudi integrat de diversos esllavissaments submarins dels marges continentals europeus, entre els quals s'inclou l'esllavissament BIG'95.

Els quatre esllavissaments del canal d'Eivissa són comparables amb l'esllavissament d'Afen, situat al canal de les Feroe – Shetland, al nord de les illes Britàniques, no tant per les seves mides (Taula 8.1) sinó **per llur geometria i la disposició de llurs lòbuls deposicionals** (Masson, 2001).

[77] *weak layer*

Nom	Àrea (km^2)	Profunditat (m)	Gruix màx. / mig (m)	Volum (km^3)	Pendent mitjà del talús (°)	Cicatrius		Recorregut (km)
						Número	Alçada (m)	
Storegga	90.000	130-3.850	200 / 60	<3.000	1,5	Moltes	>400	770
Trænadjupet	14.100	400-3.000	150 / 100	900	2,0	>2	<150	200
BIG'95	2.200	200-2.000	135 / 16	26	1,5	>5	<200	110
GEBRA	515	900-1.950	135 / 135	21	0,4	2	<160	70
Afen	40	825-1.120	20 / 10	0,2	1,5	3	<10	7
Ana	6	635-815	44 / 23	0,14	1,6	1	<30	<5
Joan	16	600-870	? / 25	0,4	2,5	1	10	<5
Nuna	10	675-860	50 / 30	0,41	3,0	2	20	<5
Jersi	8	755-910	50 / 25	0,15	1,9	1	10	<5

Taula 8.1. *Comparativa de les dades bàsiques dels esllavissaments BIG'95 i del canal d'Eivissa amb els esllavissaments d'Storegga i de Trænadjupet, al marge noruec, l'esllavissament GEBRA, a la península Antàrtica, i l'esllavissament d'Afen, al canal de les Feroe – Shetland. Dades pròpies i de Canals et al. (2004).*

No deixa de cridar l'atenció la notable quantitat de dipòsits d'esllavissament a la part més alta de la columna sedimentària a tota la Mediterrània occidental, incloent-hi els esllavissaments del canal d'Eivissa, alguns d'ells amb edats molt properes a la de l'esllavissament BIG'95. Com ja s'ha mostrat, l'esllavissament BIG'95 ocorregué fa uns 11.500 anys de calendari AP, pràcticament al límit entre el Pleistocè i l'Holocè, al final del Darrer Màxim Glacial. Durant aquest període també s'emplaçaren els anomenats esllavissament occidental (Droz et al., 2001) i oriental (Droz i Bellaiche, 1985) del ventall del Roine al Golf de Lleó. La megaturbidita de la plana abissal de Balears, de la qual encara no s'ha pogut identificar l'àrea font, s'emplaçà abans, fa uns 22.000 anys AP (Rothwell et al., 1998, 2000), durant el Darrer Màxim Glacial, quan el nivell del mar de la Mediterrània tot just banyava les vores de plataforma actuals.

CAPÍTOL 9

CONCLUSIONS

L'esllavissament BIG'95 afectà 2.200 km^2 del marge continental de l'Ebre, entre 39°30'N i 40°10'N i entre 0°55'E i 1°55'E, a profunditats compreses entre 600 i gairebé 2.000 m. El dipòsit resultant, amb un volum de 26 km^3, recobreix 2.000 km^2 del talús i el glacis del marge de l'Ebre i part del canal de València. En general, el dipòsit presenta fàcies sísmica transparent, en contrast amb la fàcies sísmica estratificada dominant al Plio-Quaternari del Mar Catalano-balear.

La cicatriu principal de l'esllavissament BIG'95 se situa entre 600 i 1.230 m de profunditat, té una llargària d'uns 20 km i una alçada màxima de 200 m. En la seva part oriental presenta una morfologia esglaonada, mentre que a la part occidental el salt topogràfic es resol mitjançant un pendent regular de fins a 17° d'inclinació o a través de dos o tres escarpaments individuals de fins a 50 m d'alçada. És la expressió en superficie d'una falla normal vergent cap al nord relacionada amb un dom volcànic que forma part del camp volcànic de les illes Columbretes.

Quatre cicatrius secundàries majors, a part d'altres menys importants, han estat identificades tant talús amunt com talús avall de la cicatriu principal. Aquestes cicatrius, d'entre 40 i 100 m d'alçada, se situen a profunditats d'entre 600 i 1.350 m. La seva presència és indicativa de la complexitat de l'esllavissament BIG'95.

Dins la regió afectada, s'ha diferenciat quatre grans àrees. L'àrea font, de la qual pràcticament tot el sediment mobilitzat va ésser desallotjat, deixant només un dipòsit de menys de 20 m de potència, conté la cicatriu principal i la majoria de les secundàries. L'àrea deposicional proximal és el principal depocentre de l'esllavissament, amb acumulacions de fins a 135 m de potència. L'àrea deposicional intermèdia, amb una potència mitjana de 10 m, presenta una sèrie de monticles irregulars de fins a 35 m d'alçada i 25 km^2 de superfície, separats per depressions lineals i de fons pla, essent llur resposta a la insonificació totalment diferent. L'àrea deposicional distal presenta gruixos inferiors a 10 m, excepte al canal de València, on arriba a tenir 35 m de potència. Té una resposta a la insonificació molt similar a la de les depressions de l'àrea deposicional intermèdia.

L'esllavissament BIG'95 va rejovenir el talús superior, destruint o colmatant diferents sistemes de canyó-canal i de canal-levée.

Els testimonis de sediment obtinguts a les àrees deposicionals mostren més alt contingut en material groller que els obtinguts a l'àrea font. Aquest fet, i les diferents retrodifusions observades dins la massa esllavissada, indiquen que aquesta està formada per dos tipus de materials amb un origen i un comportament mecànic diferenciats. El material que forma

majoritàriament l'àrea deposicional proximal, ocupa les depressions de l'àrea intermèdia i tota l'àrea distal, prové de la cicatriu principal i de les secundàries que hi ha talús amunt, i de l'ablació de, com a mínim, un sistema de canyó-canal. Aquest material presenta, a grans trets, una mobilitat relativament alta, atribuïble al fet d'haver estat fortament retreballat, ser granulomètricament força groller i haver incorporat aigua durant el transport. Aquest material més mòbil va empènyer i accelerar al llarg de més de 20 km grans blocs de sediment des de les àrees deposicionals proximal i intermèdia, fets de material més fi i cohesiu. Un cop l'energia esdevingué insuficient, els blocs quedaren aturats, generant-se així el relleu característic de l'àrea deposicional intermèdia. Mentrestant, el material més mòbil continuà fins al canal de València, aturant-se uns 110 km enllà de l'àrea font. Aquest model conceptual de la dinàmica sedimentària de l'esllavissament BIG'95 ha estat provat com a físicament possible mitjançant simulacions numèriques.

Datacions pel mètode de ^{14}C AMS indiquen que l'esllavissament BIG'95 va ocórrer entre 11.647 i 11.129 anys de calendari AP. Hom apunta la presència del dom volcànic i la falla associada, la sobrecàrrega i el sobrependent del talús, l'escapament de fluids del fons per canvis en la temperatura de l'aigua de fons, i la sismicitat, com els principals factors d'inestabilitat del marge de l'Ebre.

Quatre esllavissaments de mida relativament petita afecten el marge balear del canal d'Eivissa a profunditats d'entre 600 i 900 m. Tots ells presenten, en general, fàcies sísmica transparent, en contrast amb la fàcies sísmica estratificada de la resta del Plio-Quaternari del canal d'Eivissa. Localment, però, s'han observat blocs estratificats dins les masses esllavissades. L'esllavissament d'Ana, el dipòsit del qual té 0,11 km^3, està centrat a 38°38'30"N i 0°49'E, i afecta 6 km^2 del fons marí. L'esllavissament de Joan, centrat a 38°41'N i 0°48'E, afecta 16 km^2 del fons marí i presenta una cicatriu de fins a 10 m d'alçada. El dipòsit de l'esllavissament de Nuna, a 38°43'30"N i 0°48'E, és el resultat de dos esdeveniments que afectaren 10,3 km^2 del fons marí. Per últim, l'esllavissament de Jersi, a 38°47'30"N i 0°47'E, presenta una cicatriu de fins a 15 m d'alçada i afecta una àrea d'uns 7,9 km^2.

Els quatre esllavissaments comparteixen un mateix pla de lliscament, corresponent a un reflector d'alta amplitud i gran continuïtat, que probablement respon al concepte de nivell feble. A més, les cicatrius principals dels esllavissaments d'Ana i de Nuna estan relacionades amb estructures de tipus pockmark, molt abundants a tot el marge balear i al nord del mont de Xàbia,

de manera que pot establir-se una relació entre l'escapament de fluids i la inestabilitat d'aquest indret en particular.

Aquests quatre esllavissaments són el darrer gran esdeveniment sedimentari del canal d'Eivissa, ja que es troben al capdamunt de la sèrie quaternària, i probablement varen ocórrer simultàniament, cosa que implica un mecanisme capaç de generar un increment de l'escapament de fluids en un curt període de temps, com pot ser un terratrèmol. Aital increment hauria estat capaç d'afeblir la resistència a la cisalla del recobriment sedimentari superficial fins a generar el seguit d'esllavissaments observat.

Les Tesis Doctorals aporten respostes i un increment del coneixement, però també és freqüent que obrin noves vies i permetin plantejar noves qüestions. En el nostre cas, n'hi hauria quatre de principals.

Convindria estendre l'estudi efectuat al conjunt dels marges del Mar Catalano-balear amb l'objectiu de conèixer la freqüència de la inestabilitat, tant recent com antiga, d'identificar els indrets on aquesta és més recurrent, i d'elaborar una anàlisi acurada de riscs geològics.

L'esllavissament BIG'95 sembla tenir un potencial tsunamigènic cert. Per tant, convindria simular el possible tsunami que hauria estat capaç de generar, a fi i efecte de conèixer quins podrien ser els trams costaners afectats per un esdeveniment d'aquestes característiques si es reproduís en un futur indeterminat.

També és altament interessant determinar la naturalesa exacta del pla de lliscament dels quatre esllavissaments del canal d'Eivissa, i si aquest pla de lliscament és el producte d'algun canvi a gran escala en les condicions ambientals regionals. Caldria obtenir mostres dels materials implicats en aquests esllavissaments per a poder caracteritzar-los sedimentològicament i emprar-los en simulacions numèriques.

Convindria datar amb exactitud els quatre esllavissaments del canal d'Eivissa i, en el cas d'ésser propera la seva edat a la de l'esllavissament BIG'95 i d'altres esllavissaments a la Mediterrània occidental, cercar les causes de tal període d'inestabilització regional.

CAPÍTOL 10

BIBLIOGRAFIA

Acosta, J., Muñoz, A., Herranz, P., Palomo, C., Ballesteros, M., Vaquero, M., Uchupi, E., 2001, Pockmarks in the Ibiza Channel and western end of the Balearic Promontory (western Mediterranean) revealed by multibeam mapping: *Geo-Marine Letters*, v. 21, p. 123-130.

Acosta, J., Canals, M., López-Martínez, J., Muñoz, A., Herranz, P., Urgeles, R., Palomo, C., Casamor, J.L., 2002, The Balearic Promontory geomorphology (western Mediterranean): morphostructure and active processes: *Geomorphology*, v. 49, p. 177-204.

Alla, G., Dessolin, D., Leenhardt, O., Pierrot, S., 1972, Données du sondage sismique continu concernant la sedimentation Plio-quaternaire en Mediterranée nord-occidental. A: D.J. Stanley (ed.), *The Mediterranean Sea: A Natural Sedimentation Laboratory*: Dowden, Hutchinson & Ross, Stroudsburg, USA, p. 471-481.

Almagor, G., 1984, Salt-controlled slumping on the Mediterranean slope of central Israel: *Marine Geophysical Researches*, v. 6, p. 227-243.

Alonso, B., Maldonado, A., 1990, Late quaternary sedimentation patterns of the Ebro turbidite systems (northwestern Mediterranean): Two styles of deep-sea deposition. A: C.H. Nelson, A. Maldonado (eds.), The Ebro Continental Margin, Northwestern Mediterranean Sea: *Marine Geology*, v. 95, p. 353-377.

Alonso, B., Canals, M., Palanques, A., Rehault, J.P., 1985, A deep-sea channel in the Northwestern Mediterranean Sea: morphology and seismic structure of the Valencia Channel and its surroundings: *Marine Geophysical Researches*, v. 17, p. 469-484.

Alonso, B., Field, M.E., Gardner, J.V., Maldonado, A., 1990, Sedimentary evolution of the Pliocene and Pleistocene Ebro margin, northeastern Spain. A: C.H. Nelson, A. Maldonado (eds.), The Ebro Continental Margin, Northwestern Mediterranean Sea: *Marine Geology*, v. 95, p. 313-331.

Alonso, B., Canals, M., Got, H., Maldonado, A., 1991, Seavalleys amd related depositional systems in the Catalan Sea (northwestern Mediterranean Sea): *AAPG Bulletin*, v. 75, p. 1195-1214.

Aparicio, A., Mitjavila, J.M., Araña, V., Villa, I.M., 1991, La edad del volcanismo de las islas Columbrete Grande y Alborán (Mediterráneo occidental): *Boletín Geológico y Minero*, v. 102-104, p. 562-570.

Argand, E., 1916, Sur l'arc des Alpes Occidentales: *Eclogae Geologica Helvetica*, v. 14, p. 145-191.

Arnau, P., Liquete, C., Canals, M., 2003, Flood events and plume dispersal on the Spanish Mediterranean continental shelf: *ComDelta Open Conference, Comparing Mediterranean and Black Sea Prodeltas*, Abstract volume, p. 6.

Baraza, J., Casas, D., 1998, *Informe preliminar. Muestreo y análisis geotécnico de los testigos CALMAR-97*: Grupo de Geología, ICM, CSIC, Barcelona, Espanya, 37 pp., (inèdit).

Barley, B., 1999, Deepwater problems around the world: *Leading Edge*, v. 18, p. 488-494.

Bart, P.J., De Batist, M., Jokat, W., 1999, Interglacial collapse of Crary Trough-Mouth Fan, Weddell Sea, Antarctica: Implications for Antarctic glacial history: *Journal of Sedimentary Research*, v. 69, p. 1276-1289.

Bartolini, C., Gehin, C., Stanley, D.J., 1972, Morphology and recent sediments of the Western Alboran Basin in the Mediterranean Sea: *Marine Geology*, v. 13, p. 159-224.

Bea, R.G., 1971, How sea floor slides affect offshore structures: *Oil and Gas Journal*, v. 69, p. 88-92.

Bea, R.G., Wright, S.G., Sicar, P., Niedoroda, A.W., 1983, Wave-induced slides in South Pass Block 70, Mississippi delta: *Journal of Geotechnical Engineering*, v. 109, p. 619-644.

Berné, S., Loubrieu, B., equip CALMAR embarcat, 1999, Canyons et processus sédimentaires récents sur la marge occidentale du golfe du Lion. Premiers résultats de la campagne Calmar: *Comptes Rendus de l'Academie des Sciences de Paris*, v. 328, p. 471-477.

Biju-Duval, B., Montadert, L., 1977, Introduction to the structural history of the Mediterranean Basins. A: B. Biju Duval, L. Montadert (eds.), *Structural History of the Mediterranean Basin*: Technip, França, p. 1-12.

Blondel, P., Murton, B.J. (eds.), 1997, *Handbook of seafloor sonar imagery*: John Wiley and Sons, Chichester, Regne Unit, 314 pp.

Bondevik, S., Svendsen, J.I., Johnsen, G., Mangerud, J., Kaland, P.E., 1997, The Storegga tsunami along the Norwegian coast, its age and runup: *Boreas*, v. 26, p. 29-53.

Bryn, P., Solheim, A., Berg, K., Lien, R., Forsberg, C.F., Haflidason, H., Ottesen, D., Rise, R., 2003, The Storegga slide complex: repeated large scale sliding in response to climatic ciclicity. A: J. Locat, J. Mienert (eds.), *Submarine Mass Movements and Their Consequences*: Kluwer Academic Publishers, Holanda, p. 215-222.

Bugge, T., 1983, Submarine slides on the Norwegian continental margin, with special emphasis on the Storegga area: *Continental Shelf Institute Publication*, v. 110, 152 pp.

Bugge, T., Befring, S., Belderson, R.H., Eidvin, T., Jansen, E., Kenyon, N.H., Holtedahl, H., Sejrup, H.P., 1987, A giant three-stage submarine slide off Norway: *Geo-Marine Letters*, v. 7, p. 191-198.

Bulat, J., 2003, Imaging the Afen Slide from commercial 3D seismic – methodology and comparisons with high-resolution data. A: J. Locat, J. Mienert (eds.), *Submarine mass movements and their consequences*: Kluwer Academic Publishers, Holanda, p. 205-213.

Burrus, J., 1984, Contribution to a geodynamic synthesis of the Provençal Basin (North-western Mediterranean): *Marine Geology*, v. 55, p. 247-269.

Campbell, K.J., 1999, Deepwater geohazards: How significant are they?: *Leading Edge*, v. 18, p. 514-519.

Canals, M., 1985, *Estructura sedimentaria y evolución morfológica del talud y el glacis continentales del Golfo de León: Fenómenos de desestabilización de la cobertura plio-cuaternaria* [Tesi Doctoral]: Universitat de Barcelona, Barcelona, Espanya, 618 pp.

Canals, M, Ballesteros, E., 1996, Production of carbonate particles by phytobenthic communities on the Mallorca – Menorca Shelf, Northwestern Mediterranean Sea: *Deep-Sea Research*, v. 44, p. 611-629.

Canals, M., Catafau, E., Serra-Raventós, J., 1982, Toponímia de la mar catalano-balear (amb un glossari de termes genètics): *Bolletí de la Societat d'Història Natural de les Balears*, v. 26, p. 169-194.

Canals, M., Acosta, J., Baraza, J., Bart, P., Calafat, A.M., Casamor, J.L., De Batist, M., Ercilla, G., Farran, M., Sorribas, J.L., Tassone, A., 1994, La Cuenca Central de Bransfield (NW de la Península Antártica): primeros resultados de la campaña GEBRA-93: *Geogaceta*, v. 16, p. 132-135.

Canals, M., Alonso, B., Baraza, J., Ercilla, G., Calafat, A.M., Masson, D.G., Farran, M., Sorribas, J., Estrada, F., Cavaller, M., Prieto, M.J., Rodríguez, J.P., Maillard, N., 1995, *Estudio oceanográfico multidisciplinar del Mar Catalano-Balear; Informe de la Campaña BIG 95*. [Document intern GRC Geociències Marines]: Universitat de Barcelona, Barcelona, Espanya, 94 pp., (inèdit).

Canals, M., Cacho, I., Vaquero, M., Suc, J.P., Subayllova, D., Aloisi, J.C., Jallet, L., Moreno, E., Kerbrat, R., Floch, G., 1998, *Coring of the BIG'95 slide Ebro Margin, NW Mediterranean Sea; CALMAR Cruise 13-26 November 1997* [Document intern GRC Geociències Marines]: Universitat de Barcelona, Barcelona, Espanya, 98 pp., (inèdit).

Canals, M., Urgeles, R., Masson, D.G., Casamor, J.L., 2000a, Los deslizamientos submarinos de las Islas Canarias: *Makaronesia, Boletín de la Asociación de Amigos del Museo de Ciencias Naturales de Tenerife*, v. 2, p. 57-69.

Canals, M., Casamor, J.L., Urgeles, R., Lastras, G., Calafat, A.M., De Batist, M., Masson, D., Berné, S., Alonso, B., Hughes-Clarke. J.E., 2000b, The Ebro continental margin, Western Mediterranean Sea: Interplay between canyon-channel systems and mass wasting processes; A: C.H. Nelson, P. Weimer (eds.), *Deep-water Reservoirs of the World*: GCSSEPM Foundation 20th Annual Research Conference, Houston, Texas, Estats Units, p. 152-174, (CD edition).

Canals, M., Lastras, G., Urgeles, R., Casamor, J.L., Mienert, J., Cattaneo, A., De Batist, M., Haflidason, H., Imbo, Y., Laberg, J.S., Locat, J., Long, D., Longva, O., Masson, D.G., Sultan, N., Trincardi, F., Bryn, P., 2004, Slope failure dynamics and impacts from seafloor and shallow sub-seafloor geophysical data: An Overview: *Marine Geology*, (en premsa).

Carter, L., 2001, A large submarine debris flow in the path of the Pacific deep western boundary current off New Zealand: *Geo-Marine Letters*, v. 21, p. 42-50.

Casas, D., Ercilla, G., Baraza, J., Alonso, B., Maldonado, A., 2003, Recent mass-movement processes on the Ebro continental slope (NW Mediterranean): *Marine and Petroleum Geology*, v. 20, p. 445-457.

Cherkis, N.Z., Max, M.D., Vogt, P.R., Crane, K., Midthassel, A., Sundvor, E., 1999, Large-scale mass wasting on the north Spitsbergen continental margin, Arctic Ocean: *Geo-Marine Letters*, v. 19, p. 131-142.

Chiocci, F.L., Bosman, A., Romagnoli, C., Tommasi, P., De Alteris, G., 2003, The December 2002 Sciara Del Fuoco (Stromboli Island) submarine landslide: a first characterisation: *EGS-AGU-EUG Joint Assembly*, Niça, França.

Cita, M.B., Camerlenghi, A., Kastens, K.A., McCoy, F.W., 1984, New findings of Bronze Age homogenites in the Ionian Sea: Geodynamic implications for the Mediterranean. A: M.B. Cita, F.R. Lucchi (eds.), Seismicity and Sedimentation in the Mediterranean: *Marine Geology*, v. 55, p. 47-62.

Clavell, E., Berastegui, X., 1991, Petroleum geology of the Gulf of Valencia. A: A.M. Spencer (ed.), *Generation, accumulation and production of Europe's Hydrocarbons*: Special Publication EAPG, Oxford University Press, v. 1, p. 355-368.

Coulter, H.W., Migliaccio, R.R., 1966, Effects of the earthquake of March 27, 1954, at Valdez, Alaska: *US Geological Survey Professional Papers*, v. 542-C, 36 pp.

Crandell, D.R., Miller, C.D., Christiansen, R.L., Glicken, H.X., Newhall, C.G., 1984, Catastrophic debris avalanche from an ancestral Mount Shasta volcano, California. A: T.H. Nielsen (ed.), *Geology of the Upper Cretaceous Hornbook Formation, Oregon and California*: Society of Economic Palaeontology and Mineralogy, Tulsa, Oklahoma, Estats Units, p. 197-201.

Dañobeitia, J.J., Alonso, B., Maldonado, A., 1990, Geological framework of the Ebro continental margin and surrounding areas. A: C.H. Nelson, A. Maldonado (eds.), The Ebro Continental Margin, Northwestern Mediterranean Sea: *Marine Geology*, v. 95, p. 265-287.

De Blasio, F.V., Issler, D., Elverhøi, A., Harbitz, C.B., Ilstad, T., Bryn, P., Lien, R., Løvholt, F., 2003, Dynamics, velocity and run-out of the giant Storegga Slide. A: J. Locat, J. Mienert (eds.), *Submarine mass movements and their consequences*: Kluwer Academic Publishers, Holanda, p. 223-230.

Deplus, C., Le Friant, A., Boudon, G., Komorowski, J.C., Villemant, B., Harford, C., Ségoufin, J., Cheminée, J.L., 2001, Submarine evidence for large-scale debris avalanches in the Lesser Antilles Arc: *Earth and Planetary Science Letters*, v. 192, p. 145-157.

Dingle, R.V., 1977, The anatomy of a large submarine slump on a sheared continental margin (southeast Africa): *Journal of the Geological Society of London*, v. 134, p. 293-310.

Dott Jr., R.H., 1963, Dynamics of subaqueous gravity depositional processes: *AAPG Bulletin*, v. 47, p. 104-128.

Drago, M., 2002, A coupled debris flow – turbidity current model: *Ocean Engineering*, v. 29, p. 1769-1780.

Driscoll, N.W., Weissel, J.K., Goff, J.A., 2000, Potential for large-scale submarine slope failure and tsunami generation along the U.S. mid-Atlantic coast: *Geology*, v. 28, p. 407-410.

Droz, L., 1983, *L'éventail sous-marin profond du Rhône (Golfe du Lion): grands traits morphologiques et structure semi-profonde* [Tesi Doctoral]: Université de Paris VI, Paris, França, 195 pp.

Droz, L., Bellaiche, G., 1985, Rhone deep-sea fan: morphostructure and growth pattern: *AAPG Bulletin*, v. 69, p. 460–479.

Droz, L., Kergoat, R., Cochonat, P., Berné, S., 2001, Recent sedimentary events in the western Gulf of Lions (Western Mediterranean): *Marine Geology*, v. 176, p. 23-37.

Durand, B., Jolivet, L., Horvath, F., Séranne, M. (eds.), 1999, *The Mediterranean Basins: Tertiary extension with the Alpine orogen*: Geological Society, London, Special Publications, v. 156, 570 pp.

EarthVision, 2002, URL: *http://www.dgi.com/earthvision/index.shtml* (darrera actualització, Desembre 2002) [17 Març 2003].

El-Robrini, M., Gennesseaux, M., Mauffret, A., 1985, Consequences of the El-Asnam earthquakes: Turbidity currents and slumps on the Algerian margin (Western Mediterranean): *Geo-Marine Letters*, v. 5, p. 171–176.

Embley, R.W., 1982, Anatomy of some Atlantic margin sediment slides and some comments on ages and mechanisms. A: S. Saxov, J.K. Neiuwenhuis (eds.), *Marine Slides and Other Mass Movements*: Plenum Press, Nova York, Estats Units, p. 189-214.

Embley, R.W., Jacobi, R.D., 1977, Distribution and morphology of large submarine sediment slides and slumps on Atlantic continental margins: *Marine Geotechnology*, v. 2, p. 205-228.

Estrada, F., Ercilla, G., Alonso, B., 1997, The tecto-sedimentary evolution of the Northeastern Alboran Sea during the Plio-Quaternary. A: S. Cloetingh, M. Fernández, J.A. Muñoz, W. Sassi, F. Horvath (eds.), Structural Controls on Sedimentary Basin Formation: *Tectonophysics*, v. 382, p. 423-442.

Evans, D., King, E.L., Kenyon, N.H., Brett, C., Wallis, D., 1996, Evidence for long-term instability in the Storegga Slide region off western Norway: *Marine Geology*, v. 130, p. 281-292.

Farran, M., Maldonado, A., 1990, The Ebro continental shelf: Quaternary seismic stratigraphy and growth patterns. A: C.H. Nelson, A. Maldonado (eds.), The Ebro Continental Margin, Northwestern Mediterranean Sea: *Marine Geology*, v. 95, p. 289-312.

Field, M.E., Edwards, B.D., 1980, Slopes of the southern California borderland: a regime of mass transport, in processes of the Quaternary depositional environments of the Pacific Coast. A: M.E. Field, A.H. Bouma, I.P. Colbourn, R.G. Douglas, V.C. Ingle (eds.), *Pacific Coast Paleogeography Symposium 4*: SEPM-PS, Bakersfield, Estats Units, p. 169-184.

Field, M.E., Gardner, J.V., 1990, Pliocene-Pleistocene growth of the Rio Ebro margin, northeast Spain: A prograding-slope model: *GSA Bulletin*, v. 102, p. 721-733.

Flewellen, C.G., Millard, N.W., Rouse, I.P., 1993, TOBI, a vehicle for deep ocean survey: *Electronic and Communication Engineering Journal*, v. 5, p. 85-93.

Gardner, J.V., Prior, D.B., Field, M.E., 1999, Humboldt Slide – a large shear-dominated retrogressive slope failure: *Marine Geology*, v. 154, p. 323-338.

Garfunkel, Z., Arad, A., Almagor, G., 1979, The Palmahim disturbance and its regional setting. *GSA Bulletin*, v. 72, 56 pp.

Gary, M.R. McAfee Jr., R., Wolf, C.L. (eds.), 1974, *Glossary of Geology*: American Geology Institute, Washington DC, Estats Units, 805 pp.

Gaullier, V., Antonini, E., Benkhelil, J., Got, H., 1998, Corps gravitaires récents dans le basin Nord-Baléares: géométrie et quantification: *Comptes Rendus de l'Académie des Sciences de Paris*, v. 327, p. 677-684.

Gee, M.J.R., Masson, D.G., Watts, A.B., Allen, P.A., 1999, The Saharan debris flow: an insight into the mechanics of long runout submarine debris flows: *Sedimentology*, v. 46, p. 317-335.

Gennesseaux, M.A., Mauffret, A., Pautot, G., 1980, Les glissements sous-marins de la pente continentale niçoise et la rupture de câbles en mer Ligure (Méditerranée occidentale): *Comptes Rendus de l'Académie des Sciences de Paris*, v. 290, p. 959–962.

GMT, 2001, Disponible FTP (versió 3.4 per a DOS): *gmt.soest.hawaii.edu*, directori: pub/gmt, arxiu: netcdf-3_4_win32bin.zip (13 Abril 2001) [17 Març 2003].

GMT, 2002, URL: *http://gmt.soest.hawaii.edu* (darrera actualització, Octubre 2002) [17 Març 2003].

Goldfinger, C., Kulm, L.D., McNeill, L.C., Watts, P., 2000, Super-scale failure of the Southern Oregon Cascadia Margin: *Pure and Applied Geophysics*, v. 157, p. 1189-1226.

Gràcia, E., Dañobeitia, J., Vergés, J., equip PARSIFAL, 2002, Mapping active faults offshore Portugal (36°N-38°N): Implications for seismic hazard assessment along the southwest Iberian margin: *Geology*, v. 31, p. 83-86.

Grup de Treball ZEE, 2001, *Mapa geomagnético del mar Balear y golfo de Valencia, Mediterráneo occidental, Zona Económica Exclusiva Española.* Instituto Español de Oceanografía.

Gueguen, E., 1995, *Le Bassin Liguro-Provençal: un véritable ocean. Example de segmentation des marges et de hiatus cinématiques. Implications sur les processus d'amincissement crustal* [Tesi Doctoral]: Université de Brest, Brest, França, 315 pp.

Gueguen, E., Doglioni, C., Fernández, M., 1997, Lithospheric boudinage in the western Mediterranean: new constraints: *Terra Nova*, v. 9, p. 184-187.

Gueguen, E., Doglioni, C., Fernández, M., 1998, On the post-25 Ma geodynamic evolution of the western Mediterranean: *Tectonophysics*, v. 298, p. 259-269.

Hampton, M.A., 1972, The role of subaqueous debris flows in generating turbidity currents: *Journal of Sedimentary Petrology*, v. 42, p. 775-793.

Hampton, M.A., Lee, J.L., Locat, J., 1996, Submarine landslides: *Reviews of Geophysics*, v. 34, p. 33-59.

Hanumantha Rao, Y., Subrahmanyam, C., Rastogi, A., Deka, B., 2002, Slope failures along the western continental margin of India: a consequence of gas-hydrate dissociation, rapid sedimentation rate, and seismic activity?: *Geo-Marine Letters*, v. 22, p. 162-169.

Harbitz, C.B., 1992, Model simulations of tsunamis generated by the Storegga slides: *Marine Geology*, v. 105, p. 1-12.

Heezen, B.C., Ewing, M., 1952, Turbidity Currents and Submarine Slumps, and the 1929 Grand Banks Earthquake: *American Journal of Science*, v. 250, p. 849-873.

Heezen, B.C., Ewing, M., 1954, Orleansville earthquake and turbidity currents: *AAPG Bulletin*, v. 39, p. 2505-2514.

Heezen, B.C., Ericson, D.B., Ewing, M., 1954, Further evidence for a turbidity current following the 1929 Grand Banks earthquake: *Deep-Sea Research*, v. 1, p. 193-202.

Holcomb, R.T., Searle, R.C., 1991, Large landslides from oceanic volcanoes: *Marine Geotechnology*, v. 10, p. 19-32.

Hsü, K.J., 1977, The history of the Mediterranean salinity crisis: *Nature*, v. 267, p. 399-403.

Huang, X., Garcia, M.H., 1999, Modelling of non-hydroplaning mud flows on continental slopes: *Marine Geology*, v. 154, p. 132-142.

Huson, W.J., Fortuin, A.R., 1985, The Lithinion slide: a large submarine slide in the South Cretan Trough, eastern Mediterranean: *Marine Geology*, v. 65, p. 103–111.

IGME, 1987, *Contribución de la exploración petrolífera al conocimiento de la geología de España*: Instituto Geológico y Minero, Madrid, Espanya, 465 pp.

Imbo, Y., De Batist, M., Canals, M., Prieto, M.J., Baraza, J., 2002, The Gebra Slide: a submarine slide on the Trinity Peninsula Margin, Antarctica: *Marine Geology*, v. 193, p. 235-252.

Imran, J., Harff, P., Parker, G., 2001, A numerical model of submarine debris flow with graphical user interface: *Computers and Geosciences*, v. 27, p. 717-729.

Iverson, R.M., 1997, The Physics of debris flows: *Reviews of Geophysics*, v. 35, p. 245-296.

Jackson, D.R., Winebrenner, D.P., Ishimaru, A., 1986, Application of the composite roughness model to high-frequency bottom backscattering: *Journal of the Acoustical Society of America*, v. 79, p. 1410-1422.

Jiang, L., LeBlond, P.H., 1992, The Coupling of a submarine slide and the surface waves which it generates: *Journal of Geophysical Research*, v. 97, p. 12731-12744.

Kastens, K.A., 1984, Earthquakes as a triggering mechanism for debris flows and turbidites on the Calabrian Ridge: *Marine Geology*, v. 55, p. 13-33.

Kastens, K.A., Cita, M.B., 1981, Tsunami-induced sediment transport in the abyssal Mediterranean Sea: *GSA Bulletin*, v. 92, p. 845-857.

Kastens, K., Mascle, J., Auroux, C., i altres, 1988, ODP Leg 107 in the Tyrrhenian Sea, insights into passive margin and back-arc basin evolution: *GSA Bulletin*, v. 100, p. 1140-1156.

Kenyon, N.H., 1987, Mass-wasting features on the continental slope of northwestern Europe: *Marine Geology*, v. 74, p. 57-77.

Krastel, S., Schmincke, H.U., Jacobs, C.L., Rihm, R., Le Bas, T.P., Alibés, B., 2001, Submarine landslides around the Canary Islands: *Journal of Geophysical Research*, B3, v. 106, p. 3977-3997.

Labazuy, P., 1996, Recurrent landslides events on the submarine flank of Piton de la Fournaise volcano (Reunion Island). A: W.J. McGuire, A.P. Jones, J. Neuberg (eds.), *Volcano instability on the Earth and other planets*: Geological Society Special Publication, Geological Society of London, Londres, p. 295-306.

Laberg, J.S., Vorren, T.O., 1995, Late Weichselian submarine debris flow deposits on the Bear Island Trough Mouth Fan: *Marine Geology*, v. 127, p. 45-72.

Laberg, J.S., Vorren, T.O., 2000a, Flow behaviour of the submarine glaciogenic debris flows on the Bear Island Trough Mouth Fan, western Barents Sea: *Sedimentology*, v. 47, p. 1105-1117.

Laberg, J.S., Vorren, T.O., 2000b, The Trænadjupet Slide, offshore Norway – morphology, evacuation and triggering mechanisms: *Marine Geology*, v. 171, p. 95-114.

Laberg, J.S., Vorren, T.O., Dowdeswell, J.A., Kenyon, N.H., Taylor, J., 2000, The Andøya Slide and the Andøya Canyon, north-eastern Norwegian-Greenland Sea: *Marine Geology*, v. 162, p. 259-275.

Lastras, G., 1999, *Inventario de movimientos de masa submarinos en el Mediterráneo* [Treball de Fi de Carrera]: Universitat de Barcelona, Barcelona, Espanya, 104 pp., (inèdit).

Lastras, G., Canals, M., Hughes Clarke, J.E., Moreno, A., De Batist, M., Masson, D.G., Cochonat, P., 2002, Seafloor imagery from the BIG'95 debris flow, western Mediterranean: *Geology*, v. 30, p. 871-874.

Lastras, G., Canals, M., Urgeles, R., 2003, Lessons from sea-floor and subsea-floor imagery of the BIG'95 debris flow scar and deposit. A: J. Locat, J. Mienert (eds.), *Submarine Mass Movements and Their Consequences*: Kluwer Academic Publishers, Holanda, p. 425-431.

Lastras, G., Canals, M., Urgeles, R., De Batist, M., Calafat, A.M., Casamor, J.L., 2004a, Characterisation of a recent debris flow deposit on the Ebro margin, Western Mediterranean Sea, after a variety of seismic reflection data: *Marine Geology*, (acceptat).

Lastras, G., Canals, M., Urgeles, R., Hughes-Clarke, J.E., Acosta, J., 2004b, Shallow slides and pockmark swarms in the Eivissa Channel, Western Mediterranean Sea: *Sedimentology*, (en premsa).

Lastras, G., De Blasio, F.V., Elverhøi, A., Canals, M., 2004c, Conceptual and numerical modelling of the BIG'95 debris flow, Western Mediterranean: *Journal of Sedimentary Research*, (en revisió).

Legros, F., 2002, The mobility of long-runout landslides: *Engineering Geology*, v. 63, p. 301-331.

Locat, J., Lee, H.J., 2002, Submarine landslides: advances and challenges: Keynote paper presented at the 8th International Symposium on Landslides, Cardiff, UK, June 2000, *Canadian Geotechincal Journal*, v. 39, p. 193-212.

Locat, J., Mienert, J. (eds.), 2003, *Submarine Mass Movements and Their Consequences*: Kluwer Academic Publishers, Holanda, 552 pp.

Locat, J., Lee, H.J., Locat, P., Imran, J., 2004, Numerical analysis of the mobility of the Palos Verdes debris avalanche, California, and its implication for the generation of tsunamis: *Marine Geology*, v. 203, p. 269-280.

Longva, O., Janbu, N., Blikra, L.H., Bøe, R., 2003, The 1996 Finneidfjord Slide; seafloor failure and slide dynamics. A: J. Locat, J. Mienert (eds.), *Submarine mass movements and their consequences*: Kluwer Academic Publishers, Holanda, p. 531-538.

López Jurado, J.L., Díaz del Río, G., 1994, Dinámica asociada a las masas de agua en el canal de Ibiza en noviembre de 1990 y marzo de 1991: *Boletín del Instituto Español de Oceanografía*, v. 10, p. 3-22.

Lykousis, V., Roussakis, G., Alexandri, M., Pavlakis, P., Papoulia, I., 2002, Sliding and regional slope stability in active margins: North Aegean Trough (Mediterranean): *Marine Geology*, v. 186, p. 281-298.

Maillard, A., Mauffret, A., 1993, Structure et volcanisme de la fosse de Valence (Méditerranée nord-occidentale): *Bulletin Société géologique de France*, v. 164, p. 365-383.

Maillard, A., Mauffret, A., 1999, Crustal structure and riftogenesis of the Valencia Trough (north-western Mediterranean Sea): *Basin Research*, v. 11, p. 357-379.

Maillard, A., Mauffret, A., Watts, A.B., Torné, M., Pascal, G., Buhl, P., Pinet, B., 1992, Tertiary sedimentary history and structure of the Valencia trough (western Mediterranean): *Tectonophysics*, v. 203, p. 57-75.

Malinverno, A., Ryan, W.B.F., Auffret, G., Pautot, G., 1988, Sonar images of the path of recent failure events on the continental margin off Nice, France: *GSA Special Papers*, v. 229, p. 59-75.

Marr, J.G., Harff, P.A., Shanmugam, G., Parker, G., 2001, Experiments on subaqueous sandy gravity flows: The role of clay and water content in flow dynamics and depositional structures: *GSA Bulletin*, v. 113, p. 1377-1386.

Marr, J.G., Elverhøi, A., Harbitz, C., Miran, J., Harff, P., 2002, Numerical simulation of mud-rich subaqueous debris flows on the glacially active margins of the Svalbard-Barents Sea: *Marine Geology*, v. 188, p. 351-364.

Martí, J., Grachev, A., Mitjacila, J., Aparicio, A., Roca, E., 1990, Cenozoic magmatism in the Valencia Trough: *Terra Abstracts*, v. 2, p. 6.

Martí, J., Mitjavila, J., Roca, E., Aparicio, A., 1992, Cenozoic magmatism of the Valencia trough (western Mediterranean): relationship between structural evolution and volcanism: *Tectonophysics*, v. 203, p. 145-165.

Masson, D.G., 1996, Catastrophic collapse of the flank of El Hierro about 15,000 years ago, and the history of large flank collapses in the Canary Islands: *Geology*, v. 24, p. 231-234.

Masson, D.G., 2001, Sedimentary processes shaping the eastern slope of the Faeroe-Shetland Channel: *Continental Shelf Research*, v. 21, p. 825-857.

Masson, D.G., Canals, M., Alonso, B., Urgeles, R., Huhnerbach, V., 1998, The Canary Debris Flow: source area, morphology and failure mechanisms: *Sedimentology*, v. 45, p. 411-432.

Masson, D.G., Watts, A.B., Gee, M.J.R., Urgeles, R., Mitchell, N.C., Le Bas, T.P., Canals, M., 2002, Slope failures on the flanks of the western Canary Islands: *Earth-Science Reviews*, v. 57, p. 1-35.

Mauffret, A., Contrucci, I., Brunet, C., 1999, Structural evolution of the Northern Tyrrhenian Sea from new seismic data: *Marine and Petroleum Geology*, v. 16, p. 381-407.

McAdoo, B.G., Pratson, L.F., Orange, D.L., 2000, Submarine landslide geomorphology, US continental slope: *Marine Geology*, v. 169, p. 103-136.

Méar, Y., 1984, *Séquences et unités sédimentaires du glacis rhodanien (Méditerranée Occidentale)* [Tesi Doctoral]: Université de Perpignan, Perpinyà, França, 2 vols., 214 pp.

Mienert J., Weaver, P.P.E. (eds.), 2003, *European Margins Sediment Dynamics: Side-Scan Sonar and Seismic Images*: Springer-Verlag, Heidelberg (Germany), 310 pp.

Millot, C., 1999, Circulation in the Western Mediterranean Sea: *Journal of Marine Systems*, v. 20, p. 423-442.

Mohrig, D., Whipple, K.X., Hondzo, N.H., Ellis, C., Parker, G., 1998, Hydroplaning of subaqueous debris flows: *GSA Bulletin*, v. 110, p. 387-394.

Mohrig, D., Elverhøi, A., Parker, G., 1999, Experiments on the relative mobility of muddy subaqueous and subaerial debris flows, and their capacity to remobilise antecedent deposits: *Marine Geology*, v. 154, p. 117-129.

Moore, D.G., 1961, Submarine slumps: *Journal of Sedimentary Petrology*, v. 31, p. 343-357.

Moore, J.G, Clague, D.A., Holcomb, R.T., Lipman, P.W., Normark, W.E., Torressan, M.E., 1989, Prodigious submarine landslides on the Hawaiian Ridge: *Journal of Geophysical Research*, v. 94, p. 14465-14484.

Moore, J.G., Normark, W.R., Holcomb, R.T., 1994, Giant Hawaiian landslides: *Annual Review Earth and Planetary Science Letters*, v. 22, p. 119-144.

Mulder, T., Cochonat, P., 1996, Classification of offshore mass movements: *Journal of Sedimentary Research*, v. 66, p. 43–47.

Mulder, T., Tisot, J.P., Cochonat, P., Bourillet, J.F., 1994, Regional assessment of mass failure events in the Baie des Anges, Mediterranean Sea: *Marine Geology*, v. 122, p. 29-45.

Murton, B.J., Rouse, I.P., Millard, N.W., Flewellen, C., 1992, Deeptowed instrument explores ocean floor: *Eos transansactions of the American Geophysical Union*, v. 73, p. 225-228.

Nardin, T.R., Hein, F.J., Gorsline, D.S., Edwards, B.D., 1979, A review of mass movement processes, sediment and acoustic characteristics, and contrasts in slope and base-of-slope systems versus canyon-fan-basin floor systems: *Society of Economic Palaeontology and Mineralogy Special Publication*, v. 27, p. 61-73.

Nelson, C.H., Maldonado, A., 1988, Factors controlling depositional patterns of Ebro Turbidite Systems, Mediterranean Sea: *AAPG Bulletin*, v. 72, p. 698-716.

Nelson, C.H., Maldonado, A., 1990, Factors controlling late Cenozoic continental margin growth from the Ebro Delta to the western Mediterranean deep sea. A: C.H. Nelson, A. Maldonado (eds.), The Ebro Continental Margin, Northwestern Mediterranean Sea: *Marine Geology*, v. 95, p. 419-440.

Okura, Y., Kitahara, H., Ochiai, H., Sammori, T., Kawanami, A., 2002, Landslide fluidization process by flume experiments: *Engineering Geology*, v. 66, p. 65-78.

Palomo, C., Acosta, J., de Andrés, J., Herranz, P., Rey, J., Sanz, J.L., 1976, Perfiles geofísicos entre la península y las Islas Baleares: 2ª Asamblea Nacional de Geodesia y Geofísica, *Comunicaciones*, v. 3, p. 1615-1627.

Papatheodorou, G., Ferentinos, G., 1997, Submarine and coastal sediment failure triggered by the 1995, Ms=6.1R Aegion earthquake, Gulf of Corinth, Greece: *Marine Geology*, v. 137, p. 287-304.

Pérez-Belzuz, F., Alonso, B., Ercilla, G., 2000, Modelos de sistemas turbidíticos en el área de Motril (NE Alborán): *Geotemas*, v. 1(4), p. 213-216.

Piper, D.J.W., McCall, C., 2003, A synthesis of the distribution of submarine mass movements on the Eastern Canadian Margin. A: J. Locat, J. Mienert (eds.), *Submarine mass movements and their consequences*: Kluwer Academic Publishers, Holanda, p. 291-298.

Piper, D.J.W., Cochonat, P., Morrison, M.L., 1999, The sequence of events around the epicentre of the 1929 Grand Banks earthquake: initiation of debris flows and turbidity current inferred from sidescan sonar: *Sedimentology*, v. 46, p. 79-97.

Pratson, L.F., J. Imran, G. Parker, J. Syvitski, E. Hutton, 2000, Debris flows versus turbidity currents: a modelling comparison of their dynamics and deposits. A: A. Bouma, C. Stone (eds.), Fine-Grained Turbidite Systems: AAPG Memoir 72, *SEPM Special Publication*, v. 68, p. 57-72.

Prior, D.B., Coleman, J.M, 1978, Disintegrative retrogressive landslides on very-low-angle subaqueous slopes, Mississippi delta: *Marine Geotechnology*, v. 3, p. 37-60.

Prior, D.B., Doyle, E.H., Neurauter, T., 1986, The Currituck Slide, Mid-Atlantic continental slope – revisited: *Marine Geology*, v. 73, p. 25-45.

Rebesco, M., Della Vedova, B., Cernobori, L., Aloisi, G., 2000, Acoustic facies of Holocene megaturbidites in the Eastern Mediterranean: *Sedimentary Geology*, v. 135, p. 65-74.

Rehault, J.P., Boillot, G., Mauffret, A., 1984, The Western Mediterranean Basin geological evolution: *Marine Geology*, v. 55, p. 447-477.

Riba, O., Galí, S., Susagna, M.T., Reguant, S., Canals, M., Mata, J.M., Santanach, P., Serrat, D., Vaquer, R., Martí, J., Melgarejo, J.C., Martinell, J., Colombo, F., i altres, 1997, *Diccionari de Geologia*: Institut d'Estudis Catalans, Ed. Enciclopèdia Catalana, Barcelona, Espanya, 1407 pp.

Robertson, A.H.F, Grasso, M., 1995, Overview of the Late Tertiary-recent tectonic and palaeo-environmental development of the Mediterranean region: *Terra Nova*, v. 7, p. 114-127.

Roca, E., 1992, *L'estructura de la Conca Catalano-Balear: paper de la compressió i de la distensió en la seva gènesi* [Tesi Doctoral]: Universitat de Barcelona, Barcelona, Espanya, 340 p.

Roca, E., 1994, La evolución geodinámica de la Cuenca Catalano-Balear y áreas adyacentes desde el Mesozoico hasta la actualidad: *Acta Geológica Hispánica*, v. 29, p. 3-25.

Roca, E., Sans, M., Cabrera, L., Marzo, M., 1999, Oligocene to Middle Miocene evolution of the central Catalan margin (northwestern Mediterranean): *Tectonophysics*, v. 315, p. 209-233.

Rosenbaum, G., Lister, G.S., Duboz, C., 2002, Reconstruction of the tectonic evolution of the western Mediterranean since the Oligocene. A: G. Rosenbaum, G.S. Lister (eds.), Reconstruction of the evolution of the Alpine-Himalayan Orogen: *Journal of the Virtual Explorer*, v. 8, p. 107-126.

Rothwell, R.G., Thomson, J., Kähler, G., 1998, Low sea-level emplacement of a very large Late Pleistocene "megaturbidite" in the western Mediterranean: *Nature*, v. 392, p. 377-380.

Rothwell, R.G., Reeder, M.S., Anastasakis, G., Stow, D.A.V., Thomson, J., Kähler, G., 2000, Low-stand emplacement of megaturbidites in the Western and Eastern Mediterranean Sea: *Sedimentary Geology*, v. 135, p. 75-88.

Ryan, W.B.F., Stanley, D.J., Hersey, J.B., Falquist, D., Allan, T.D., 1970, The tectonics and geology of the Mediterranean Sea. A: A.F. Maxwell (ed.), *The Sea, ideas and observation on progress in the study of the sea*: Wiley Interscience, Nova York, Estats Units, v. 4, p. 387-492.

Ryan, W.B.F., Hsu, K.I., i altres, 1973, *Initial report of the Deep Sea Drilling Project*: US Government Printing Office, Washington DC, Estats Units, v. 13.

Sàbat, F., Roca, E., Muñoz, J.A., Vergés, J., Santanach, P., Sans, M., Massana, E., Estévez, A., Santisteban C., 1997, Role of extension and compression in the evolution of the eastern margin of Iberia: the ESCI-València trough seismic profile: *Revista de la Sociedad Geológica de España*, v. 8, p. 431-448.

Satake, K., 2001, Tsunami modelling from submarine landslides: *Proceedings of the International Tsunami Symposium*, Seattle, Estats Units, p. 665-674.

Savelli, C., 1988, Late Oligocene to Recent episodes of magmatism in and around the Thyrrhenian Sea: implications for the processes of opening in a young inter-arc basin of intra-orogenic (Mediterranean) type: *Tectonophysics*, v. 146, p. 163-181.

Savostin, L.A., Sibuet, J.C., Zonenshain, L.P., Le Pichon, X., Roulet, M.J., 1986, Kinematic evolution of the Tethys belt from the Atlantic Ocean to the Pamirs since the Triassic: *Tectonophysics*, v. 123, p. 1-35.

Simrad Norge, 1994, *Simrad TOPAS PS 018 operator manual* [Document intern Simrad Norge]: Stjordal, Noruega, 68 pp.

Simrad Subsea, 1991, *Product description. Simrad EM 12 multibeam echosounder* [Document intern Simrad Subsea]: Horten, Noruega, 31 pp.

Smith, W.H.F, Sandwell, D.T., 1997, Global seafloor topography from satellite altimetry and ship depth soundings: *Science*, v. 277, p. 1957-1962.

Smith, D.E., Kolenkiewicz, R., Nerem, R.S., Dunn, P.J., Torrence, M.H., Robbins, J.W., Klosko, S.M., Williamson, R.G., Pavlis, E.C., 1994, Contemporary global horizontal crustal motion: *Geophysics Journal International*, v. 119, p. 511-520.

Soler, R., Martínez, W., Megías, A.G., Abeger, J.A., 1983, Rasgos básicos del Neógeno del Mediterráneo español: *Mediterránea Serie de Estudios Geológicos*, v. 1, p. 71-82.

SwathEd, 1998, URL: *http://www.omg.unb.ca/~jhc/SwathEd.html* (darrera actualització, Maig 1998) [17 Març 2003].

Tappin, D.R., Matsumoto, T., Watts, P., Satake, K., McMurtry, G.M., Matsuyama, M., Lafoy, Y., Tsuji, Y., Kanamatsu, T., Lus, W., Iwabuchi, Y., Yeh, H., Matsumotu, Y., Nakamura, M., Mahoi, M., Hill, P., Crook, K., Anton, L., Walsh, J.P., 1999, Sediment slump likely caused Papua New Guinea tsunami: *Eos Transactions of the American Geophysical Union*, v. 80, p. 329-340.

Tappin, D.R., Watts, P., McMurtry, G.N., Lafoy, Y., Matsumoto, T., 2001, The Sissano, Papua New Guinea tsunami of July 1998 – offshore evidence on the source mechanism: *Marine Geology*, v. 175, p. 1-23.

Tapponnier, P., 1977, Evolution tectonique du ssystème alpin en Méditerranée: poinçonnement et écrasement rigide-plastique: *Bulletin Société géologique de France*, v. 19, p. 437-460.

Urgeles, R., 1999, *Esllavissaments gegants a les Illes Canàries: les illes d'El Hierro i La Palma* [Tesi Doctoral]: Universitat de Barcelona, Barcelona, Espanya, 210 pp.

Urgeles, R., Canals, M., Baraza, J., Alonso, B., Masson, D.G., 1997, The most recent megalandslides on the Canary islands: The El Golfo debris avalanche and the Canary debris flow, West Hierro Island: *Journal of Geophysical Research*, v. 102, p. 20305-20323.

Urgeles, R., Masson, D.G., Canals, M., Watts, A., Le Bas, T., 1999, Recurrent giant landslides on the west flank of La Palma, Canary Islands: *Journal of Geophysical Research*, v. 104, p. 25331-25348.

Urgeles, R., Canals, M., Masson, D.G., 2001a, Flank stability and processes off the western Canary Islands: A review from El Hierro and La Palma: *Scientia Marina*, v. 65, p. 21-31.

Urgeles, R., Lastras, G., Calafat, A.M., Willmott, V., Casamor, J.L., Buryak, S., Shashkin, P., Frigola, J., Amblàs, D., 2001b, *Large landslides on the slope and rise of the Ebro continental margin. Final Cruise Report TTR-11 Leg 2b (BIGIMAGE) on board the R.V. Professor Logachev, August 16-20, 2001* [Document intern GRC Geociències Marines]: Universitat de Barcelona, Barcelona, Espanya, 33 pp., (inèdit).

Urgeles, R., Locat, J., Lee, H.J., Martin, F., 2002, The Saguenay Fjord, Quebec, Canada: integrating marine geotechnical and geophysical data for spatial seismic slope stability and hazard assessment: *Marine Geology*, v. 185, p. 319-340.

Urgeles, R., Lastras, G., Canals, M., Willmott, V., Moreno, A., Casas, D., Baraza, J., Berné, S., 2003, The BIG'95 debris flow and adjacent unfailed sediments in the NW Mediterranean Sea: geotechnical – sedimentological properties, and dating. A: J. Locat, J. Mienert (eds.), *Submarine Mass Movements and Their Consequences*: Kluwer Academic Publishers, Holanda, p. 479-487.

Watts, A.B., Platt, J.P., Bulh, P., 1993, Tectonic evolution of the Alboran Sea Basin: *Basin Research*, v. 5, p. 153-177.

Weaver, P.P.E., Wynn, R.B., Kenyon, N.H., Evans, J.M., 2000, Continental margin sedimentation, with special reference to the north-east Atlantic margin: *Sedimentology*, v. 47 (suppl. 1), p. 239-256.

Wessel, P., Smith, W.H.F., 1998, New, improved version of the Generic Mapping Tools Released: *Eos Transactions of the American Geophysical Union*, v. 79, p. 579.

WIN4GMT, 2002, URL: *http://www.icm.csic.es/geo/gma/geo6es.html* (darrera actualització, Gener 2002). Disponible FTP (versió 2.1): *cucafera.cmima.csic.es*, directori: pub/web/gma, arxiu: W4Gsetup.exe (24 Gener 2002) [17 Març 2003].

Wynn, R.B., Masson, D.G., Stow, D.A.V., Weaver, P.P.E., 2000, The Northwest African slope apron: a modern analogue for deep-water systems with complex seafloor topography: *Marine and Petroleum Geology*, v. 17, p. 253-265.

APÈNDIX

Índex de figures i taules

Índex de figures i taules

CAPÍTOL 1

CAPÍTOL 2

CAPÍTOL 3

CAPÍTOL 4

CAPÍTOL 5

CAPÍTOL 6

CAPÍTOL 7

CAPÍTOL 8